Impacts of Temperature-Dependent Heating Demand on Wintertime Emissions

Cara Scalpone

A Thesis submitted in partial fulfillment of
the requirements for the degree of

Master of Science
(Atmospheric and Oceanic Sciences)

at the
UNIVERSITY OF WISCONSIN-MADISON
August 2025

Abstract

Impacts of Temperature-Dependent Heating Demand on Wintertime Emissions

By Cara Scalpone

Most residences are heated by burning fuels, such as natural gas, heating oil, or wood, which emits combustion byproducts into the atmosphere. Space heating demand is dependent on outdoor temperatures, so the impact of residential heating on wintertime pollution covaries with changes in atmospheric dynamics and meteorologically-dependent chemical processes. However, current representations of emissions from non-wood residential fuel combustion (RFC) in atmospheric modeling are based on fixed monthly or seasonal allocations that do not vary with daily temperature. To improve the representation of these emissions, a method for temporally allocating annual residential fuel combustion emissions that reflects temperature-dependent changes in heating demand based on heating degree days (HDDs) was developed. The temperature-dependent daily scaling (DS) approach was applied to create an hourly RFC emissions inventory gridded to a 12 km domain covering the contiguous U.S. The DS approach was compared to a seasonal scaling (SS) approach that had a fixed temporal allocation for winter, spring, summer, and fall. Across all climate regions, the DS approach resulted in a redistribution of emissions toward March and November relative to the SS approach. RFC emissions contributed substantially to the total anthropogenic NOx and SO_2 emissions in some grid cells, particularly during the heating season. DS had a greater range in hourly emission rates relative to SS, with higher median peak emission rates across all climate regions. Using a diurnal profile to represent hourly heating demand resulted 18% to 28% more emissions to allocated to nighttime hours compared to the default profile. The temperature-based DS approach offers improvements to the representation of heating demand over fixed temporal allocation methods, enabling future

investigation into parsing the co-variable impacts of emissions, meteorology, and chemistry on wintertime air pollution.

Acknowledgements

This research was made possible by the guidance and support from many people throughout my time in graduate school. First, I would like to thank my advisor, Professor Tracey Holloway, for her mentorship and direction in navigating the balance of research, life, and graduate school. Tracey's encouragement has helped me take on challenges and opportunities that I otherwise would not have pursued.

I would like to thank the members of my Graduate Advising Committee, Professor Ankur Desai and Professor Brad Pierce, for providing guidance and advice on courses and helping to define the scope of my M.S. research.

Conducting the emissions processing necessary for this work would not have been possible without help from Mark Jansen at the Lake Michigan Air Directors Consortium (LADCO) to set up the software, and Pete Pokrandt to run the software on our computers. The expert emissions and data science assistance from Holloway Group members Dr. Monica Harkey and Summer Acker helped me work through many technical issues along the way.

I would especially like to thank all the professors, staff, and other graduate students within the Atmospheric and Oceanic Sciences Department and the Energy Analysis and Policy certificate program who have welcomed and supported me throughout graduate school. In particular, the academical, professional, and emotional support offered Lizzy Kysela and Cecilia Orth have been irreplicable in navigating graduate school thus far.

A huge thank you goes toward my family, boyfriend, and friends scattered across the country. Your willingness and patience to listen to me talk about air quality and my newly acquired fun facts about the weather have endlessly affirmed my decision to continue pursing my path toward a Ph.D. in AOS and a career in atmospheric research.

The work presented in this thesis was funded by Audi Settlement funds awarded by the State of Wisconsin to the Holloway Group. During the preparation of this work, I used generative artificial intelligence tools GPT-4o and Google Gemini version 2.5 for assistance in Python scripting for data analysis and figures, and copy-editing a completed thesis draft for word choice and organization. After using these tools, I reviewed, evaluated, and edited any output, and I am fully responsible for the contents of this thesis.

Contents

List of Figures

List of Tables

List of Abbreviations

CAA	Clean Air Act
CDD	cooling degree day
CMAQ	Community Multiscale Air Quality model
CONUS	contiguous United States
$ClNO_2$	nitryl chloride
CO	carbon monoxide
CTM	chemical transport model
DS	daily scaling
EI	emissions inventory
ERA	ECMWF Reanalysis
EQUATES	U.S. Environmental Protection Agency's Air QUAlity TimE Series Project
HDD	heating degree day
HNO_3	nitric acid
IECC	International Energy Conservation Codes
IQR	interquartile range
LADCO	Lake Michigan Air Directors Consortium
LPG	liquified petroleum gas
MCIP	Meteorology - Chemistry Interface Processor
MODIS	Moderate Resolution Imaging Spectroradiometer
N_2O_5	dinitrate pentoxide
NAAQS	National Ambient Air Quality Standard
NAM	North American Mesoscale forecast system

NEI	National Emissions Inventory
NO	nitrogen oxide
NO_2	nitrogen dioxide
NO_X	nitrogen oxides (NO + NO_2)
OHH	outdoor hydronic heater
PM	particulate matter
$PM_{2.5}$	fine particulate matter (less than 2.5-micron diameter)
RFC	non-wood residential fuel combustion
RRTGM	Rapid Radiative Transfer Model for GCMs
RWC	residential wood combustion
SCC	source classification code
SEDS	State Energy Data System
SMOKE	Sparse Matrix Operator Kernel Emissions
SO_2	sulfur dioxide
SS	seasonal scaling
TEMPO	Tropospheric Emissions: Monitoring of Pollution
U.S. EPA	United States Environmental Protection Agency
U.S. EIA	United States Energy Information Administration
VOC	volatile organic compound
WRF	Weather Research and Forecasting model

Chapter 1 Introduction

1.1 Overview of Wintertime Air Quality

Nitrogen oxides ($NO_X = NO + NO_2$) are a group of atmospheric gases that are emitted by natural sources, such as soils (Almaraz et al., 2018; Hall et al., 1996) and lightning (Allen et al., 2021; Schumann & Huntrieser, 2007), and anthropogenic sources, such as vehicles and electricity generation as a byproduct of combustion (Lee et al., 1997; U.S. EPA, 2021a). NO_X are harmful to human and environmental health, and are precursors to the formation of detrimental secondary air pollutants, ozone and fine particulate matter ($PM_{2.5}$). Both short- and long-term exposure to high concentrations of NO_X, ozone, and $PM_{2.5}$ in ambient air have been shown to worsen cardiovascular and respiratory health, and increase mortality (Beelen et al., 2014; Cai et al., 2016; Chen et al., 2007; Dedoussi et al., 2020; Hoek et al., 2013; Turner et al., 2017; Yang et al., 2018). Environmentally, the oxidation of nitrogen dioxide (NO_2) produces nitric acid (HNO_3), a component of acid rain, which can harm terrestrial ecosystems and agriculture by stripping soil of essential nutrients (Jacob, 1999; Krug & Frink, 1983; Likens et al., 1972).

Because of these detrimental health and environmental impacts, outdoor air quality in the United States is regulated by the United States Environmental Protection Agency (U.S. EPA) under the Clean Air Act (CAA) (Clean Air Act, 1970). The U.S. EPA sets National Ambient Air Quality Standards (NAAQS) for air pollutants that pose a risk to human health, called criteria air pollutants, which include NO_2, ozone, and $PM_{2.5}$. NO_X emissions were also controlled under Title IV-Acid Deposition Control from the CAA Amendments of 1990, which set controls for emissions from power plants to reduce acid rain.

Concentrations of NO_X, $PM_{2.5}$, and ozone vary regionally and seasonally, influenced by interconnected changes in emissions, meteorology, and chemical processes. Ambient NOx

concentrations are highest in the wintertime (Van Der A et al., 2008) due to increases in cold-weather emissions, such as residential heating (Chatoutsidou & Lazaridis, 2024), and a longer atmospheric residence time of NOx, or NOx lifetime. NOx lifetime—the time that NOx persist in the atmosphere before being removed by physical and chemical loss pathways—is estimated from aircraft and satellite observations to be between 2 and 11 hours in the summer, and between 6 and 29 hours in the winter (Jaeglé et al., 2018; Kenagy et al., 2018; Lange et al., 2022). In the winter, $PM_{2.5}$ pollution episodes are dominated by particulate nitrate and ammonium nitrate, for which NOx is an essential precursor (Cheng et al., 2024; Hand et al., 2012; Turkiewicz et al., 2006). While high ozone episodes predominantly occur during the summer, high ozone concentrations can occur in the winter, particularly in valleys surrounded by mountains during prolonged winter inversions (Mansfield & Hall, 2013; Matichuk et al., 2017). Isolating the covariable influences of emissions, meteorology, and chemical processes on wintertime air quality at local and regional scales is difficult with observations alone.

Parsing these factors could be achieved through simulations of the atmosphere using chemical transport models (CTM), such as the U.S. EPA's Community Multiscale Air Quality model (CMAQ). Given meteorological and emissions inputs, CMAQ simulates hourly atmospheric composition on a three-dimensional grid using complex parameterizations of chemical processes (Appel et al., 2021b). However, the accuracy of CMAQ and all CTMs are limited by simplifications to chemical processes that are necessary for computing resources, and the accuracy of inputs, such as emissions inventories. To isolate the impacts of meteorology-dependent emissions on wintertime air quality using CMAQ, that dependence must be represented in the emissions inputs.

This study aims to improve the representation of one key temperature-dependent emissions source sector: residential fuel combustion for home heating. To improve the representation of these emissions, we developed a method for temporally allocating annual residential fuel combustion emissions that reflects local variability in temperature-dependent changes in heating demand.

1.2 Wintertime NO_X Chemistry and Meteorology Interactions

The physical and chemical loss pathways determining the atmospheric lifetime of NO_X are modulated by meteorological variables, such as temperature, relative humidity, and boundary layer height (e.g., Jaeglé et al., 2018; Kenagy et al., 2018; Lange et al., 2022; Ying, 2011). Physical loss pathways for NO_X within the boundary layer include wet and dry deposition and mixing with the free troposphere, which is controlled by atmospheric stability and advective transport. In the midlatitudes, the role of meteorology in NO_X chemistry becomes more pronounced in winter when shorter days and lower solar radiation reduce photochemical reactivity, and lower concentrations of biogenic volatile organic compounds (VOCs) reduce VOC reactivity.

Chemical loss pathways involve the transformation of NO_X to other chemical species, such as nitric acid (HNO_3), dinitrogen pentoxide (N_2O_5), or nitryl chloride ($ClNO_2$). N_2O_5 and $ClNO_2$ form at night and can act as reservoir species of NO_X, as NO_X can be rereleased in the daytime with the thermal dissociation of N_2O_5 and photolysis of $ClNO_2$ if they have not been removed by other processes (Kenagy et al., 2018). HNO_3 (and N_2O_5 through conversion to HNO_3) is a precursor for secondary particulate nitrate (Jaeglé et al., 2018; Mezuman et al., 2016; Ying, 2011), which is a substantial component of wintertime $PM_{2.5}$ species (Hand et al., 2012). Colder temperatures and higher humidity impact this loss pathway by increasing the production of $ClNO_2$ and favoring the partitioning of HNO_3 to particulate nitrate (Jaeglé et al., 2018; Kenagy et al., 2018).

A shallow boundary layer, either due to nocturnal stagnation or wintertime inversions, can increase the role of N_2O_5 chemistry. A study of a wintertime pollution episode in California's central valley showed that wintertime inversions limiting boundary layer growth lead to high concentrations of NO_X and a rapid increase in particulate nitrate (Ying, 2011). Similarly, persistent cold air pool events in Salt Lake City, Utah have been associated with high particulate nitrate concentrations due to atmospheric stagnation (Sun et al., 2021). Furthermore, low VOC reactivity in the winter suggests that NO_X lifetimes increase with increasing concentrations (Laughner & Cohen, 2019; Valin et al., 2013). Because of the impacts of meteorology and time of day on the fate of NOx in the atmosphere, accurate representations of when NO is emitted by temperature-dependent emissions sources is essential for capturing the impacts on ambient NO_X, $PM_{2.5}$, and ozone concentrations.

1.3 Residential Fuel Combustion Emissions

Residential fuel combustion for home heating is one important temperature-dependent emissions source sector, as energy demand for space heating is directly dependent on outdoor temperatures (Quayle & Diaz, 1980; Ranson et al., 2014). In the United States, most residences are heated by burning fuels such as natural gas, heating oil, or wood (U.S. Energy Information Association (EIA), 2023), releasing combustion emissions into the atmosphere. Studies on the air quality impacts of residential heating have focused on the role of wood and biomass burning, which contributes roughly a third of organic aerosols observed in some regions of North America in winter (Jeong et al., 2008; Schroder et al., 2018). Residential heating emissions contribute to increased mortality in the U.S., particularly due to the contribution to $PM_{2.5}$ from wood burning (Arunachalam et al., 2016; Dedoussi et al., 2020).

In the 2020 Residential Energy Consumption Survey from the U.S. EIA, wood was reported to be the primary heating fuel source in less than 2% of homes in the U.S., with most homes relying on natural gas boilers (~51%), and ~8% of homes using fuel oil, kerosene, or propane (U.S. EIA, 2023). For non-wood residential fuel combustion (RFC), NO_X are the major pollutant of concern. In the 2017 National Emissions Inventory (NEI) from the U.S. EPA, RFC contributed 2.6% of total annual anthropogenic NOx emissions across the U.S., and as much as 29.8% in some counties (Figure 1.1; U.S. EPA, 2021a). Electrification of building heating would decrease or remove home heating emissions, so quantifying the spatial and temporal contribution of RFC emissions to ambient wintertime air quality is important to understand the impact of such efforts.

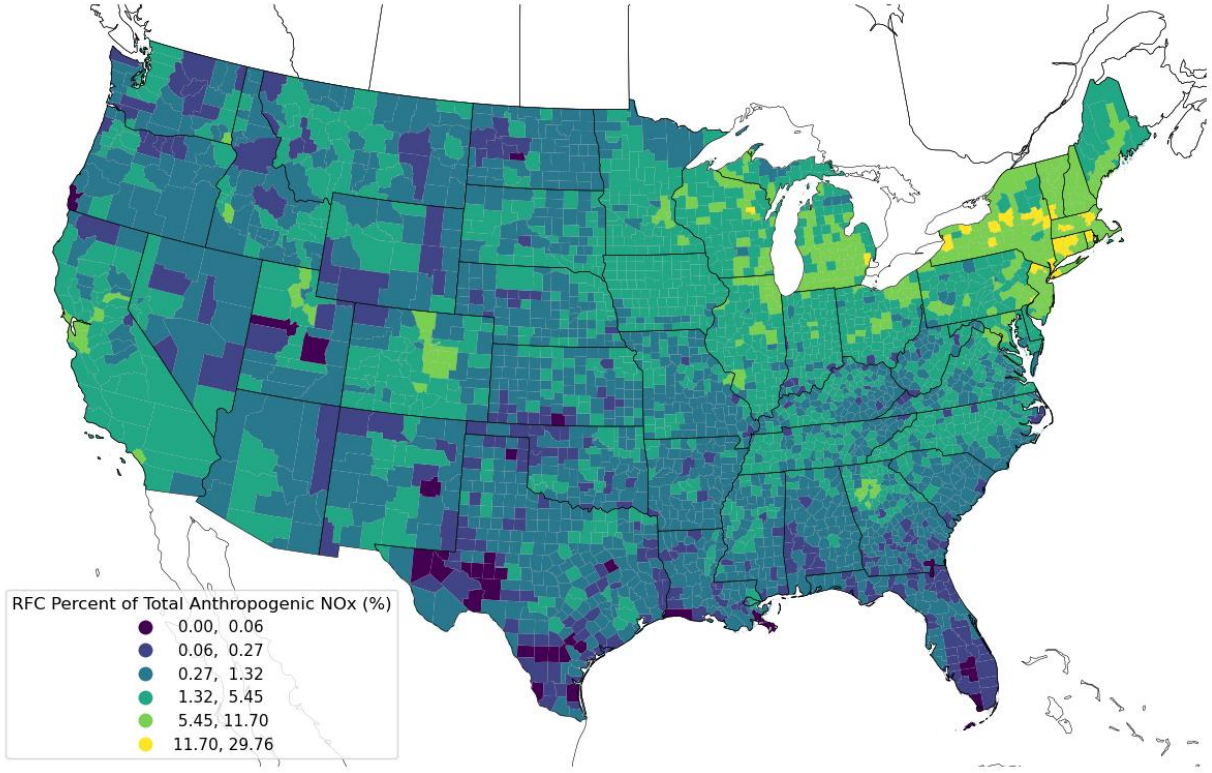

Figure 1.1. The percentage of annual total anthropogenic NOx from RFC per county in the 2017 NEI. The upper bin boundary of each bin corresponds to the 10th, 25th, 50th, 75th, 90th percentiles of the data, respectively, with the final bin extending to the maximum percentage.

1.3.1 Estimating Residential Fuel Combustion Emissions

Residential fuel combustion emissions for all fuel types (e.g., wood, natural gas, etc.) are part of the nonpoint emissions sector, also called area source emissions, which include any stationary emissions sources without a specific release point. The general approach for estimating annual residential fuel combustion emissions for a given area is to estimate the annual consumption of each fuel type (i.e., activity data) and multiply the consumption by emission factors specific to each fuel and pollutant. To prepare an emissions inventory for use in a CTM such as CMAQ, annual emissions are allocated in space to a user-defined horizontal grid, and in time as an hourly emission rate using an emissions processing software.

1.3.1.1 Residential Wood Combustion (RWC)

For the U.S. EPA's NEI and CMAQ modeling platforms, residential wood combustion (RWC) emissions are estimated based on outdoor temperatures. Annual RWC county-level wood consumption is calculated using variables parameterized from a regression analysis that used a temperature-based metric, heating degree days (HDDs), as a predictor (U.S. EPA, 2023b). For the 2017 and 2020 NEIs, wood consumption was estimated based on the number of homes in a county, the fraction of homes using each appliance type, the burn rate for each appliance, and a county-specific wood density factor (U.S. EPA, 2021a, 2023b). These county-level activity estimates were then multiplied by empirically-derived emissions factors specific to appliance and wood types.

For modeling applications, annual RWC emissions are allocated to a user defined grid using spatial surrogates based on the number of housing units using wood as a primary fuel source (Adelman, 2016). Emissions are then distributed to each day based on daily minimum temperature, using a county-specific annual-to-day profile that was developed from a regression analysis designed to predict observed $PM_{2.5}$ concentrations using meteorological variables (Adelman et al.,

2010). Days with minimum temperatures above a 50°F threshold are assigned zero emissions (U.S. EPA, 2022, 2025). This daily allocation method was first implemented in the U.S. EPA's 2007 modeling platform, published in 2012, which replaced the prior approach of uniformly allocating emissions by season (U.S. EPA, 2012).

1.3.1.2 Non-Wood Residential Fuel Combustion (RFC)

Emissions from RFC—which includes natural gas, distillate heating oil, liquid petroleum gas (LPG), kerosene, and coal—are not estimated or allocated in time based on temperature for either the annual county-level NEI or U.S. EPA's modeling platforms.

The methodology used to estimate annual county-level emissions for the 2014, 2017, and 2020 NEIs (U.S. EPA, 2021a, 2021c, 2023a) calculates activity data with state-level energy consumption data from the U.S. EIA State Energy Data System (SEDS). The state-level consumption data is distributed to each county by the proportion of houses that reported using each fuel type in the U.S. Census Bureau's 5-year estimate Census Detailed Housing Information. The county-level fuel consumption is multiplied by empirically-derived emissions factors specific to each fuel type for all chemical species that are relevant for estimating hazardous and criteria air pollutants (U.S. EPA, 1996). Similar methods have been used to develop annual RFC emissions estimates in other countries, such as Canada (Environment and Climate Change Canada, 2025), Italy (Aste et al., 2009, 2013), and Belgium (Cornette & Blondeau, 2024).

For the U.S. EPA's modeling platforms, annual RFC emissions are allocated to a 12 km horizontal domain using spatial surrogates for each fuel type (Adelman, 2016). Annual emissions are then allocated in time to create hourly estimates for emission rates using profiles for annual-to-month, month-to-day-of-week, and diurnal profiles. For the annual-to-month profiles, each month is allocated a fixed fraction of emissions either by season (for model years 2019 and earlier

platforms, e.g., Foley et al., 2023) or month (for model years 2020-2022 platforms, e.g., U.S. EPA, 2025). The month-to-day-of-week profiles are flat, so each day in a season or month is allocated equal emissions. These temporal allocations of RFC emissions do not include any temperature or meteorological dependence to determine daily emissions, despite previous research identifying direct correlations between heating energy use and outdoor temperatures (Quayle & Diaz, 1980; Ranson et al., 2014). The daily co-variability between RFC emissions and meteorology is not represented, so current atmospheric modeling is not able to parse the impact of RFC emissions on wintertime pollution episodes from meteorology and chemistry.

1.4 Research Objectives

For this study, we develop and evaluate an hourly emissions inventory for RFC that reflects daily variability due to temperature-based changes in heating demand. To achieve this goal, we created an annual-to-day temporal allocation method for annual RFC emissions based on a temperature-based proxy for heating demand, heating degree days (HDD). Furthermore, we use a diurnal profile for hourly allocation that more closely represents heating demand than the profile currently used for RFC in the U.S. EPA's emissions modeling.

In this thesis, we investigate how using temperature-based daily scaling (DS) approach impacts the allocation of RFC emissions compared to a seasonal-scaling (SS) approach across climate regions in the U.S. We assess how changing the diurnal allocation of emissions impacts the nocturnal and daytime emission distributions. Chapter 2 of this thesis details the data and methodology used in this study. Chapter 3 presents the results and evaluation of the DS RFC emissions inventory, with a primary focus on NOx emissions. Chapter 4 discusses key findings and conclusions in context of previous studies are discussed, and poses future research directions.

Chapter 2 Data and Methods

2.1 Overview

We created an hourly, gridded temperature-dependent emissions inventory (EI) for non-wood residential fuel combustion (RFC) for the contiguous United States (CONUS) (i.e. the lower 48 states and Washington D.C.). The emissions inventory was developed for the 2019 emissions year to integrate with the U.S. Environmental Protection Agency's (U.S. EPA) Air QUAlity TimE Series Project (EQUATES) 2019 modeling platform for the Community Multiscale Air Quality (CMAQ) model (U.S. EPA, 2021b; U.S. EPA Office of Research and Development, 2024). Annual county-level RFC emissions from the U.S. EPA's 2017 National Emissions Inventory (NEI) were allocated in space to a 12 km by 12 km grid following U.S. EPA methods (Foley et al., 2023), and in time using a new temporal scaling approach that uses daily temperature to allocate emissions based on heating degree days (HDDs). HDDs are a measure of heating demand based on average daily temperature, which assumes that no heating is required when outdoor temperatures are above a certain reference temperature (typically 18.3°C, or 65°F). HDDs are widely used to estimate energy demand required for space heating in the peer-reviewed literature (e.g., Gesangyangji et al., 2024; Kennard et al., 2022; Petri & Caldeira, 2015; Thom, 1954) and by the U.S. Department of Energy (U.S. EIA, 2024). Using HDDs allows us to assign heating emissions proportionally with temperature to days on which we expect home heating to be required, and not to days with warmer outdoor temperatures.

A flowchart describing the processing steps to develop the temperature-scaled emissions inventory for RFC is shown in Figure 2.1. Annual, county-level RFC emissions from the 2017 NEI were processed using the U.S. EPA's emissions processing software, the Sparse Matrix Operator Kernal Emissions (SMOKE) program (Baek & Seppanen, 2021) to prepare unscaled daily

emissions files. The annual-to-day HDD-based scaling factors were applied to the unscaled emissions files resulting in daily temperature-dependent RFC emissions files. The data sources, scaling factor development, SMOKE emissions processing steps, and the post-processing steps, are described in the sections to follow.

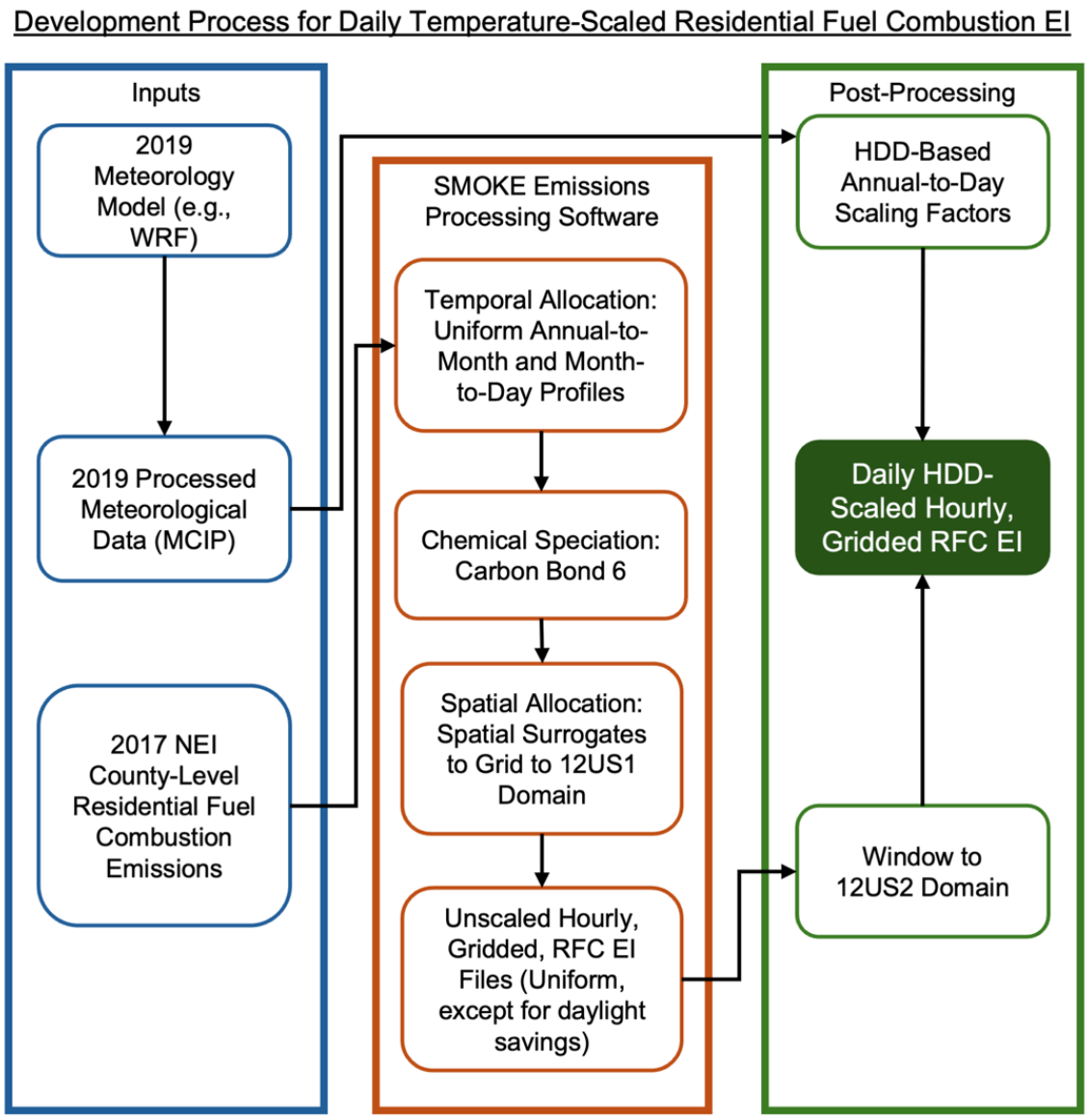

Figure 2.1. Flowchart of the development process for temperature-scaled RFC EI.

2.2 Data Sources

The EQUATES 2019 modeling platform includes a collection of inputs published by the U.S. EPA for the CMAQ photochemical model to simulate hourly atmospheric chemistry across CONUS for 2019 (Foley et al., 2023; U.S. EPA, 2021b). The EQUATES 2019 inputs include hourly, gridded meteorology, emissions inventories, and initial and boundary conditions on a 12 km horizontal grid covering CONUS with 35 vertical layers, called the "12US1" domain (Figure 2.2). The EQUATES 2019 CMAQ-ready inputs are windowed to a smaller domain that includes less area of Canada and Mexico, called the "12US2" domain (Figure 2.2). In addition to the CMAQ-ready inputs, the U.S. EPA provides the ancillary files and programs required to create the emissions inventories using U.S. EPA's emissions processing software, the Sparse Matrix Operator Kernal Emissions (SMOKE) program (Baek & Seppanen, 2021). Many emissions sectors including RFC in the 2019 EQUATES modeling platform are based on annual county-level emissions from the 2017 NEI (Foley et al., 2023), which are allocated in space and time using SMOKE. The U.S. EPA also published monthly and annual emissions summaries from the EQUATES project for select chemical species, which were used in this work to compare with the temperature-based RFC emissions inventory.

The 2019 meteorological inputs from the EQUATES project were derived from simulations conducted in Weather Research and Forecasting (WRF) model version 4.1.1 for 2019, then processed using the Meteorology - Chemistry Interface Processor (MCIP) version 5.0. WRF was run with a hybrid, terrain-following vertical coordinate system (Beck et al. 2020). Other WRF inputs and settings selected by the U.S. EPA included: 500 m land cover data from the Moderate Resolution Imaging Spectroradiometer (MODIS); sea surface temperature from the North American Mesoscale Forecast System (NAM); data assimilation analysis fields from NAM, with

ECMWF Reanalysis (ERA) data substituted when NAM data were missing; Morrison microphysics; Rapid Radiative Transfer Model for GCMs (RRTMG) longwave and shortwave radiation; Pleim Surface Layer and Pleim-Xiu Land-Surface model; ACM2 boundary layer mixing; the Kain-Fritsch + Ma and Tan (2009) trigger 2 (KF2) sub-grid convection scheme; three-dimensional grid nudging and indirect soil nudging; and no lightning assimilation (U.S. EPA, 2021b).

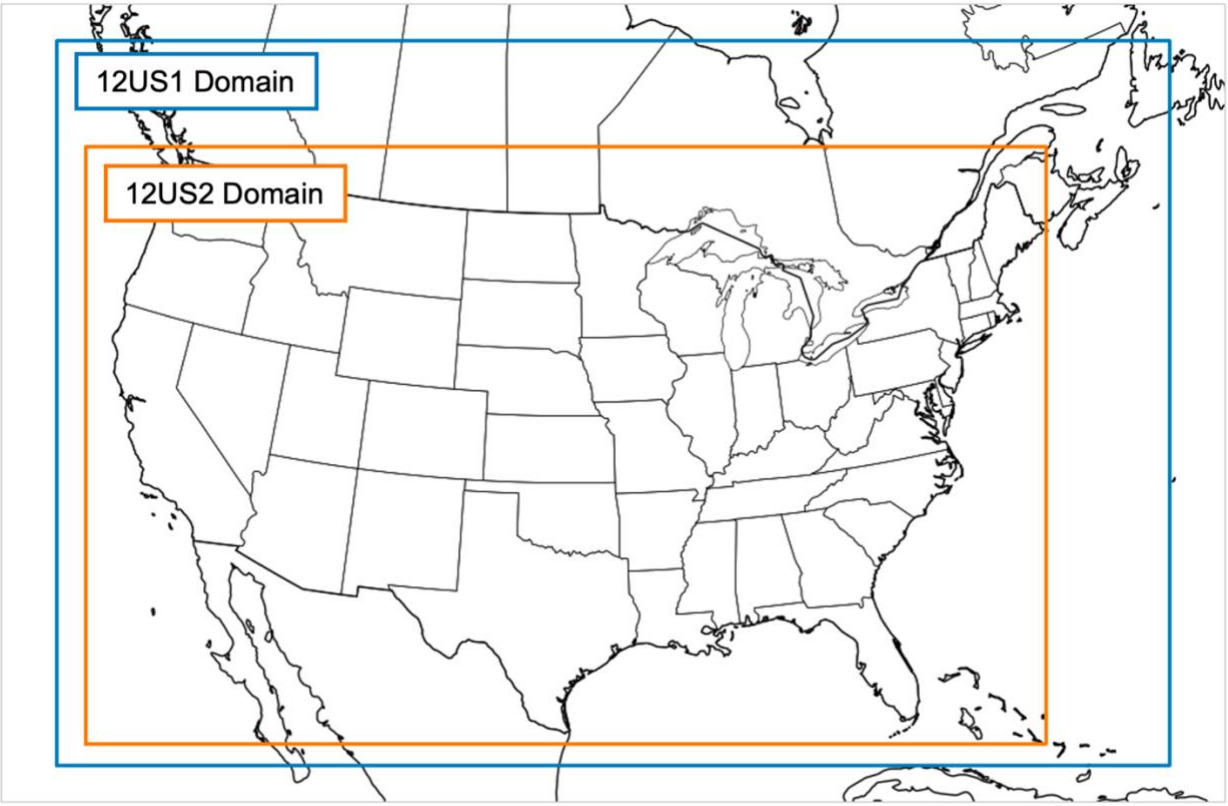

Figure 2.2. Horizontal extent of the 12US1 and 12US2 modeling domains.

2.3 Temperature-Dependent Annual-to-Day Temporal Scaling Factors

We developed annual-to-day temporal scaling factors for each grid cell of the 12US2 modeling domain to allocate a proportion of annual total RFC emissions to each day based on HDDs, using a reference temperature of 18.3°C (65°F) per the U.S. EIA. RFC emissions only

include emissions from U.S. based sources, which is covered by the 12US2 domain. The annual-to-day temporal scaling factors were developed to be multiplied by daily gridded emissions files for RFC emissions as a post-processing step following the SMOKE emissions processing described below. Two-meter air temperature data from the EQUATES 2019 MCIP meteorological files were used to calculate daily HDD at each grid cell (i, j) of the 12US2 domain ($HDD_{d,i,j}$) following Equation 1, where $\bar{T}_{d,i,j}$ is the average daily temperature at grid cell (i, j).

$$HDD_{d,i,j} = \begin{cases} 18.3 - \bar{T}_{d,i,j}, & if\ \bar{T}_{d,i,j} < 18.3°C \\ 0, & otherwise \end{cases} \quad (1)$$

The MCIP files have the Coordinated Universal Time (UTC) time zone, therefore daily average temperatures at each grid cell were based on days defined by the UTC time zone. Daily scaling factors at each grid cell ($SF_{d,i,j}$) were calculated as the daily HDDs divided by the annual total HDDs (Equation 2)

$$SF_{d,i,j} = \frac{HDD_{d,i,j}}{\sum_{d=1}^{365} HDD_{d,i,j}} \quad (2)$$

Daily emission files for nonpoint sources from SMOKE version 4.8.1 (the version used for this research, and by the U.S. EPA for the EQUATES 2019 modeling platform; Baek & Seppanen, 2021) are four dimensional arrays of hourly, gridded emissions in NetCDF file format with 25 hours. The 25th hour of the daily files is the first hour of the following day. To multiply the scaling factors by the daily emissions files, the scaling factors were saved in daily NetCDF files with dimensions matching the emissions files, with the 25th time step equal to the scaling factors for the following day. Scaling factors were developed using Python version 3.11.4.

2.4 Temperature-Dependent RFC Emissions Inventory

To apply the scaling factors to RFC emissions, we needed emissions files that included only RFC emissions. In the U.S. EPA's emissions modeling platforms, RFC emissions are included

in the nonpoint emissions sector. The nonpoint emissions sector, also called area source emissions, includes any stationary emissions sources that do not have a specific release point. While some nonpoint sources are prepared separately, such as area fugitive dust or residential wood combustion, most nonpoint source categories are prepared as one combined category. RFC emissions are grouped with other nonpoint emissions categories in all U.S. EPA's emissions modeling platforms, which were the foundation of the 2019 EQUATES modeling.

To separate the residential fuel combustion emissions from other nonpoint emissions source categories, I used the U.S. EPA's emissions processing software, SMOKE version 4.8 (Baek & Seppanen, 2021). SMOKE is a Fortran-based program used to create photochemical-model ready emissions inventories from emissions inputs, typically from the NEI for nonpoint sources, though other inputs can be used. The annual emissions inventories are temporally allocated to hourly values, chemically speciated such that all model-ready emissions are mapped to the appropriate chemical species for the user-specified chemical mechanism, then spatially allocated to a user defined grid by spatial surrogates.

In the EQUATES 2019 SMOKE ancillary files, temporal allocation of annual RFC emissions occurs by applying one annual-to-month, one month-to-day-of-week, and one day-to-hour profile to the entire domain. Representative days for each day of the week, weekends, and holidays are output, not daily files, though there is no distinction between these day types for RFC. Representative days are used for other source categories included in nonpoint emissions, but not for RFC. Therefore, in the EQUATES platform, RFC emissions have seasonal and hourly variability, but not weekly. Chemical speciation occurs by mapping the chemical species in the NEI to the Carbon Bond version 6 with Aerosol Extension version 7 (CB6AE7) chemical mechanism. The CB6AE7 maps to 56 chemical species including nitrogen oxide (NO), nitrogen

dioxide (NO_2), sulfur dioxide (SO_2), and many volatile organic compound (VOC) species. Finally, emissions are gridded from the county-level to the 12 km 12US1 domain using spatial surrogates.

2.4.1 SMOKE Emission Processing Runs

Two SMOKE runs were conducted to prepare RFC emissions for this analysis: one using the EQUATES 2019 default seasonal scaling (SS) approach for temporal allocation, and one to be temporally allocated using our temperature-dependent daily scaling (DS) approach. For the SS run, RFC emissions were isolated from other nonpoint emissions sources without modification to the temporal allocation or other settings in SMOKE. These files are equivalent to the RFC portion of the nonpoint emissions in the EQUATES 2019 platform, which have not previously been isolated for an RFC-specific assessment. The second SMOKE run was conducted to be scaled by the HDD-based DS factors in post-processing, with modifications to the temporal allocation profiles from the EQUATES 2019 defaults (see Figure 2.1).

For both SMOKE runs, the 2017 NEI nonpoint emissions input file from the EQUATES 2019 SMOKE ancillary files[1] was modified to only include emissions from the five source classification codes (SCC) associated with RFC emissions, which are tied to fuel type—natural gas (2104006000), distillate oil (2104004000), liquified petroleum gas (2104007000), kerosene (2104011000), and coal (2104002000). While the coal source category was included for consistency with previous NEI versions, there are zero RFC emissions from coal in the 2017 NEI.

For the SS run, no changes were made to the temporal allocation profiles, chemical speciation, or spatial allocation from the EQUATES 2019 settings. The EQUATES 2019 default

[1] Nonpoint emissions input file from EQUATES 2019 ancillary SMOKE files: '2017NEIpost_NONPOINT_20210129_08nov2021_v6.csv'

annual-to-month, month-to-day-of-week, and day-to-hour temporal profiles are shown in Figure 2.3. SMOKE applies all temporal profiles in local time, then shifts to UTC accounting for time zone and daylight-saving time. The annual-to-month profile assigns a proportion of emissions to each season[2] for each RFC SCC except for kerosene, which uses a flat annual-to-month profile (Figure 2.3a).[3] The month-to-day-of-week profile is flat for all RFC SCCs,[4] such that all days within a season have identical emissions (Figure 2.3b). The day-to-hour diurnal profile allocates the emissions in a bell-curve that peaks in midday local time (Figure 2.3c).[5] This diurnal profile (profile 26) is typically used for source categories that do not have source-specific diurnal data (Beidler, 2025). However, because heating demand typically increases during colder nighttime hours, this profile is not likely to be representative of diurnal RFC emission rates.

Though SMOKE outputs 101 representative day files, the SS emissions files fall into one of five categories with identical emissions within each: winter months (December, January, February); spring before daylight savings starts (on March 9, 2019); spring months after daylight savings starts (March 9 to May 31); fall months before daylight savings ends (September to November 2); and fall after daylight savings ends (November 2 to November 30).

For the second RFC SMOKE run intended for post-processing to apply the HDD-scaling factors (DS), the only changes made to the first run were to the temporal profiles used in temporal allocation of RFC emissions (Figure 2.3). A flat annual-to-month profile was applied for all RFC

---

[2] In the EQUATES 2019 platform, RFC SCCs except kerosene use monthly profile number 485 in SMOKE ancillary file: "amptpro_general_2011platform_tpro_monthly_6nov2014_12oct2021_v9"

[3] In the EQUATES 2019 platform, kerosene uses the flat monthly profile number 262 in SMOKE ancillary file: "amptpro_general_2011platform_tpro_monthly_6nov2014_12oct2021_v9"

[4] All RFC SCCs use the flat weekly number 7 defined in SMOKE ancillary file: "amptpro_general_2011platform_tpro_weekly_6nov2014_09sep2016_v2"

[5] In the EQUATES 2019 platform, all RFC SCCs use diurnal profile 26 defined in SMOKE ancillary file: "amptpro_general_2011platform_tpro_hourly_6nov2014_07oct2021_v9"

SCCs, and the flat month-to-day-of-week profile. For the diurnal profile, the default diurnal profile 26 was replaced with the profile developed for outdoor hydronic heaters (SCC=2104008610), which is included in the residential wood combustion source category.[6] The updated diurnal profile allocates most emissions to evening and morning hours local time, and fewer emissions to midday (Figure 2.3). In the resulting SMOKE output, the unscaled emissions are identical across all 101 representative days, except for offsets due to standard versus daylight saving time.

[6] Outdoor hydronic heater diurnal profile 1500 define in SMOKE ancillary file: "amptpro_general_2011platform_tpro_hourly_6nov2014_07oct2021_v9"

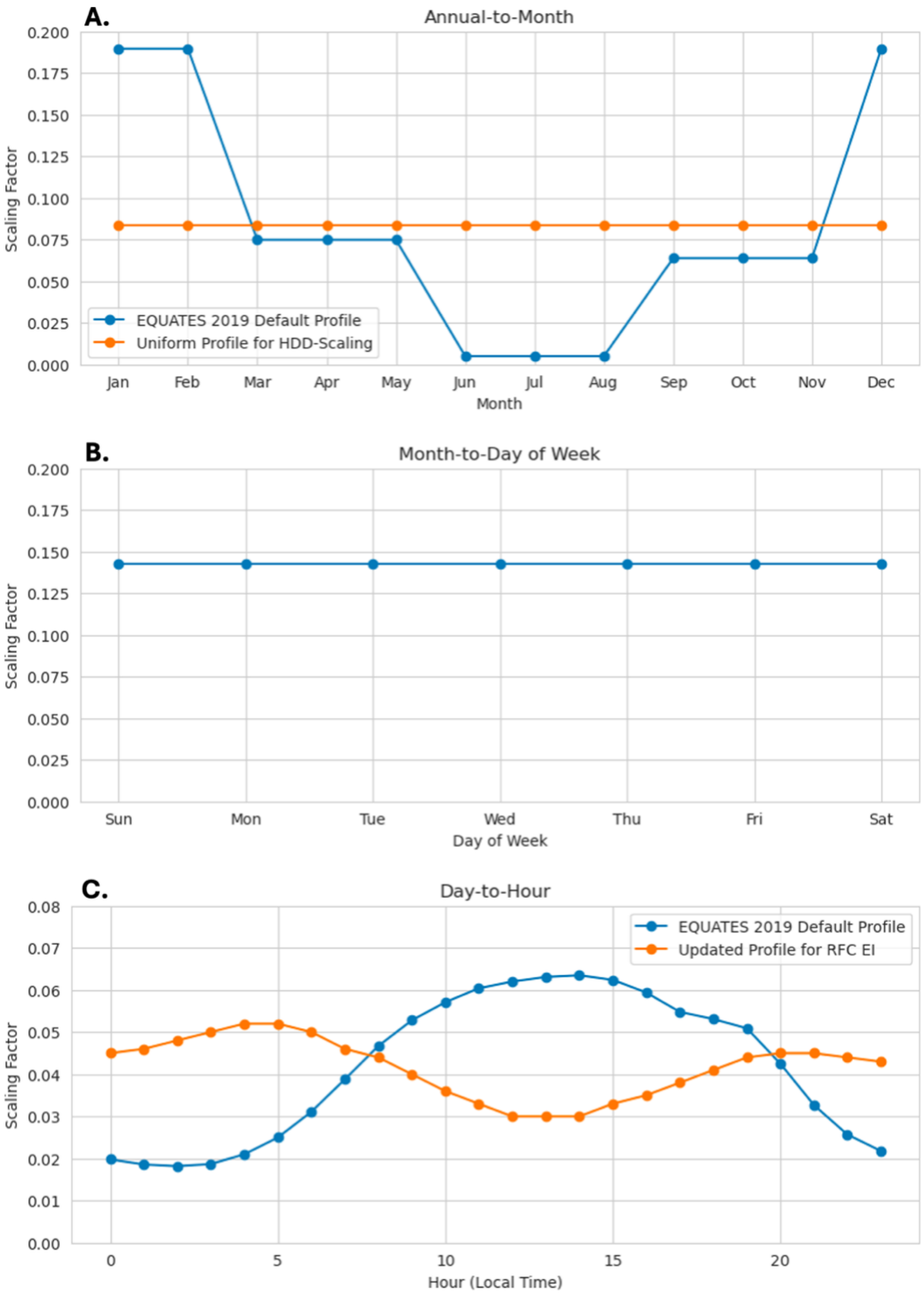

Figure 2.3. Temporal allocation profiles used in SMOKE. (A) Annual-to-month profile for RFC SCCs in EQUATES 2019 modeling platform, excluding kerosene, and the flat profile used for HDD-scaling, which is also the EQUATES default for kerosene; (B) flat month-to-day-of-week profile used in both the EQUATES platform and HDD-scaling; (C) day-to-hour profiles for the EQUATES platform and for the HDD-scaled emissions.

2.4.2 RFC Emissions Post-Processing

Following each SMOKE run, the emission output files were spatially windowed from the 12US1 domain to the 12US2 domain (Figure 2.2). Next, representative daily emissions files were mapped to each calendar date accounting for temporal allocation and daylight savings time shifts. For the SS run, five representative files were used to map onto the day of the year: one for winter months; one for spring before daylight savings starts (on March 9, 2019); one for spring months after daylight savings starts (March 9 to May 31); one for fall months before daylight savings ends (September to November 2); and one for fall after daylight savings ends (November 2 to November 30). For the DS run, one representative file was used for dates with standard time, and one representative file was used for dates with daylight saving time.

Each daily emissions file included 56 variables of chemical species with hourly emission rates in either moles per second (mol/s) or grams per second (g/s). To generate the DS RFC emissions files, the HDD-based scaling factors were applied to the flat daily emission files using the following operation (Equation 3):

$$E_{S,v,i,j} = E_{U,v,i,j} * 365 * SF_{i,j} \quad (3)$$

where $E_{S,v,i,j}$ is the scaled hourly emission rate (mol/s or g/s) for each variable *v* at grid cell (i, j), $E_{U,v,i,j}$ is the unscaled hourly emission rate, $SF_{i,j}$ is the array of daily HDD-based scaling factors (in units of years per day), and 365 is the number of days over which the emissions inventory was uniformly distributed in SMOKE (units of days per year). The resulting emission files represent daily, temperature-scaled emission for the RFC source sector, prepared such that they can be merged with the EQUATES 2019 modeling platform to be used for photochemical modeling applications.

2.5 Climate Regions for Evaluation of RFC Emissions

To evaluate the regional impacts of the temperature-scaling approach and associated changes to RFC emissions, we mapped the 12US2 grid cells to climate zones as defined by the 2021 International Energy Conservation Code (IECC). IECC climate zones for CONUS are split into seven thermal regimes (1-7), ranging from very hot (zone 1) to very cold (zone 7), and three moisture zones (A-C): humid (A), dry (B), and marine (C) (Antonopoulos et al., 2022; Figure 2.4). Thermal and moisture classifications are determined in the IECC for each county based on annual average HDDs, cooling degree days (CDD), and precipitation (International Code Council, 2025). We allocated a shapefile of IECC climate zones by county to the 12US2 domain, such that each grid cell of the modeling domain was assigned one climate zone (Figure 2.4). For this research, we focus on the RFC emissions in zones 2 through 7, as the very hot climate zone (zone 1) has little to no heating demand (Antonopoulos et al., 2022).

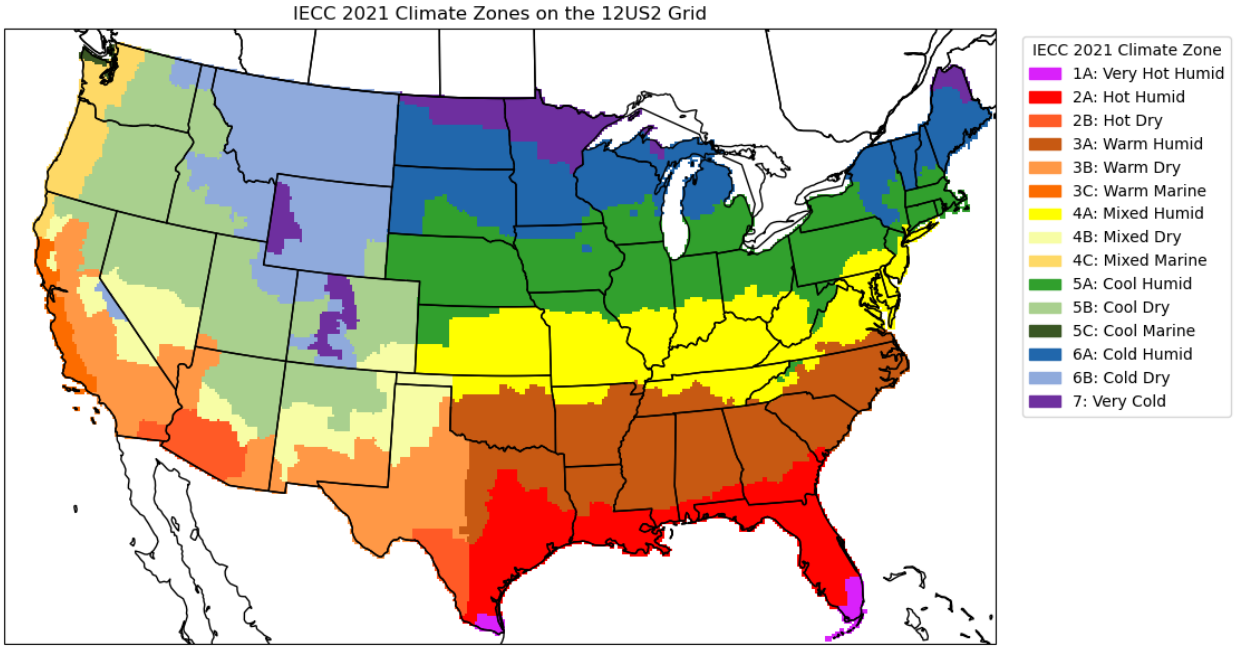

Figure 2.4. IECC Climate Zones gridded onto the 12US2 domain to classify each grid cell.

2.5.1 Regional Examples of Temperature-Based Scaling Factors

For illustrative purposes, we discuss examples of how daily mean temperatures were translated to daily scaling factors for two representative grid cells: one in a hot climate, Houston, Texas, and one a cold climate, Minneapolis, Minnesota (Figure 2.5b-d). These two locations were identified from the counties with the highest 2019 populations[7] within the IECC hot zone (zone 2) and the IECC cold zone (zone 6). Figure 2.5a shows the annual total HDDs derived from the EQUATES 2019 WRF/MCIP files for each grid cell overlapping CONUS of the 12US2 domain. Annual total HDDs range across CONUS from 7.2 in the far southeast of CONUS, to 7,930.3 in the mountainous regions in the west (Figure 3.1a). Figure 2.5b-d steps through daily mean temperatures (Figure 2.5b), the calculated HDDs (Figure 2.5c), and the final DS factors for each location, with the SS factors for comparison (Figure 2.5d).

Minneapolis, MN had 4,486 annual total HDDs (Figure 2.5a). Daily mean two-meter air temperatures in Minneapolis, MN ranged from -29.1°C to 28.9°C throughout the year (Figure 2.5b). In Minneapolis, days with mean temperature greater than or equal to 18.3°C only occurred between May through September. Since days with mean temperature greater than 18.3°C have 0 HDDs, HDDs in Minneapolis was equal to 0 for some days in May, June, and September, and all days in July and August (Figure 2.5c).

In Figure 2.5d, the comparison of the final scaling factors for the DS approach compared with the scaling factors used for the SS approach is shown (Figure 2.5d). In Minneapolis, there was a greater allocation of emissions to days in early spring months (March and April) and late

[7] Data for county population in 2019 were the Annual Resident Population Estimates from the U.S. Census Bureau, which were based on the 2010 Census (U.S. Census Bureau, 2020).

fall months (October and November) in the DS approach compared to the SS approach, when cold temperatures were nearly as prevalent as in the winter months (Figure 2.5d). This suggests that the SS approach overallocates emissions to winter months in Minneapolis. Conversely, May and September had lower scaling factors in the DS approach than in the SS approach. The day with the coldest mean daily temperature (-29.1°C in late January) had the highest scaling factor at ~0.01, meaning ~1% of annual total RFC emissions were allocated to that day for that grid cell.

Houston experienced 623.5 HDDs (Figure 2.5a), with daily mean temperatures ranging from 4.7°C to 31.9°C throughout the year (Figure 2.5b). Every month except for January had days where daily mean temperature was higher than the HDD reference temperature, 18.3°C. As a result, there were days in all months except January where HDD was 0, indicating no heating demand (Figure 2.5c). Comparing the DS approach scaling factors to the SS approach scaling factors, heating emissions in Houston were reallocated to fewer individual days, since most days of the year were warmer than 18.3°C and therefore not expected to require residential heating (Figure 2.5d).

Because the scaling factors represent the fraction of annual total emissions allocated to a given day, the sum of scaling factors over the year at a given location is equal to 1 (Figure 2.5d). The magnitude of the DS factors for Houston are often larger than the DS factors for Minneapolis because Houston experienced fewer days with heating demand than Minneapolis. Minneapolis had more days with heating demand than Houston, therefore emissions are allocated across more days and individual days may have a lower fraction of emissions, i.e. lower scaling factors. The magnitude of the scaling factors is not analogous to the magnitude of annual emissions, which is dependent on total fuel consumption and mix of heating fuel type (e.g. natural gas, propane, etc.).

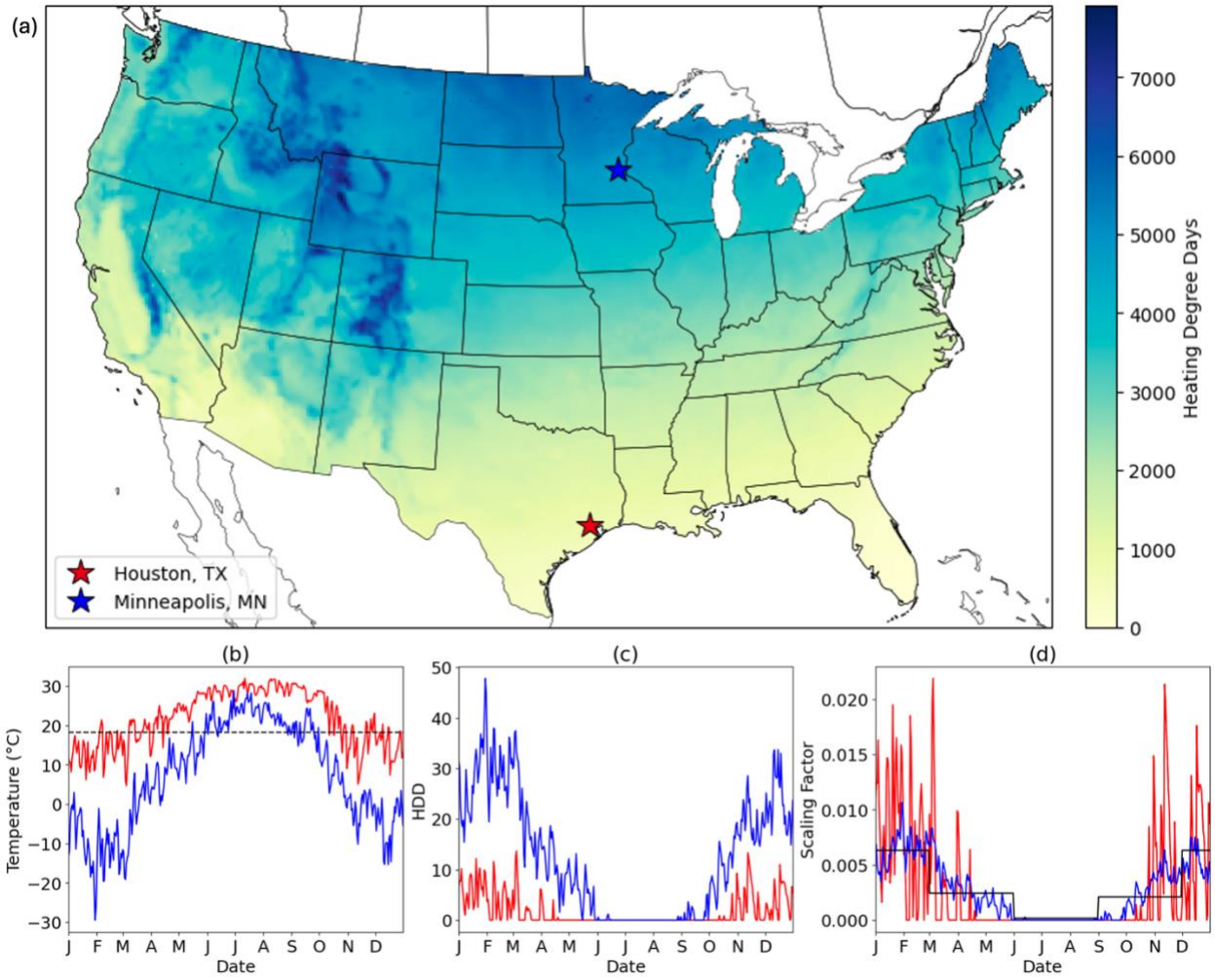

Figure 2.5. (a) A map of the annual total heating degree days calculated from the two-meter air temperature (°C) in from the EQUATES 2019 MCIP output, with a red star marking Houston, TX and a blue star marking Minneapolis, MN. (b-d) Daily timeseries for Houston (red lines) and Minneapolis (blue lines) for (b) the average daily 2-meter air temperature, with a dashed line indicating the 18.3°C threshold for HDDs; (c) the HDDs calculated from the daily mean temperature; and (d) the daily temperature-based scaling factors developed for annual-to-day scaling of RFC, with the seasonal-scaling (SS) default profile for comparison in black.

2.6 Assumptions and Limitations

Methods for estimating emissions for area sources such as RFC are inherently based on assumptions due to the lack of observational data. In our method, the application of temperature-based scaling assumes that daily heating demand directly correlates with ambient outdoor temperature, and that RFC emissions directly correlate with daily heating demand. This assumption is based on the use of the U.S. EIA's proxy for heating demand, HDDs. Other meteorological variables, such as humidity and wind speed, may also impact heating demand and building energy efficiency but were not directly considered in the HDD-based DS approach.

One key assumption with using HDDs for the temporal allocation is that no heating is required on days with average daily mean temperatures greater than or equal to 18.3°C. In the U.S., space heating is the primary end use for residential fuel consumption, with water heating as the second highest end use (U.S. EIA, 2023). While most RFC emissions would be attributable to space heating, the HDD assumption may not capture the energy consumption patterns of water heating, as water heating demand may be less directly correlated with outdoor ambient temperature compared to space heating. Our method allocates zero emissions to days without heating demand as defined by HDDs, which is a simplification that does not necessarily reflect fuel combustion for fuel end uses other than space heating.

Another assumption in our methodology is the application of a diurnal profile developed for wood-burning outdoor hydronic heaters (OHH) to represent the diurnal profile in RFC emissions from all fuel types (U.S. EPA, 2022). The OHH diurnal profile was chosen to replace the EQUATES 2019 default profile, which allocates most emissions of midafternoon (Figure 2.3c), because it was developed based on heating behavior and is relatively evenly distributed across the day. In the U.S. EPA's modeling platforms, emission estimates for other types of wood-burning

furnaces use a profile with more temporal variability and discrete changes in emissions (U.S. EPA, 2022). Ideally, distinct diurnal profiles derived from empirical data specific to residential fuel combustion would be applied for each fuel type (natural gas, kerosene, heating oil) to more accurately reflect diurnal heating patterns.

Chapter 3 Results

In this chapter, we assess the HDD-based daily-scaling (DS) approach and the resulting temperature-dependent RFC emissions inventory compared to the seasonal-scaling (SS) approach. A comprehensive evaluation of the DS RFC emissions inventory would require simulations using a photochemical grid model, and comparison against ground-based and remotely sensed observations, which will represent the first phase on my Ph.D. research.

The first section of this chapter focuses on the effects of the DS approach on RFC NO_X emissions. The impacts of incorporating heating demand on scaling factors across climate regions is presented, as well as the translation of the scaling factors to daily NO_X emissions for two representative grid cells. Changes to the diurnal allocation of RFC emissions are then discussed with respect to their implications for nighttime and daytime emissions, and the contribution of RFC NO_X emissions to total anthropogenic NO_X emissions in time. Following the discussion of NO_X emissions, results are presented showing how the DS approach impacts the relative contribution of RFC emissions to total anthropogenic emissions for sulfur dioxide (SO_2), primary fine particulate matter ($PM_{2.5}$), carbon monoxide (CO), volatile organic compounds (VOCs). This chapter concludes with a summary of key findings.

3.1 Impact of the DS Approach on RFC NO_X Emissions

The temperature-based DS approach temporally redistributes annual RFC NO_X emissions relative to the SS approach, resulting in substantial percent changes in monthly total emissions (Figure 3.1). The monthly differences are a direct result of the temporal allocation approaches, as total annual emissions are constant between the DS and SS approaches. Incorporating heating demand to distribute emissions in time in the DS approach led to increases in the emissions allocated to March and November across nearly the entire domain compared to the SS approach

(Figure 3.1c-d). Conversely, the winter months (January, February, and December), exhibited a mixed pattern of increases and decreases in allocated emissions between DS and SS across CONUS. In January, DS decreased emissions in the north and northwest, and increased emissions in the south and southeast relative to SS (Figure 3.1a). In February, DS increased emissions compared to SS in some central states and in the southwest, but decreased them elsewhere, with up to a 100% decrease in the southeast (Figure 3.1b). In December, DS decreased emissions allocated to much of the country relative to SS, with increases in emissions to southern states (Figure 3.1e).

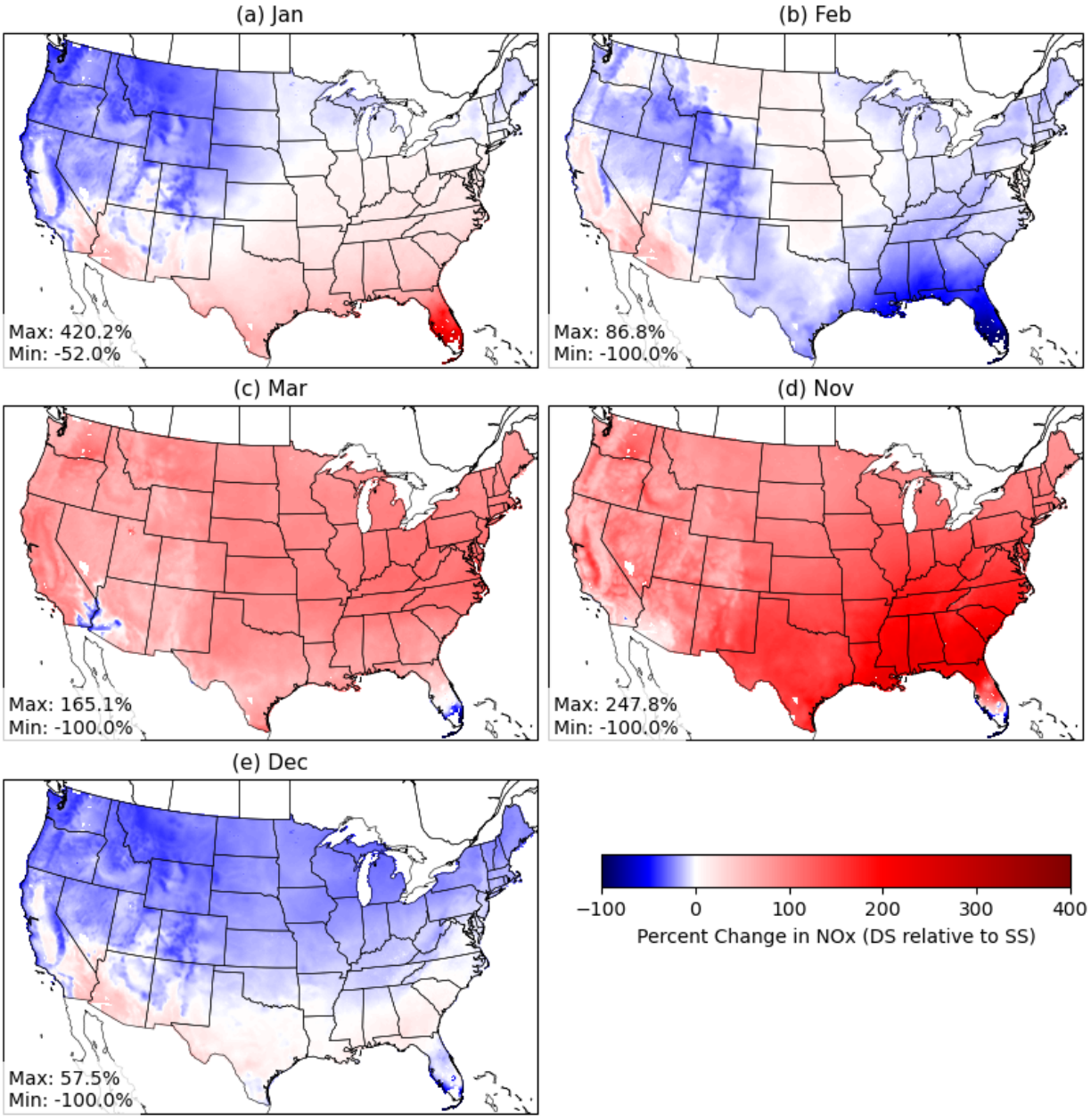

Figure 3.1. Percent change in RFC NO_X emissions between the DS approach and SS approach for (a) January, (b) February, (c) March, (d), November, and (e) December, with maximum and minimum values listed.

The spatial patterns in emissions changes between the SS and DS approaches shown in Figure 3.1 can be explained by the differences in the HDD-based daily scaling factors by climate region. Figure 3.2 shows the median daily scaling factors over time by International Energy Conservation Code (IECC) climate zone (see Figure 2.4 in Chapter 2: Methods and Data), with

shading representing the interquartile range (IQR) of the data. All plots in Figure 3.2 show the SS profile for reference, which is identical across the domain. Across all climate zones, DS varied from day-to-day with heating demand (Figure 3.2). Winter months (January, February, December) for all zones had some days where DS had a higher median fraction of emissions allocated than SS, and some days with a lower median fraction of emissions allocated. In the cool to very cold climates (zones 5-7; Figure 3.2d-f), where daily winter temperatures are predominantly below 18.3°C, days with high scaling factors in the winter reflected periods with particularly high heating demand. This could be the influence of extreme cold events that would not be captured by the SS approach.

In March and November, the DS approach allocates a greater fraction of emissions than SS approach for all climate zones. In temperate climates, November through March are often considered part of the heating season (Belova et al., 2018; Gesangyangji et al., 2024; Hartley & Robinson, 2000; Shen & Liu, 2016). Gesangyangji et al. (2024) defined heating seasons as months when heating demand (defined by HDDs) exceeded cooling demand (defined by cooling degree days). Based on historical data from 1986-2010, March and November were part of the heating season for all U.S. states except for Florida (Gesangyangji et al., 2024). The universal increase in median scaling factor in March and November when accounting for heating demand in the DS approach suggests that the SS approach may underestimates RFC emissions in the beginning and end of the heating season.

All climate zones calculated with DS had at least one day with median scaling factor equal to 0, indicating no heating demand. The median scaling factors in the hot climate zone (zone 2), had the greatest range of all climate zones (Figure 3.2a). In zone 2, days with median temperatures

below 18.3°C are uncommon, therefore colder days were assigned a high fraction of annual RFC emissions (Figure 3.2a).

For the warm to cool climates (zones 3-4), there were nearly no emissions allocated to summer months for the humid (A) and dry (B) moisture regimes. However, marine zones (3C, 4C, 5C)—which contain counties along the Pacific Coast in Washington, Oregon, and California—have the highest fraction of emissions allocated to summer months of all climate zones (Figure 3.4b-d). Because higher fractions of RFC emissions are allocated to summer months in marine zones, winter months—particularly January and December—are assigned a lower fraction of emissions for DS compared to SS. While zones 3, 4 and 5 have differing magnitudes of heating demand (by definition), the distribution of the heating requirements are similar throughout the year between their dry and humid counterparts.

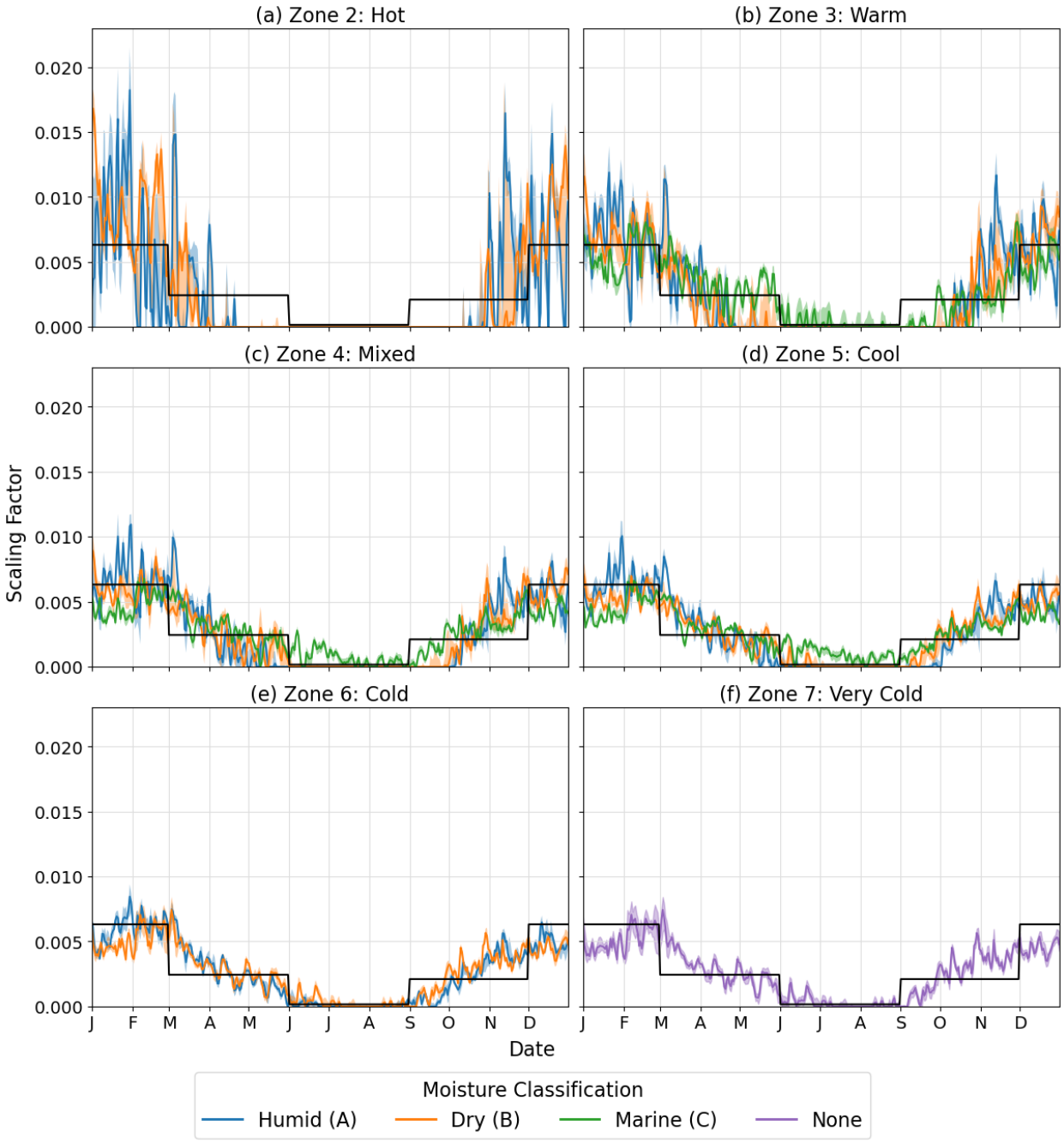

Figure 3.2. Median DS factor by IECC climate zone (subplots by thermal zones 2-7, with individual lines separating moisture classifications), with shading showing the IQR, and black reference lines showing the SS factors. IECC climate zone 7 does not have moisture classifications.

From Figure 3.2, the DS approach generally allocates more emissions to March and November and less to May and September compared to the SS approach. The spatial patterns of which months have the greatest increases and decreases in annual RFC fraction from the DS approach to the SS approach are shown in Figure 3.3. Across the 12US2 domain, nearly all grid cells have the greatest increase in RFC fraction allocated to either March or November (Figure 3.3a). Some locations in Florida, Texas, New Mexico and southern California have the greatest increase in allocation in January or December, as fewer days with heating demand in hot climates results in a greater allocation to individual cold days in winter months (Figure 3.3a). Along some mountain ranges and in the cool marine climate zone (5C), the greatest increase in RFC fraction occurred in June (Figure 3.3a). Across most grid cells, the greatest decrease in RFC fraction occurred in May or September (Figure 3.3b). The other months with the largest decreases were January, February and December, particularly in northern regions where a higher proportion of emissions were reallocated to March and November and away from core winter months (Figure 3.3b). For example, mountainous regions in the Northwest predominantly had the largest decreases in the winter months because ambient temperatures are cold enough to have heating demand year-round. Overall, the DS approach reflects regional and seasonal heating demand by redistributing RFC emissions away from May through September, and toward March and November when heating demand can be as pronounced as during winter months.

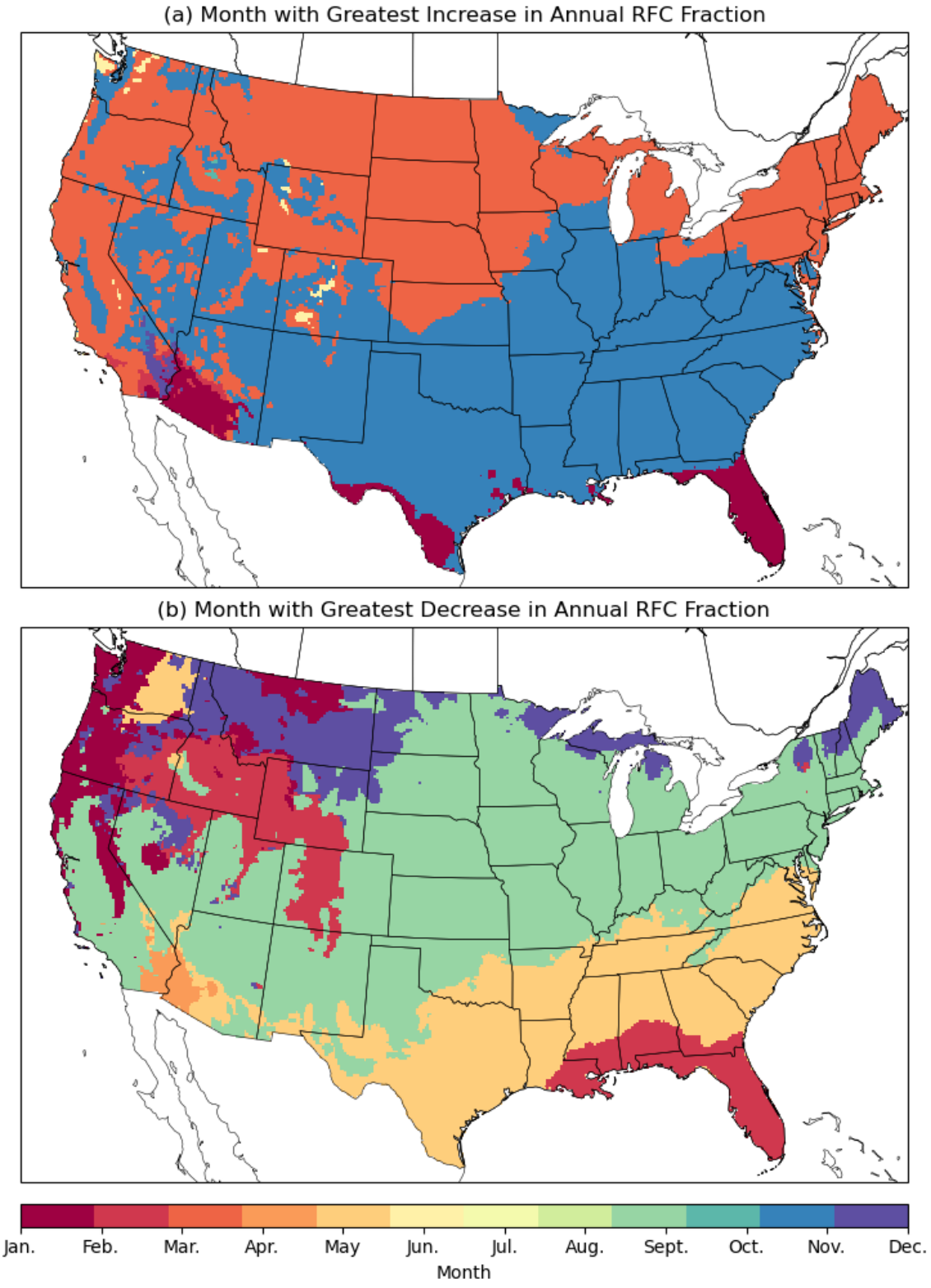

Figure 3.3. Maps showing which month has (a) the greatest increase in annual RFC fraction from SS to DS, and (b) the greatest decrease in annual RFC fraction from SS to DS at each grid cell.

The median percent change in NOx emissions for DS relative to SS for January, February, March, November, and December are summarized by IECC climate region in Table 3.1, providing further insight into the spatial patterns shown in Figure 3.1. For most mixed to very cold climate regions (zones 4-7), winter months had a negative percent change in NOx emissions between DS and SS (Figure 3.1; Table 3.1). Hot (zone 2) and warm (zone 3) climate regions showed more diverse median percent changes in winter. The hot-dry zone (2B) and warm-dry zone (3B) showed median increases for all months in November through March. In March and November, all climate regions had a median increase in emissions with DS relative to SS, ranging from 33.3% in zone 2B to 103% in zone 4A in March, and 42.4% in zone 2B to 183.7% in zone 3A in November.

Table 3.1. Median percent change in NOx emissions from SS to DS by IECC climate zone for January, February, March, November, and December, with interquartile range (IQR) in parentheses. Shading emphasizes positive median values with light pink or dark pink, and negative median values with light blue or dark blue dark blue. Light color shading indicates if the median ± the IQR changes parity (e.g., from positive to negative or vice versa).

Climate Zone	**Climate Zone Name**	**Median Percent Change (%; IQR in parentheses)**				
		Jan. (%)	*Feb. (%)*	*Mar. (%)*	*Nov. (%)*	*Dec. (%)*
2A	Hot-Humid	54.4 (24.0)	-32.3 (34.1)	66.3 (17.1)	175.5 (69.7)	4.4 (9.0)
2B	Hot-Dry	46.3 (14.6)	44.5 (59.1)	33.3 (47.0)	42.4 (131.4)	29.5 (26.2)
3A	Warm-Humid	25.4 (12.5)	-9.6 (13.8)	86.8 (18.7)	183.7 (45.8)	-0.4 (7.4)
3B	Warm-Dry	16.8 (23.4)	0.7 (27.2)	71.4 (33.0)	126.0 (69.9)	6.7 (16.4)
3C	Warm-Marine	-20.7 (13.6)	7.1 (18.1)	90.3 (24.4)	58.3 (28.6)	-16.7 (16.4)
4A	Mixed-Humid	11.4 (7.6)	-3.2 (13.9)	103.0 (13.3)	144.8 (33.9)	-11.2 (4.7)
4B	Mixed-Dry	-1.9 (14.9)	-5.7 (12.8)	72.6 (22.5)	108.2 (46.2)	-8.1 (10.0)
4C	Mixed-Marine	-33.1 (8.8)	-10.4 (8.9)	66.5 (14.7)	70.9 (25.9)	-29.8 (9.2)
5A	Cool-Humid	1.0 (10.4)	-1.4 (11.4)	94.5 (8.6)	112.7 (19.8)	-19.0 (4.8)
5B	Cool-Dry	-16.4 (13.6)	-11.0 (8.6)	67.9 (18.5)	92.8 (25.1)	-18.6 (10.4)
5C	Cool-Marine	-38.7 (9.8)	-12.9 (9.8)	55.9 (8.3)	65.3 (28.5)	-36.0 (8.6)
6A	Cold-Humid	-5.6 (7.5)	-0.5 (15.0)	86.5 (6.3)	89.5 (16.0)	-21.9 (5.1)
6B	Cold-Dry	-25.8 (9.9)	-9.0 (26.6)	76.7 (18.5)	84.6 (11.2)	-27.7 (8.8)
7	Very Cold	-8.1 (15.0)	-6.5 (19.8)	74.1 (12.0)	82.5 (13.1)	-22.6 (4.2)

3.1.1 Regional Patterns in Monthly RFC NO_X Emissions

While heating demand—and therefore relative changes between DS and SS—may be comparable within climate regions, the magnitude of RFC emissions in the 2017 NEI varies considerably within regions and across the country. Annual emissions estimates are based total fuel consumption, which relates to population, and mix of heating fuel type (e.g. natural gas, heating oil, etc.). Maps of monthly DS RFC NO_X emissions are shown in Figure 3.4. The highest NO_X emissions from RFC were in cities in the Northeast and Midwest—particularly New York City, Boston, Chicago, and Detroit. A grid cell within New York City, NY, a city on the northeast Atlantic coast of CONUS and the most populous city in the U.S., contained the maximum monthly total RFC NO_X emissions for January through May, and October through December, ranging from 72.7 tons in May to 450.2 tons in January. A grid cell over San Francisco, a city in California on the central Pacific coast, had the maximum monthly total RFC NO_X emissions in June through September, ranging from 6.1 tons in September to 12.4 tons in July.

Though the western U.S. had substantial heating demand, as seen in the map of annual total HDDs (see Chapter 2, Figure 2.5), low populations across much of the western U.S. result in low RFC emissions, often with the highest monthly total NO_X emissions of less than 0.001 tons. Sections of the U.S. particularly in the southern states had no RFC emissions allocated to months between May and September. The winter months (January, February, and December) and March and November had similar magnitudes of emissions for much of the country using the DS approach.

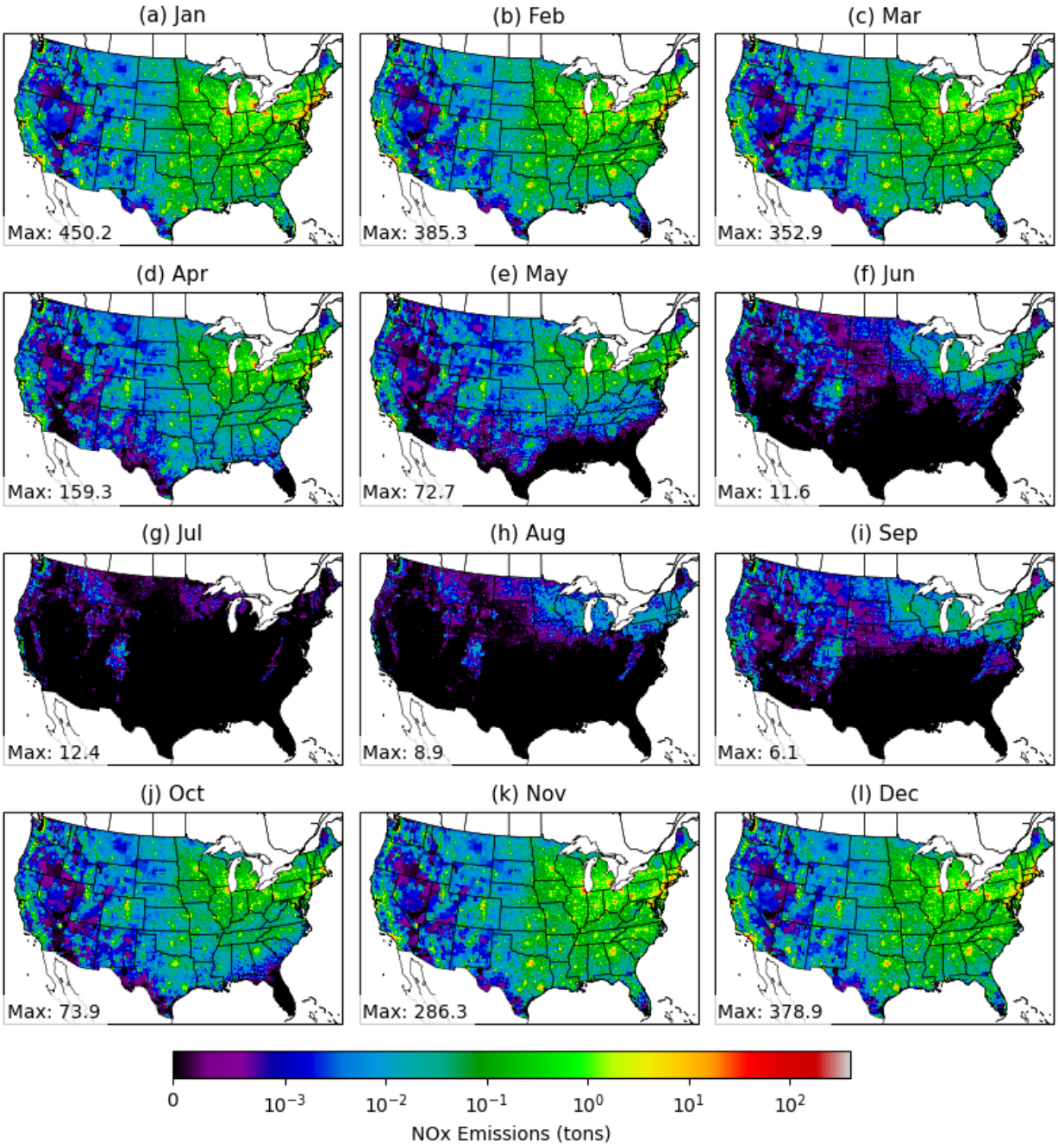

Figure 3.4. DS RFC NOx emissions by month in metric tons, with labels listing the maximum value across the domain.

3.1.2 Temporal Variability in RFC NO_X Emission Rates at Representative Grid Cells

Incorporating heating demand in the DS approach introduced daily variability in RFC heating emissions. Illustrative examples of how the DS approach translated to hourly NO_X emission rates in January, February, March, November, and December at representative grid cells in Minneapolis, MN and Houston, TX are shown in Figure 3.5. These cities had the highest 2019 populations in the cold and hot IECC climate zones respectively (see Chapter 2, Section 2.5.1). Hourly NO_X emission rates are in grams per second (g/s), indicating the rate of emissions assigned to the entire hour.

In the SS approach, the magnitude of emissions was higher in the Minneapolis grid cell compared to the Houston grid cell because Minneapolis had higher annual total emissions in the NEI: 293.5 tons in Minneapolis and 76.3 tons in Houston. SS emissions were identical for all days of a given season for each respective location, with emissions peaking at midday (Figure 3.5). DS emissions were variable across days, with emissions peaking during evening hours (Figure 3.5). The changes in peak emissions timing were due to the change in the diurnal profile between the SS and DS approaches.

In the winter months (January, February, December) in Minneapolis, DS had a greater range in hourly emission rates than SS; SS emissions ranged from 9.3 g/s to 32.5 g/s and DS emissions ranged from 8.1 g/s to 45.2 g/s. The maximum DS emissions rate (45.2 g/s) was in January, corresponding to the coldest day of the year when with mean daily air temperature was -29.1°C (Figure 3.5a). DS emission rates in March and November in Minneapolis were in a lower range than the winter emission rates, ranging from 4.4 g/s to 35.4 g/s. Though the March and November emission range was lower than the DS winter months, it represented a considerable

increase from the SS range of 3.1 g/s to 10.9 g/s in fall months (including November) and 3.7 g/s to 12.8 g/s in spring months (including March).

In Houston, the DS approach allocated zero emissions to many days due to sporadic heating demand. January was the only month when all days had non-zero DS emissions (Figure 3.5f). Houston DS emission rates in the winter months (January, February, and December) had a greater range that SS emission rates, ranging from 0 g/s to 21.4 g/s in the DS approach and 2.4 g/s to 8.4 g/s in the SS approach. The two highest daily emission rates, 24.1 g/s and 23.5 g/s, occurred in March and November respectively, as those were the days with the coldest temperatures of the year. SS emission rates ranged from 0.8 g/s to 2.8 g/s in fall months (including November) and 0.9 g/s to 3.3 g/s in spring months (including March). (Figure 3.5h-i).

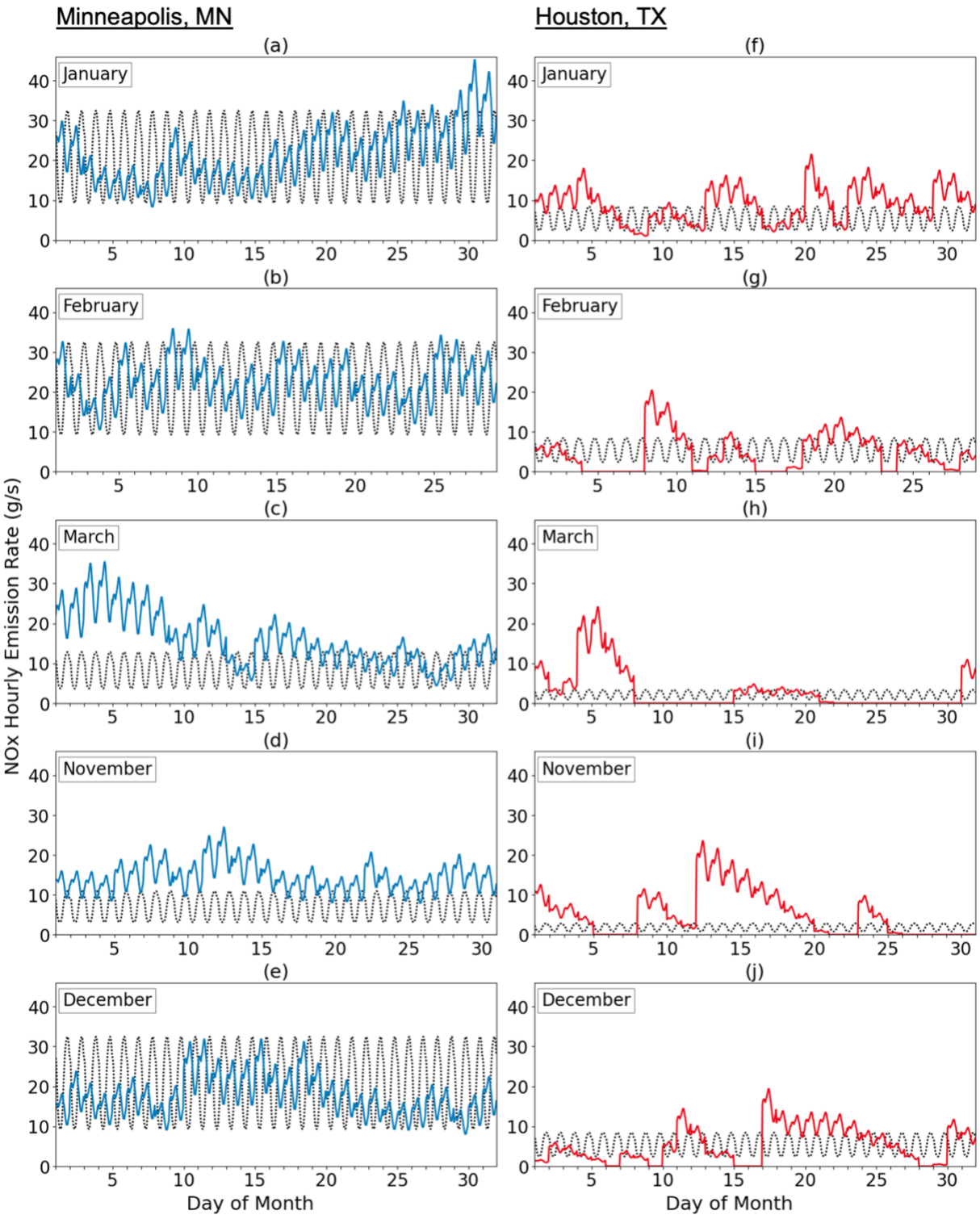

Figure 3.5. Hourly NO_X emission rates (g/s) over time for DS (solid lines) and SS (black dotted lines) for individual grid cells in Minneapolis, MN (a-e; blue solid lines) and in Houston, TX (f-j; red solid lines) in January (a, f), February (b, g), March (c, h), November (d, i), and December (e, j).

The DS approach introduced variability with temperature in daily emission rates throughout the year compared to the SS approach. In the SS approach, every day is assigned one of four emission rates depending on season, which can be seen for the Minneapolis and Houston grid cells in Figure 3.6. Daily DS NO_X emission rates ranged from 0 tons/day to 3.12 tons/day in Minneapolis, with a maximum daily emission rate 70% higher than the maximum daily SS emission rate (1.84 tons/day; Figure 3.6a). DS in Minneapolis resulted in 107 days with zero emissions. In Houston, daily DS NO_X emission rates ranged from 0 tons/day to 1.67 tons/day, with a maximum daily emission rate 249% higher than the maximum daily SS emission rate (0.48 tons/day; Figure 3.6b). In Houston, 241 days of the year had zero emissions in the DS approach.

As the daily variability in DS emissions is derived from temperature variability, daily NO_X emission rates are directly correlated with outdoor air temperature (Figure 3.6c-d). In the SS approach, emission rates do not relate to temperature, as the flat emission rates per season span a range of temperatures (Figure 3.6c-d). From these examples, we see that the DS approach results in temperature-dependent day-to-day variability in RFC emissions, introducing a greater range of daily emission rates with higher peak values than the SS approach.

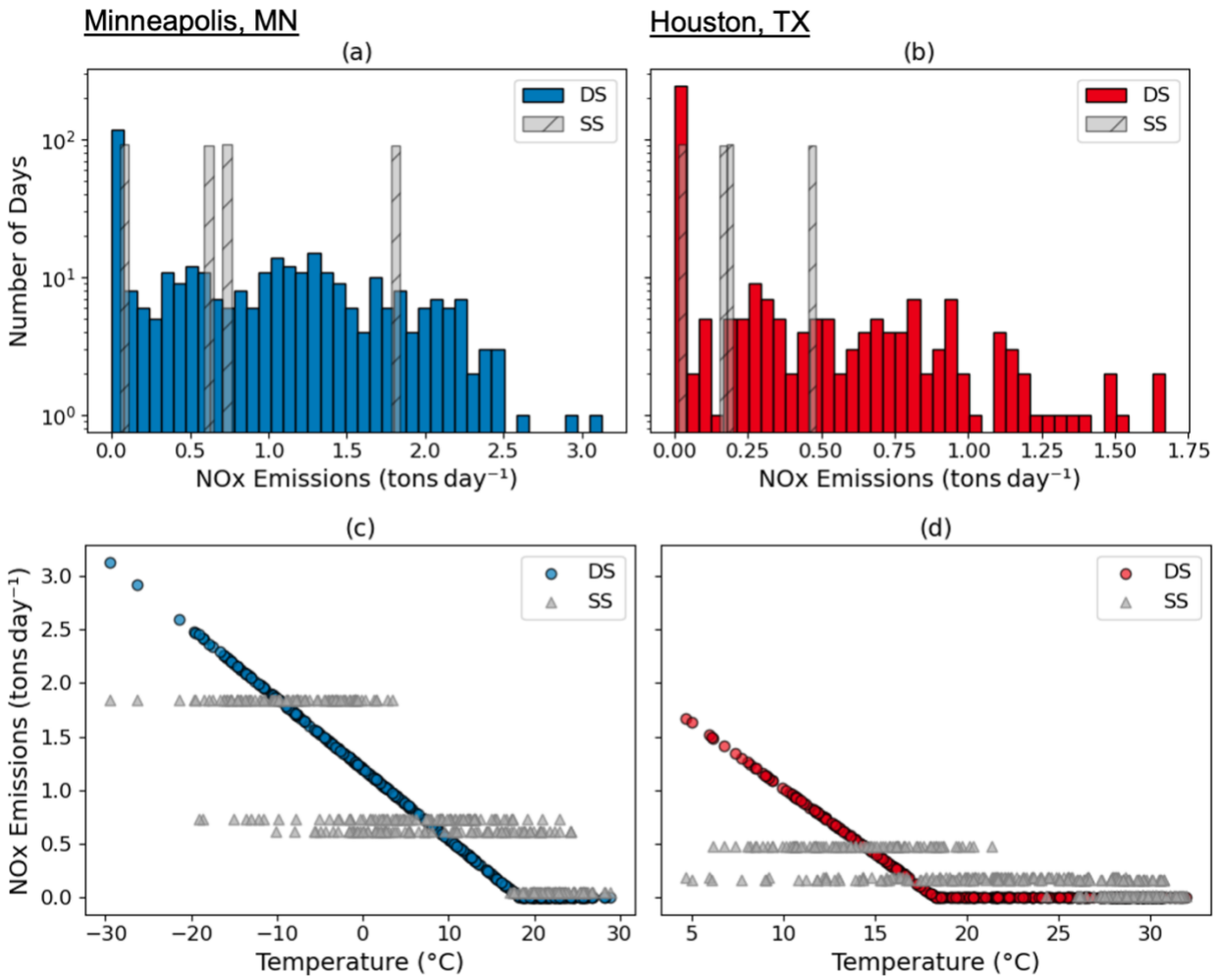

Figure 3.6. (a, b) Histograms of daily NO_X emission rate (tons day-1) for DS (solid bars) and SS (gray, hatched bars) in (a) Minneapolis, MN (blue) and (b) Houston, TX (red). (c, d) The relationship between daily mean two-meter air temperature (°C) and NO_X emission rate (tons day^{-1}) for DS (circles) and SS (triangles) in (c) Minneapolis, MN (blue) and (d) Houston, TX (red).

3.1.3 Change in Peak NO_X Emissions by Climate Zone

The median percent changes in maximum daily emission rates from DS relative to SS for each IECC climate zone are shown in Figure 3.7, with ranges indicating the 25th and 75th percentiles. Across climate zones, median percent changes in maximum daily emissions ranged from 7.1% percent in the cool-marine climate (zone 5C) to 223.0% in the hot-humid climate (zone 2A). In general, warmer climates had higher median percent changes in maximum daily emissions

compared to cooler climates. This is a result of the number of days which are assigned heating emissions due to heating demand (Table 2). Warmer climates had a higher number of days with zero emissions than cooler climates (Table 2). In a warm climate with fewer days with heating, more emissions are allocated to an individual day, resulting in a higher relative increase compared to climates with more consistent heating demand.

Humid climates (moisture classification A) in the hot through cold climates (zones 2-6) had higher median percent changes than their respective dry climates (moisture classification B; Figure 3.7). Mixed and cool marine climates (moisture classification C) had the lowest percent increases of all zones (Figure 3.7), and some of the lowest median number of days with zero emissions (Table 2).

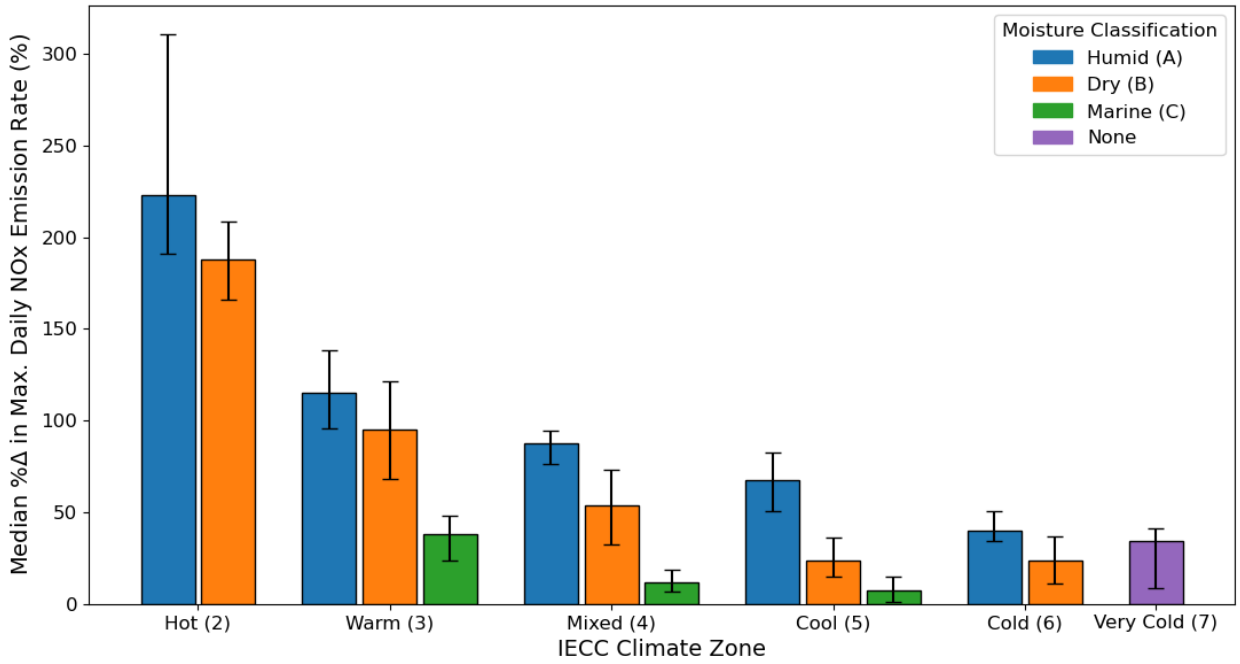

Figure 3.7. Median percent change in the maximum daily NOx emission rate from DS relative to SS, with bars indicating the 25th and 75th percentiles.

Table 3.2. Median number of days with zero heating emissions by IECC climate zone, with IQR in parentheses.

Climate Zone	Climate Zone Name	Median Number of Days with Zero Emissions (IQR)
2A	Hot-Humid	230 (34)
2B	Hot-Dry	229 (26.25)
3A	Warm-Humid	184 (23)
3B	Warm-Dry	170 (38)
3C	Warm-Marine	100 (69)
4A	Mixed-Humid	149 (17)
4B	Mixed-Dry	127 (46)
4C	Mixed-Marine	24 (38)
5A	Cool-Humid	110 (29)
5B	Cool-Dry	86 (36)
5C	Cool-Marine	7 (13.25)
6A	Cold-Humid	70 (23)
6B	Cold-Dry	56 (40)
7	Very Cold	50 (30)

3.1.4 Impact of Diurnal Allocation Profile

Figure 3.8 shows the percentage of RFC NO_X emissions allocated to nighttime hours for DS (Figure 3.8a), for SS (Figure 3.8b), and the difference between the DS and SS values (Figure 3.8c). Nighttime hours were defined at each grid cell as hours when the surface insolation from the MCIP/WRF meteorology file was equal to 0 W/m^2. For the diurnal profile used with the DS approach, between 57.0% and 64.8% of NO_X emissions were allocated to nighttime hours (Figure 3.8a). The diurnal profile used with the SS approach allocated between 34.6% and 41.1% of emissions to nighttime hours (Figure 3.8b). Across the domain, the change resulted in an increase of emissions allocated to nighttime of 18.2% to 28.3% from SS to DS. The reallocation of NO_X emissions from daytime to nighttime has substantial implications for atmospheric composition due

to the distinct chemical processes that occur between night and day with differing impacts on the lifetime of NO_X, and production of ozone and secondary $PM_{2.5}$.

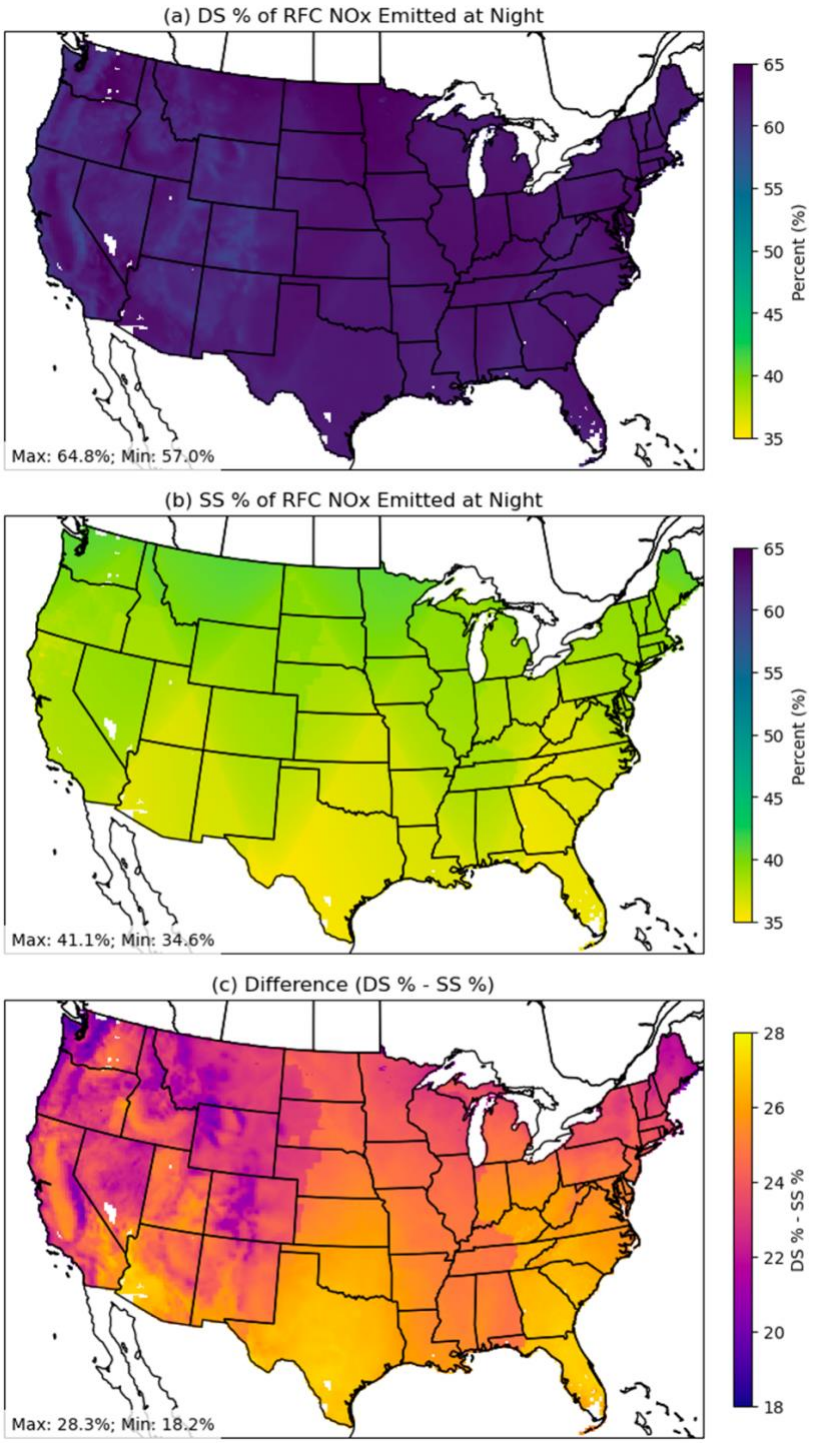

Figure 3.8. (a, b) Percentage of NO_X emissions allocated to nighttime hours (a) DS, (b) SS, and (c) the difference between the percentages in (a) and (b) (DS % - SS %).

3.1.5 RFC Contribution to Total Anthropogenic NO_X Emissions

Because RFC emissions are grouped within the nonpoint sector in emissions processing, gridded RFC emissions have not previously been made available by the U.S. EPA. While the National Emissions Inventory (NEI) allows the quantification of the contribution of RFC emissions to total annual anthropogenic emissions on a county-scale (see Figure 1.1), the contribution of RFC emissions on the gridded modeling domains, or in a higher resolution time than annually, have not previously been available. Upon request, the U.S. EPA provided annual and monthly emission summary data for the EQUATES 2019 platform on the 12US1 grid for total anthropogenic emissions of species including nitrogen oxides (NO_X), sulfur dioxide (SO_2), primary particulate matter ($PM_{2.5}$), carbon monoxide (CO), and regulatory volatile organic compounds (VOCs) (U.S. EPA, 2021b).

Figure 3.9 shows the total annual emissions of NO_X RFC (Figure 3.9a), the emissions from all anthropogenic sources in the EQUATES 2019 platform provided by the U.S. EPA (Figures 3.9b), and the percent contribution of the RFC sector to total anthropogenic NO_X emissions (Figure 3.9c). As with the monthly RFC NO_X emissions distributions (Figure 3.4), the highest NO_X emissions from RFC were in cities in the Northeast and Midwest, such as New York City, Boston, Chicago, and Detroit (Figure 3.9a). For all anthropogenic NO_X emissions, the highest contributing source sector is mobile source combustion, which can be seen in Figure 3.9b in the lattice-like distribution of high emissions corresponding to roadways, with the highest emissions in urban areas.

On average, RFC NO_X emissions contributed 4.7% to total annual anthropogenic NO_X emissions, with a maximum contribution of 68.7% to a grid cell in the mountainous regions in the west. In grid cells with a percent contribution to annual total anthropogenic NO_X above the 99th

percentile (49.0%), annual NO_X emissions from RFC ranged from 0.0014 tons/year to 2.8 tons/year. In grid cells with RFC NO_X emissions in the 99th percentile (36.2 tons/ year), the percent contribution to total anthropogenic NO_X ranged from 0.4% to 20.2%.

Compared to the annual contribution, RFC emissions allocated using the DS approach contributed to a greater fraction of total anthropogenic NO_X in winter months, March, and November—between 7.7% and 9.7% on average (Figure 3.10). In January, when the domain average contribution of RFC emissions was highest, the grid cells with RFC NO_X emissions in the 99th percentile (7.5 tons/month) contributed between 1.0% to 34.2% to total anthropogenic NO_X. Grid cells with the highest percent contribution of RFC emissions to total emissions in January (99th percentile = 61.4%) had very low monthly RFC NO_X emissions, ranging from 7.8 x 10^{-9} tons/month to 0.059 tons/month.

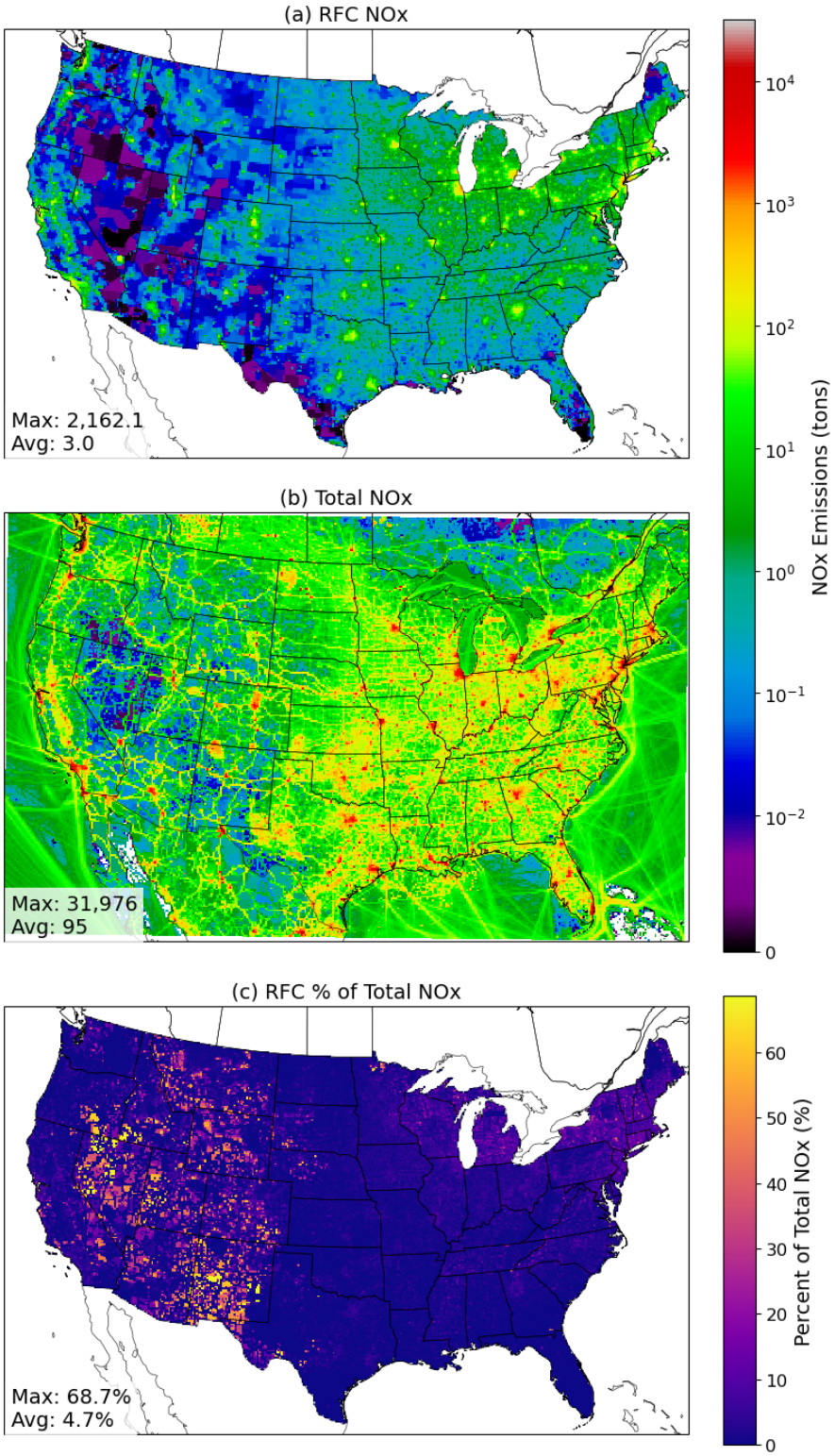

Figure 3.9. (a) Annual RFC NOx emissions (tons) on the 12US2 grid, isolated using SMOKE. (b) Annual NOx emissions (tons) from all anthropogenic sources in the EQUATES 2019 modeling platform. (c) RFC NOx percent contribution to total annual anthropogenic NOx emissions.

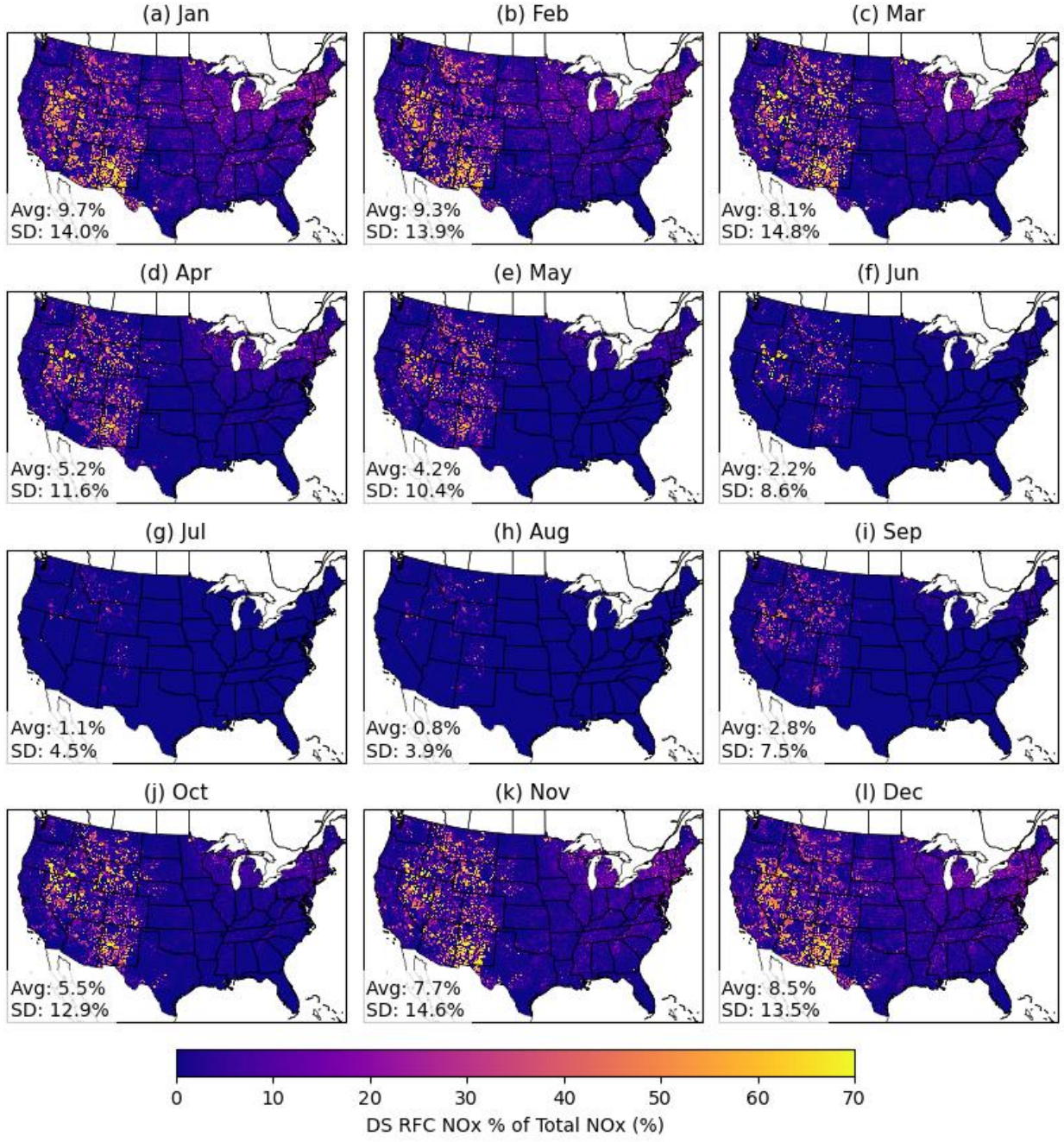

Figure 3.10. Monthly percent contribution of DS RFC NO_X emissions to total NO_X emissions.

To understand where and when incorporating the DS approach has the greatest impact to total anthropogenic NO_X, the difference between percent contribution to monthly anthropogenic NO_X using the DS and SS approaches in shown in Figure 3.11. The spatial patterns in positive or

negative percent changes are analogous to the percent changes in monthly emissions shown in Figure 3.1.

The highest magnitude of changes in relative contribution of RFC to total anthropogenic NO_X between DS and SS occur where either total NO_X emissions are especially low making RFC a greater contributor, such as rural regions in the west, or where RFC NO_X emissions are especially high, such as urban areas in the Midwest and Northeast. Across the winter months, grid cells with DS RFC NO_X emissions in the 99th percentile (between 6.3 tons/month in February and 7.5 tons/month in January) had differences in the percent contribution with SS ranging between -8.6% and 6.3%. In March and November, grid cells with DS RFC NO_X emissions in the 99th percentile (between 5.3 tons/month and 5.1 tons/month, respectively) had increases in the percent contribution with SS, ranging between 0.02% and 14.9%. The largest difference in percent contribution in grid cells with high monthly NO_X emissions occurred over an urban area in the Southeast, Atlanta, Georgia. In Figure 3.11, a lattice network of regions with little to no change in relative contribution are grid cells along major roadways, where mobile NO_X sources have a larger contribution compared to other areas.

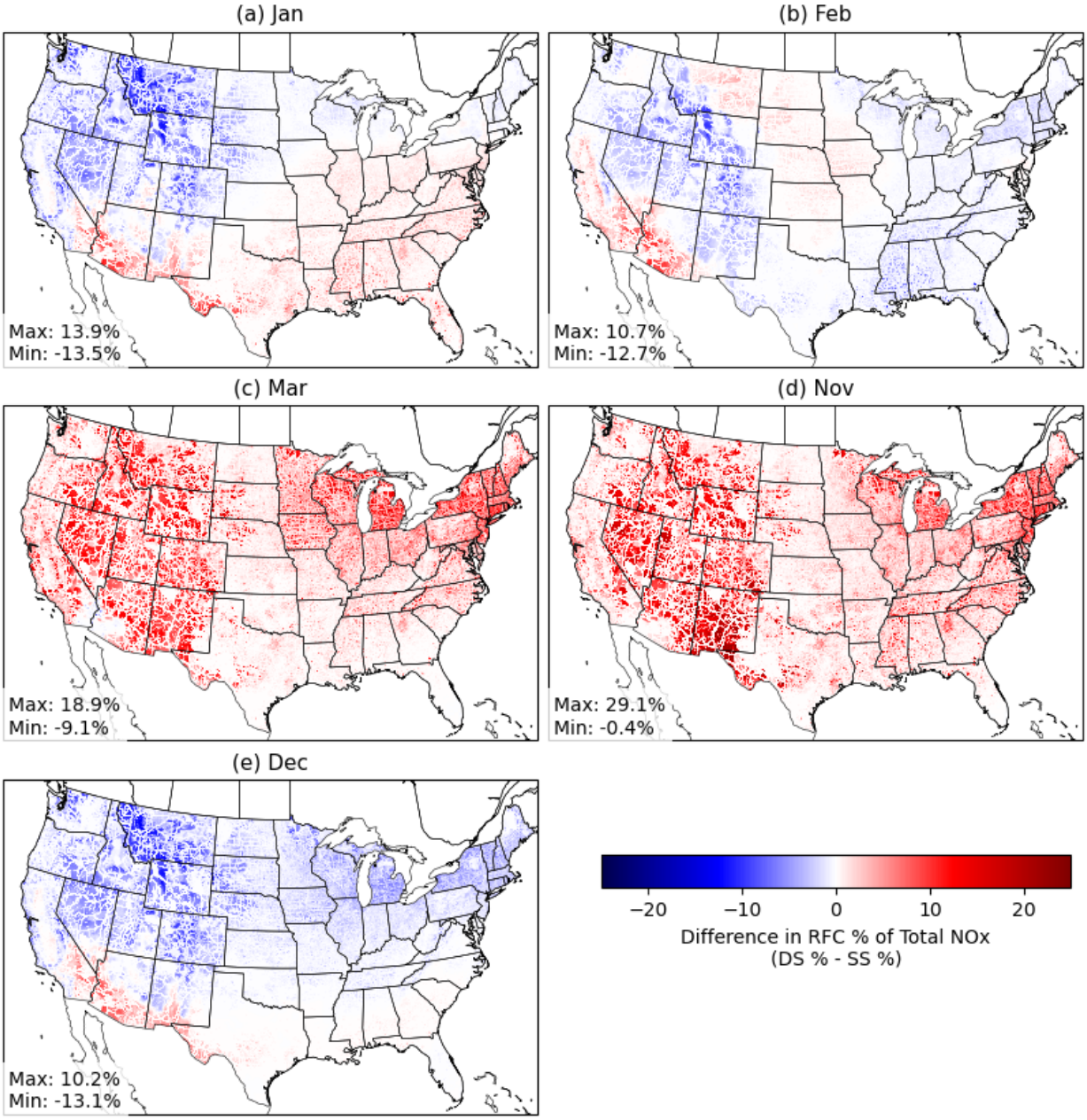

Figure 3.11. The difference between the percent contribution of RFC NO_X emissions to total anthropogenic NO_X emissions for DS and for SS in (a) January, (b) February, (c) March, (d) November, and (e) December.

3.2 Impact of DS for Other Chemical Species from RFC

While NO_X is the primary pollutant of interest for this study, RFC emits other chemical species relevant to air quality and human health, including SO_2, primary $PM_{2.5}$, CO, and VOCs.

The DS and SS approaches are applied consistently across all RFC emissions, so the relative impacts of DS compared to SS shown for NO_X in Section 3.1 are analogous to all chemical species emitted by RFC. This section discusses the impact of the DS approach on RFC contributions to total anthropogenic emissions of SO_2, $PM_{2.5}$, CO, and VOCs.

3.2.1 Sulfur Dioxide

In the 2017 NEI, RFC contributed 0.52% of total SO_2, with the largest portion of RFC SO_2 emissions from heating oil combustion (U.S. EPA, 2021a). At the county-level, the median percent contribution of RFC SO_2 to total anthropogenic SO_2 was 0.03%, but the maximum contribution was 73% (U.S. EPA, 2021a). The highest percentage contribution to country-level emissions were in New England, particularly New Hampshire and Connecticut. High SO_2 emissions in these regions relates to the widespread use of heating oil as a primary heating fuel (Northeast States for Coordinated Air Use Management (NESCAUM), 2005).

Figure **3.12** shows the total gridded annual SO_2 emissions from RFC (Figure **3.12**a) and from all anthropogenic sources (Figure **3.12**b), and the percent contribution of the RFC sector to total anthropogenic SO_2 emissions (Figure **3.12**c). The highest SO_2 emissions from RFC were across states the Northeast, with the maximum grid cell having 180 tons (Figure **3.12**a). The highest anthropogenic SO_2 emissions (maximum of 148,114 tons) were at individual grid cells across the country, since stationary combustion from coal-fired power plants and industrial boilers are the highest emitters of SO_2 (Figure **3.12**b; U.S. EPA, 2021a). On average, RFC NO_X emissions contributed 13.1% to total annual anthropogenic SO_2 emissions in a given grid cell, with a maximum contribution of 100% (Figure **3.12**c).

On a monthly basis, RFC emissions allocated using the DS approach contributed to between 20.6% and 23.6% in the heating season months (November through March) (Figure **3.13**).

The difference between the monthly percent contribution of RFC SO_2 to total anthropogenic SO_2 using DS and SS in the heating season months ranged from -21.6% in February to 27.7% in November (Figure **3.14**).

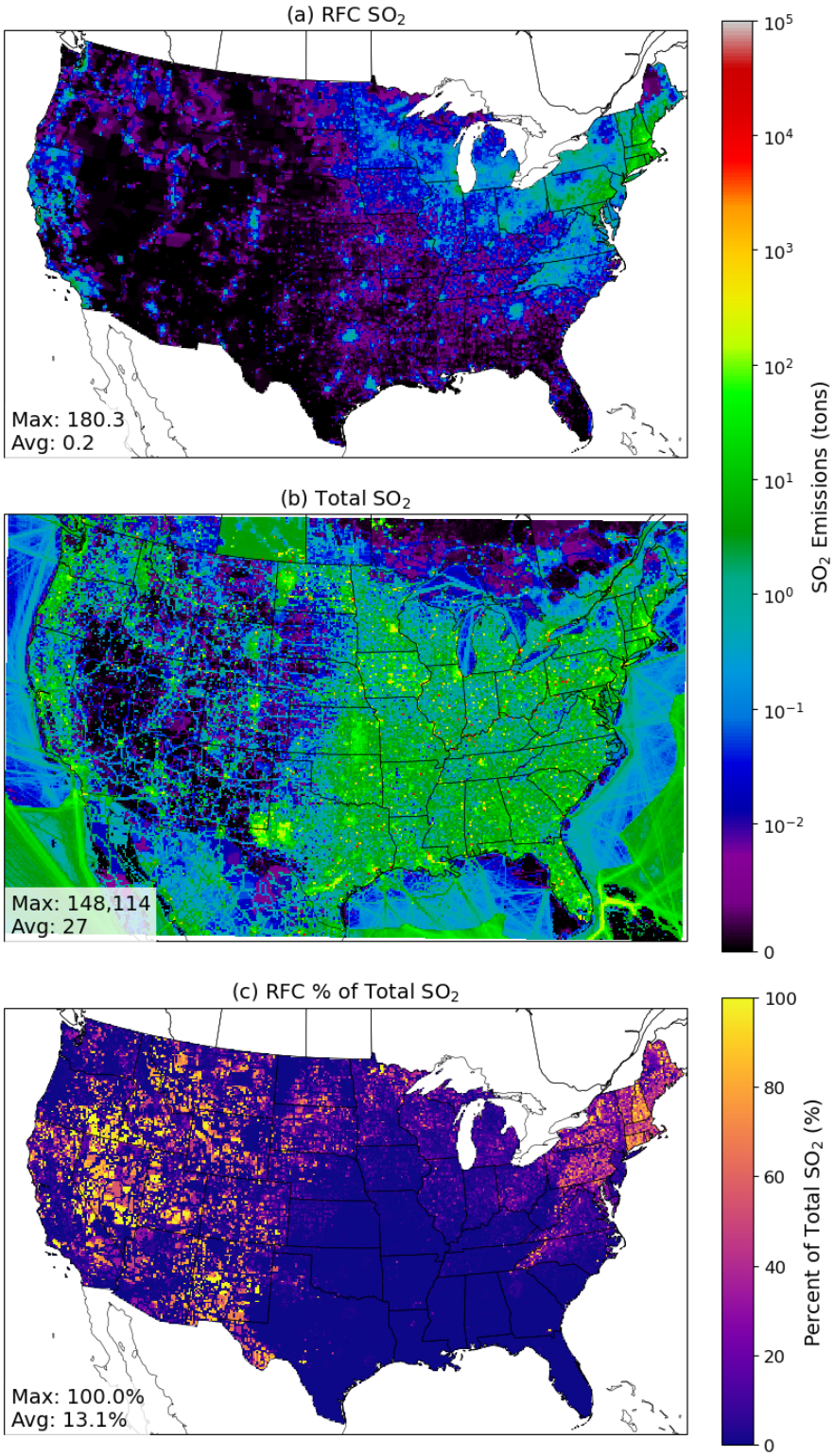

Figure 3.12. (a) Annual RFC SO_2 emissions (tons) on the 12US2 grid, isolated using SMOKE. (b) Annual SO_2 emissions (tons) from all sources in the EQUATES 2019 modeling platform. (c) RFC SO_2 percent contribution to total annual SO_2 emissions.

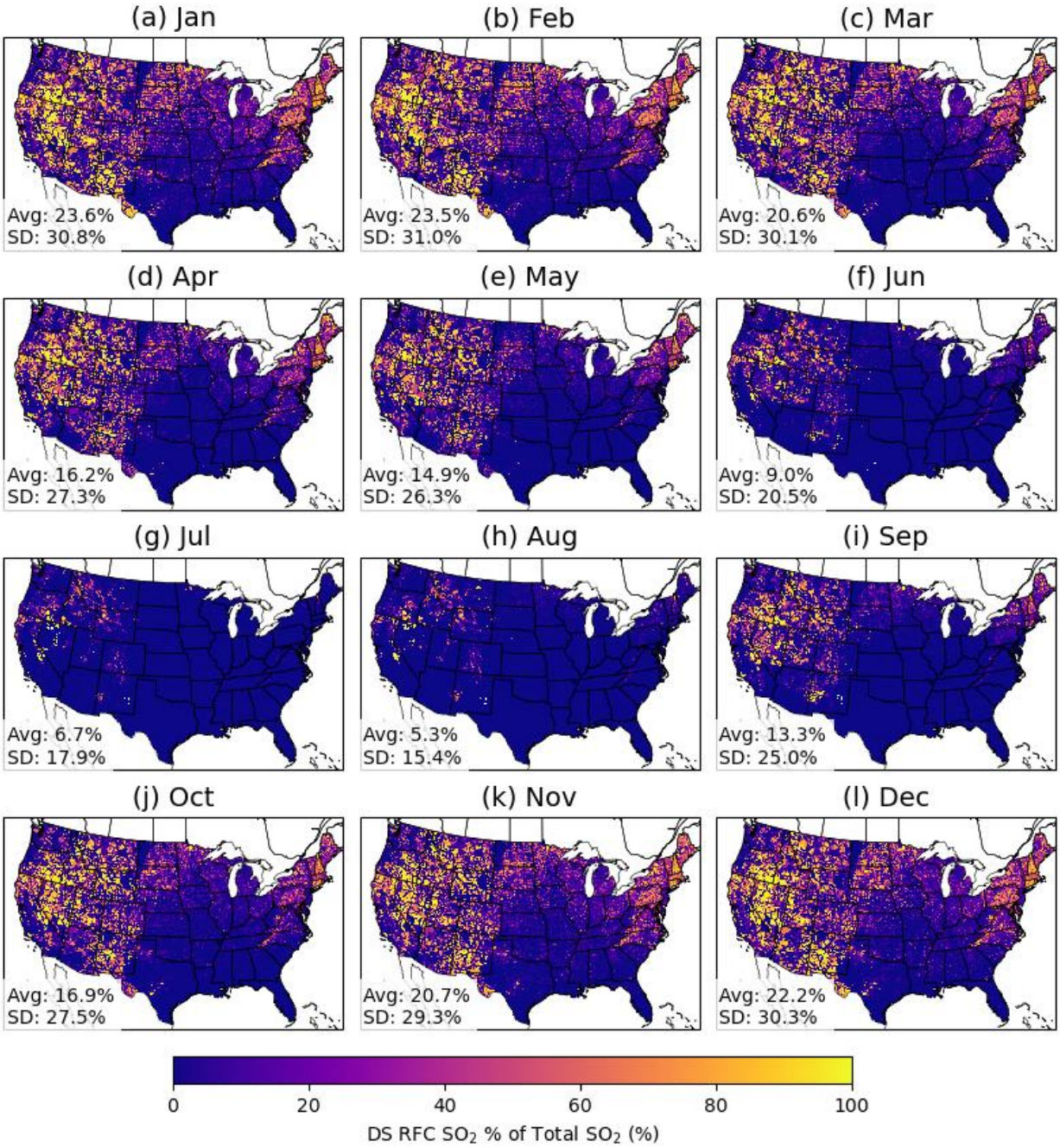

Figure 3.13. Monthly percent contribution of DS RFC SO_2 emissions to total SO_2 emissions.

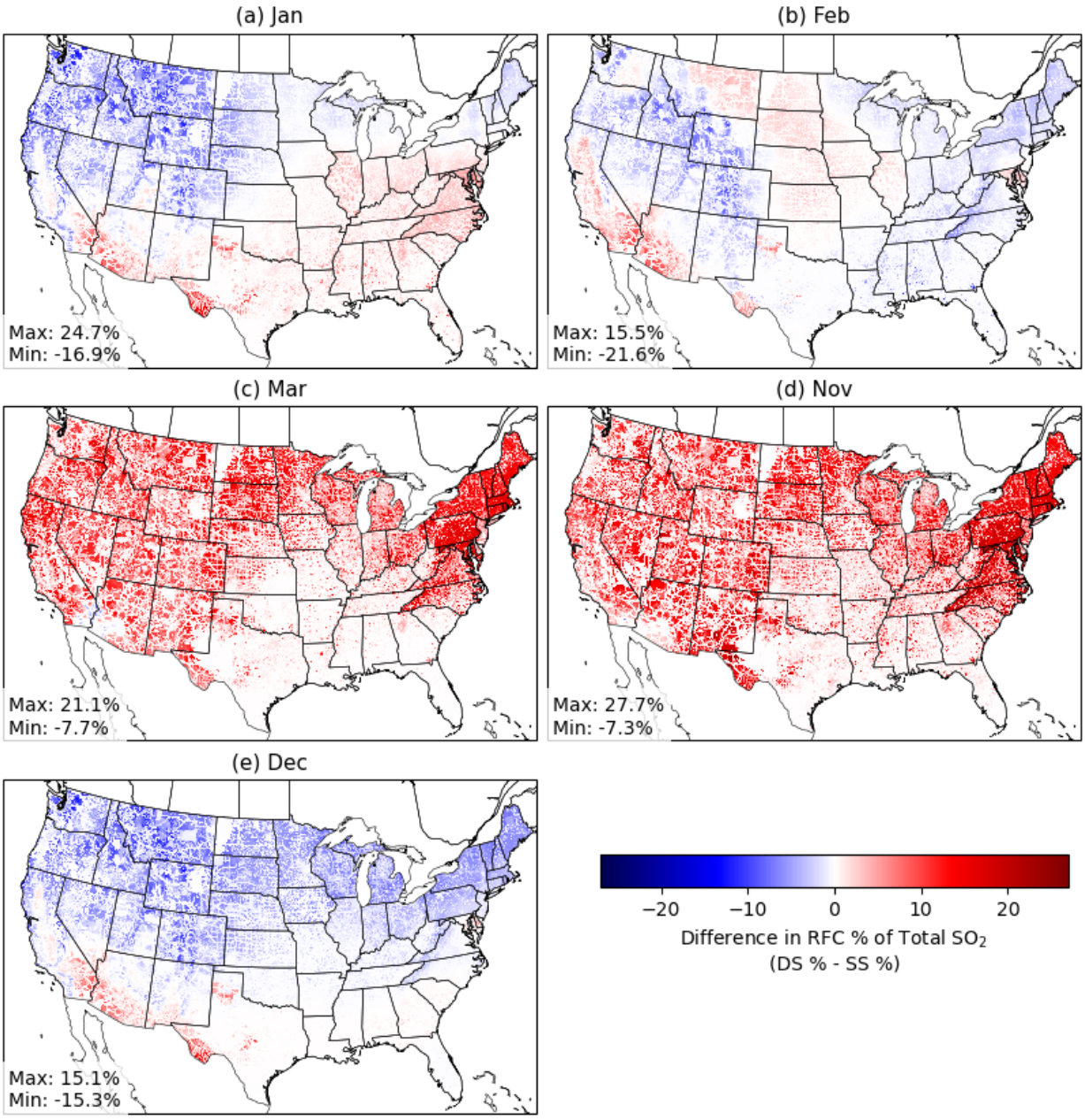

Figure 3.14. The difference between the monthly percent contribution of RFC SO_2 emissions to total SO_2 emissions from all sources for DS and for SS in (a) January, (b) February, (c) March, (d) November, and (e) December.

3.2.2 Fine Particulate Matter

In the 2017 NEI, RFC contributed 0.13% to total annual anthropogenic primary $PM_{2.5}$ (U.S. EPA, 2021a). At the county-level, the median percent contribution of RFC primary $PM_{2.5}$ to total anthropogenic primary $PM_{2.5}$ was 0.01%, with a maximum contribution of 12% (U.S. EPA,

2021a). The highest percentage contribution to country-level primary $PM_{2.5}$ were in the northeast, and in the central Pacific coast of California.

In the SMOKE speciation step, $PM_{2.5}$ is disaggregated into more detailed species (e.g., elemental carbon, nitrate, sulfate). Therefore, DS RFC primary $PM_{2.5}$ was calculated as the sum of all fine particulate species defined for the speciation (Simon, 2015). Figure 3.15 shows the total annual emissions of primary $PM_{2.5}$ from RFC (Figure 3.15a), from all anthropogenic sources (Figures 3.15b), and the percent contribution of the RFC sector to total anthropogenic primary $PM_{2.5}$ emissions (Figure 3.15c).

The highest primary $PM_{2.5}$ emissions from RFC were in urban areas in the Midwest, Northeast, and California, with the maximum grid cell having 278 tons (Figure 3.15a). High anthropogenic primary $PM_{2.5}$ emissions (maximum of 10,468 tons) were concentrated in cities but also occurred outside of urban areas (Figure 3.15b). The highest source contributors to total anthropogenic primary $PM_{2.5}$ include agricultural dust, road and construction dust, waste disposal and prescribed burns (U.S. EPA, 2021a). On average, RFC $PM_{2.5}$ emissions contributed 2.1% to total annual anthropogenic $PM_{2.5}$ emissions in a given grid cell, but up to a maximum contribution of 100% in regions in the west with very low total emissions (Figure 3.15c).

On a monthly basis, RFC primary $PM_{2.5}$ emissions allocated using the DS approach contributed to an average of between 1.6% and 2.1% during the heating season months (November through March) (Figure 3.16). The difference between the monthly percent contribution of RFC $PM_{2.5}$ to total anthropogenic $PM_{2.5}$ using DS and SS in the heating season months ranged from -12.6% in January and 23.4% in November (Figure 3.17).

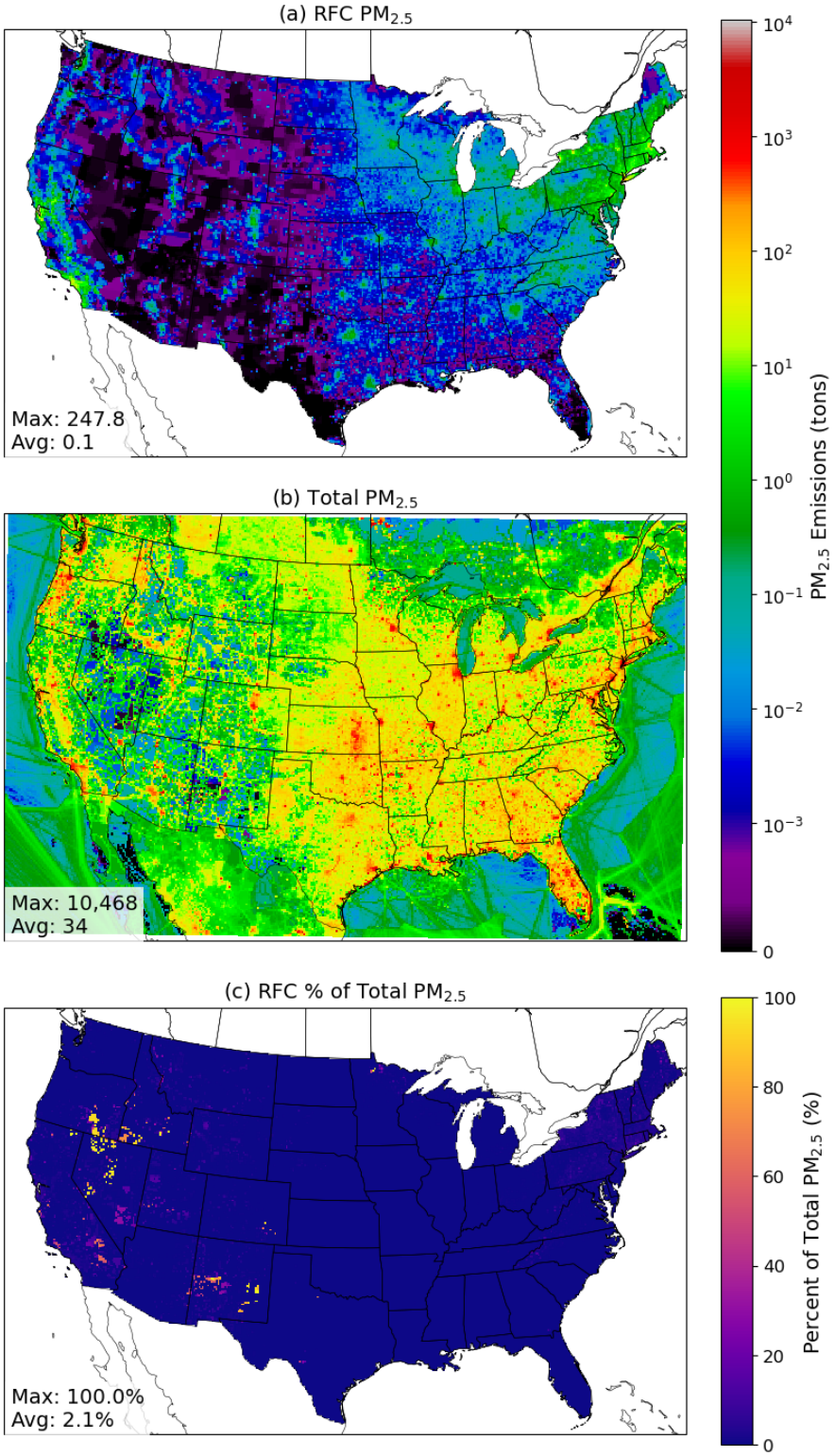

Figure 3.15. (a) Annual RFC $PM_{2.5}$ emissions (tons) on the 12US2 grid, isolated using SMOKE. (b) Annual $PM_{2.5}$ emissions (tons) from all sources in the EQUATES 2019 modeling platform. (c) RFC $PM_{2.5}$ percent contribution to total annual $PM_{2.5}$ emissions.

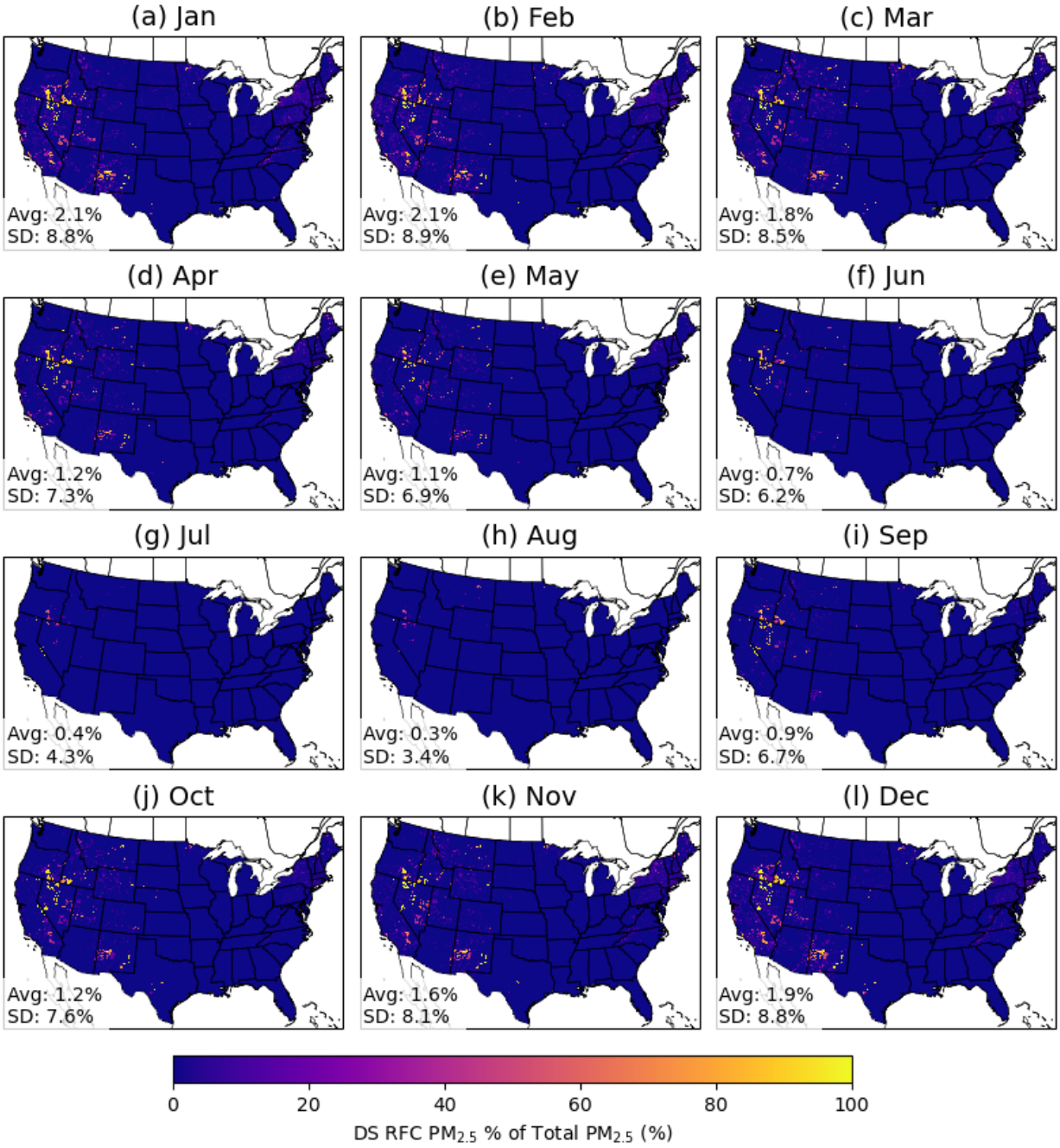

Figure 3.16. Percent contribution of DS RFC $PM_{2.5}$ emissions to total monthly $PM_{2.5}$ emissions by month.

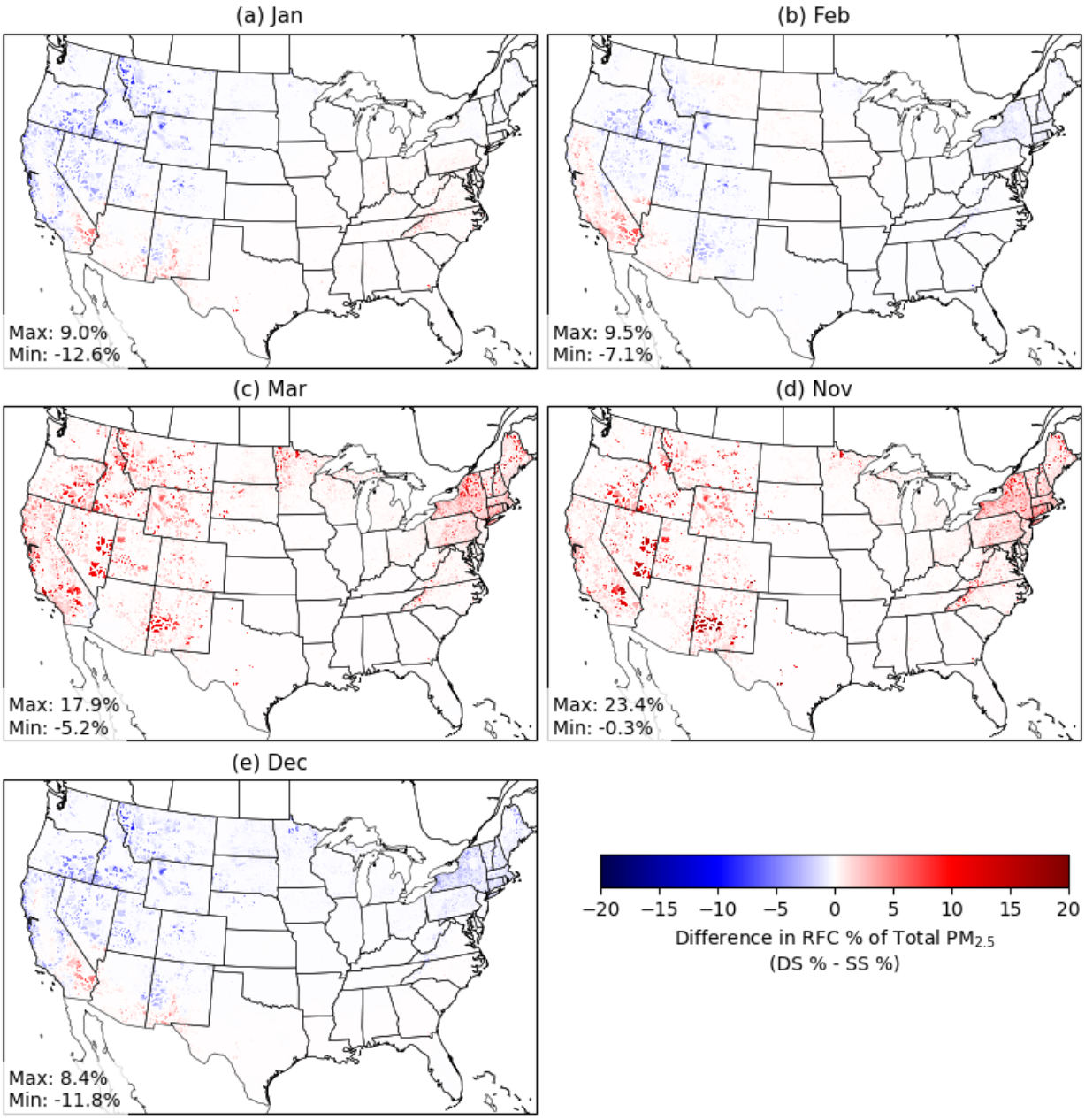

Figure 3.17. The difference between the percent contribution of RFC $PM_{2.5}$ emissions to total $PM_{2.5}$ emissions from all sources for DS and for SS in (a) January, (b) February, (c) March, (d) November, and (e) December.

3.2.3 Carbon Monoxide

In the 2017 NEI RFC contributed 0.13% of total annual anthropogenic CO emissions (U.S. EPA, 2021a). At the county-level, RFC does not contribute substantially to total anthropogenic CO

emissions; the median percent contribution was 0.1%, and the maximum contribution was 2.6% (U.S. EPA, 2021a).

Figure 3.18 shows the gridded total annual emissions of CO from RFC (Figure 3.18a), from all anthropogenic sources (Figures 3.18b), and the percent contribution of the RFC sector to total anthropogenic CO emissions (Figure 3.18c). The highest CO emissions from RFC were comparable to the spatial distribution of NO_X and $PM_{2.5}$ emissions from RFC, with high values in urban areas in the Midwest, Northeast, and California. The grid cell maximum for annual RFC CO emissions was 1,208.8 tons (Figure 3.18a). High annual anthropogenic CO emissions (grid cell maximum of 110,589 tons) occurred primarily across the eastern half of CONUS, and in urban areas (Figure 3.18b). The highest source contributors to total anthropogenic CO include mobile sources, residential wood combustion, and prescribed burns (U.S. EPA, 2021a). On average, RFC CO emissions contributed less than 0.7% to total annual anthropogenic CO emissions per grid cell, but up to a maximum contribution of 100% in regions with low total emissions in the west (Figure 3.18c).

On a monthly basis, RFC CO emissions allocated using the DS approach contributed to an average of between 1.3% and 1.6% in the heating season months (November through March) (Figure 3.19). The difference between the monthly percent contribution of RFC CO to total anthropogenic CO using DS and SS in the heating season months ranged from -10.5% in February and 24.4% in November (Figure 3.20).

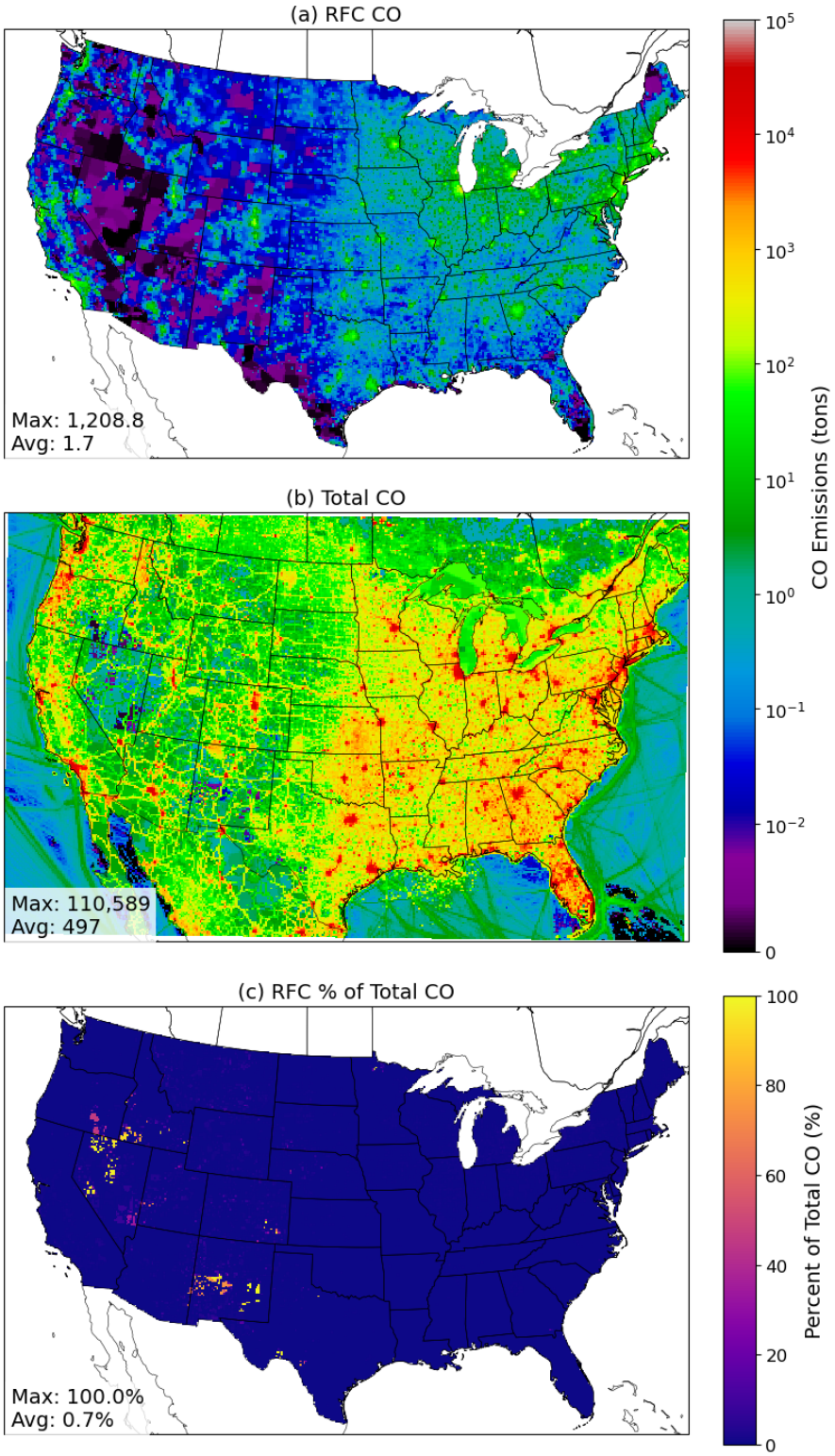

Figure 3.18. (a) Annual RFC CO emissions (tons) on the 12US2 grid, isolated using SMOKE. (b) Annual CO emissions (tons) from all sources in the EQUATES 2019 modeling platform. (c) RFC CO percent contribution to total annual CO emissions.

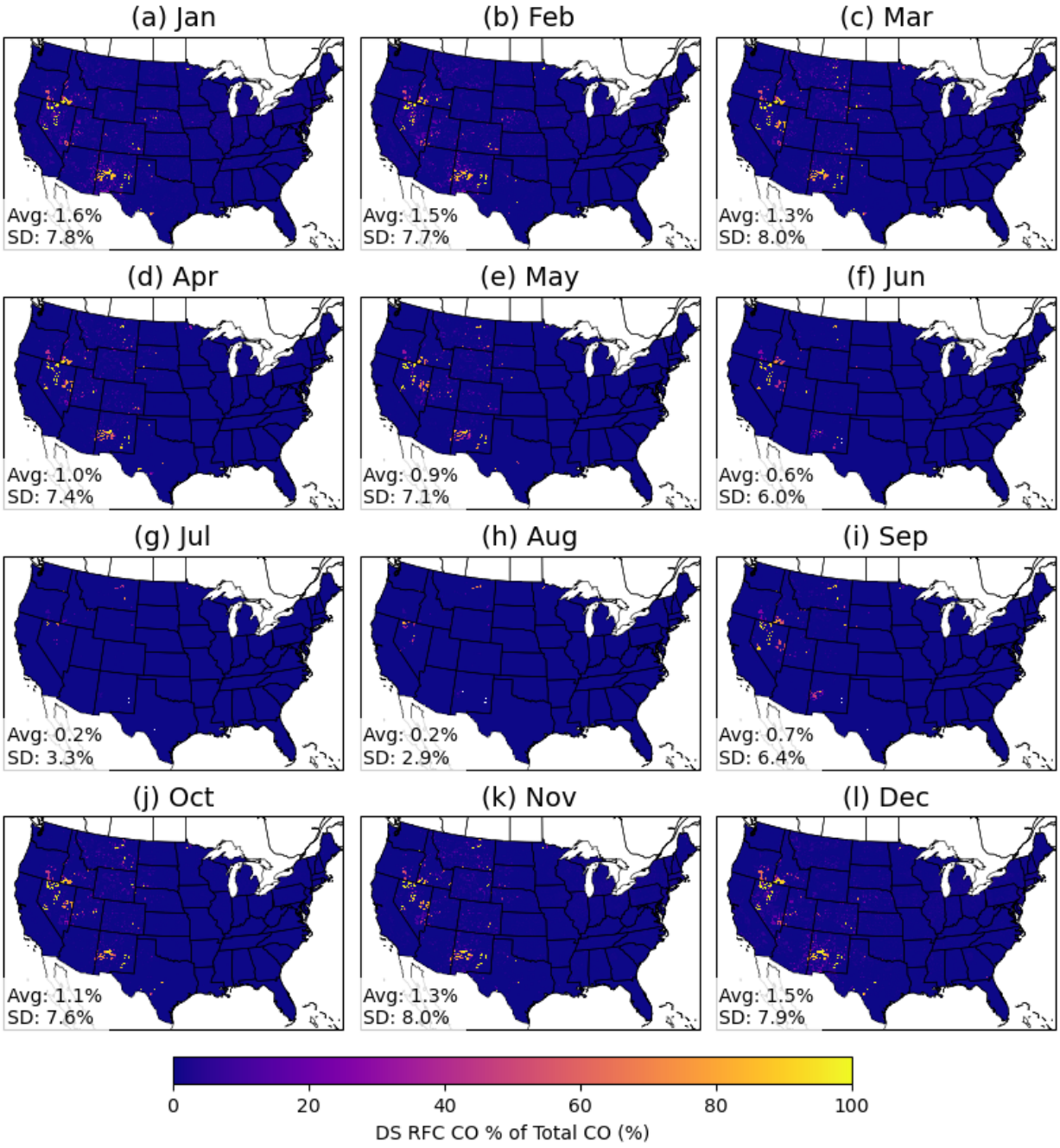

Figure 3.19. Monthly percent contribution of DS RFC CO emissions to total anthropogenic CO emissions.

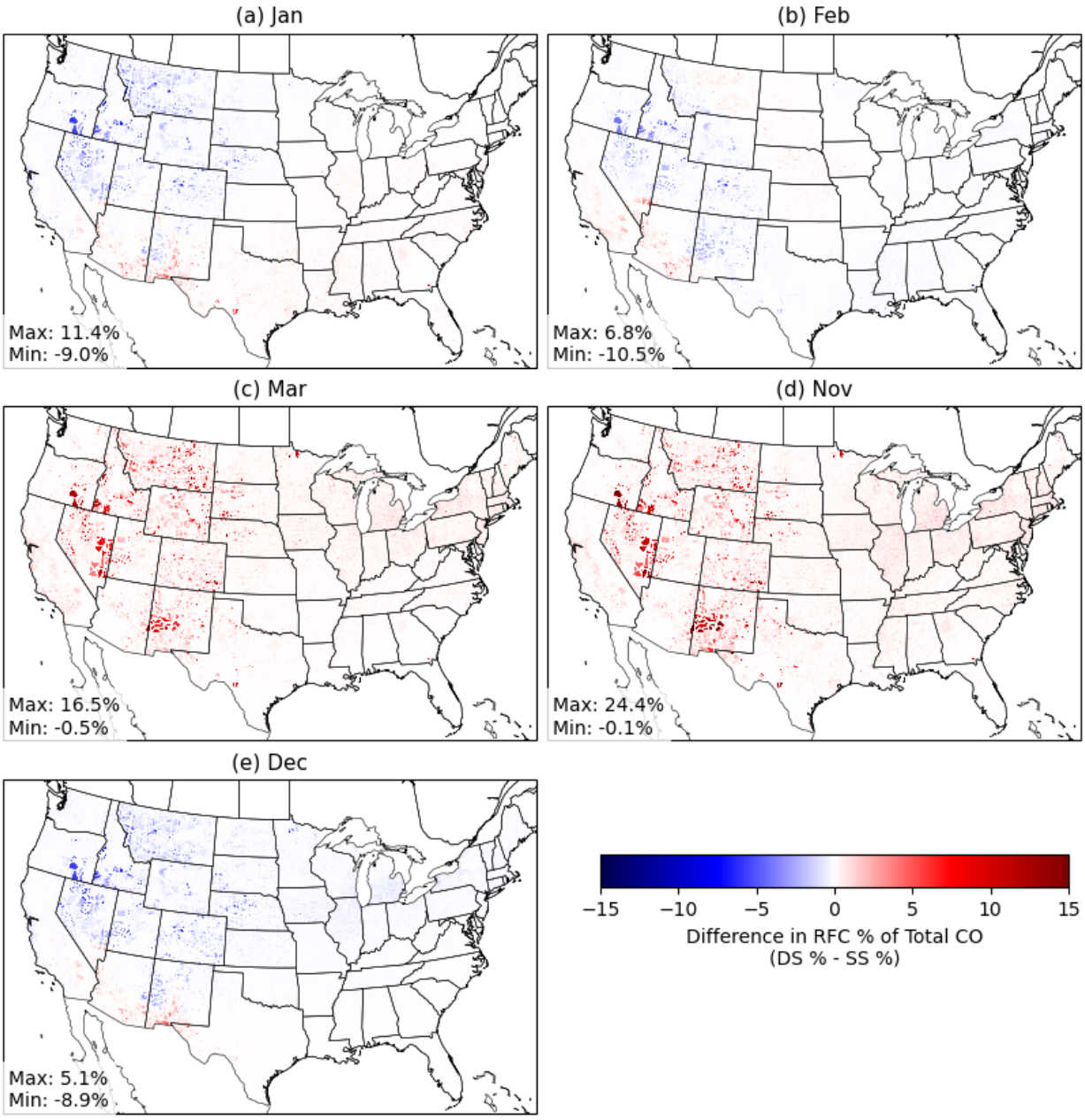

Figure 3.20. The difference between the percent contribution of RFC CO emissions to total anthropogenic CO emissions for DS and for SS in (a) January, (b) February, (c) March, (d) November, and (e) December.

3.2.4 Volatile Organic Compounds

In the 2017 NEI, RFC contributed 0.08% of total annual anthropogenic (i.e., non-biogenic) VOCs (U.S. EPA, 2021a). At the county-level, RFC does not contribute substantially to total

anthropogenic VOC emissions. The median percent contribution to county-level emissions 0.05%, with a maximum contribution of 1.2%.

Figure 3.21 shows the gridded total annual emissions of VOC from RFC (Figure 3.21a), from all anthropogenic sources (Figures 3.21b), and the percent contribution of the RFC sector to total anthropogenic VOC emissions (Figure 3.21c). The highest VOC emissions from RFC were in urban areas in the Midwest, Northeast, and California, and had maximum value of 159.3 tons (Figure 3.21a). High anthropogenic VOC emissions (grid cell maximum of 26,016 tons) occurred in hotspots across CONUS, as one of the largest contributing sources for VOCs is oil and gas production (Figure 3.21c; U.S. EPA, 2021a). On average, RFC VOC emissions contributed 0.1% to total annual anthropogenic VOC emissions per grid cell, but up to a maximum contribution of 100% in regions with low total emissions (Figure 3.21c).

On a monthly basis, RFC VOC emissions allocated using the DS approach contributed to an average of between 0.2% and 0.3% in the heating season months (November through March) (Figure 3.22). The difference between the monthly percent contribution of RFC VOC to total anthropogenic VOC using DS and SS in the heating season months ranged from -1.3% in January to 5.6% in November (Figure 3.23).

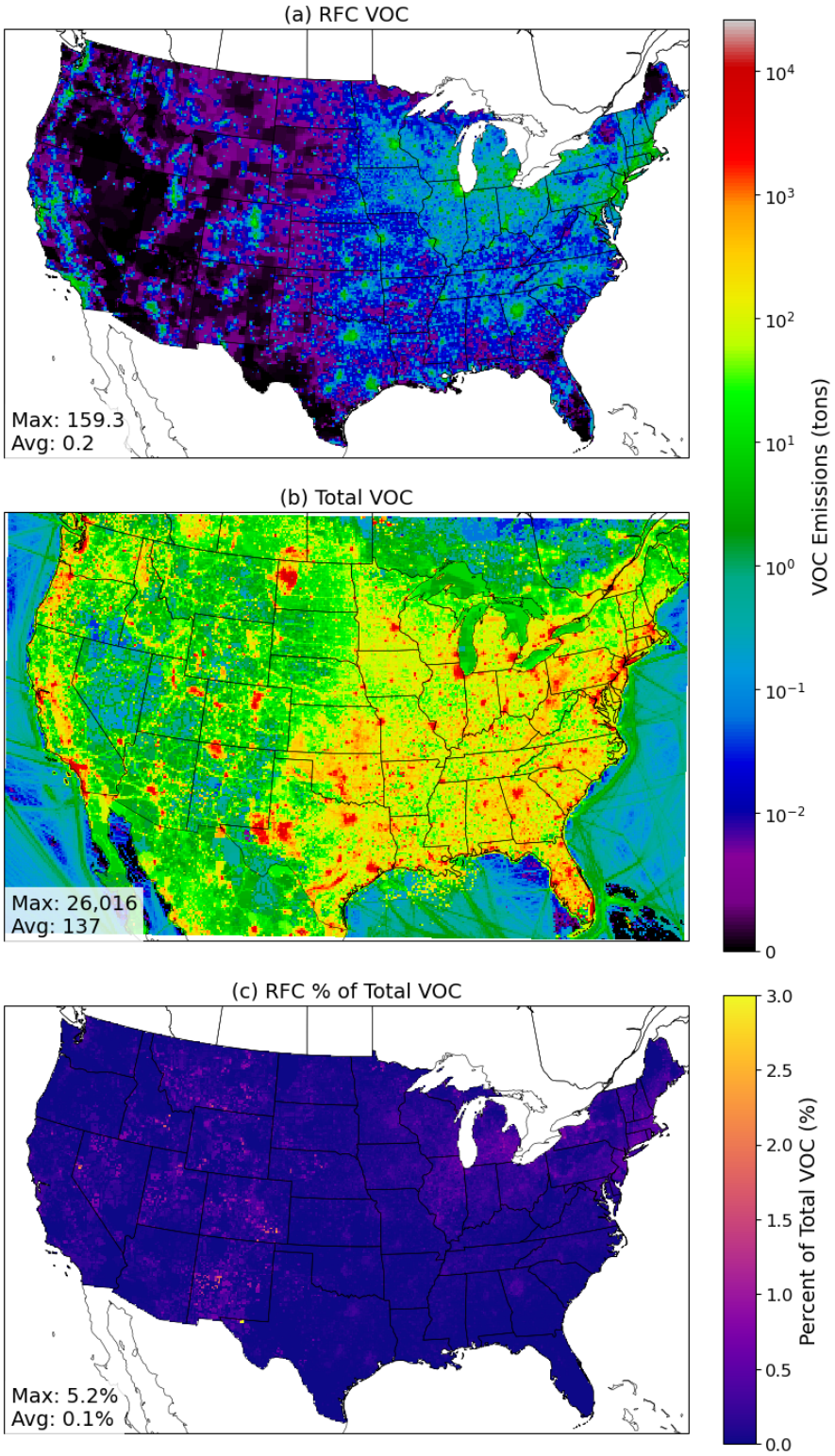

Figure 3.21. (a) Annual RFC VOC emissions (tons) on the 12US2 grid, isolated using SMOKE. (b) Annual VOC emissions (tons) from all sources in the EQUATES 2019 modeling platform. (c) RFC VOC percent contribution to total annual VOC emissions.

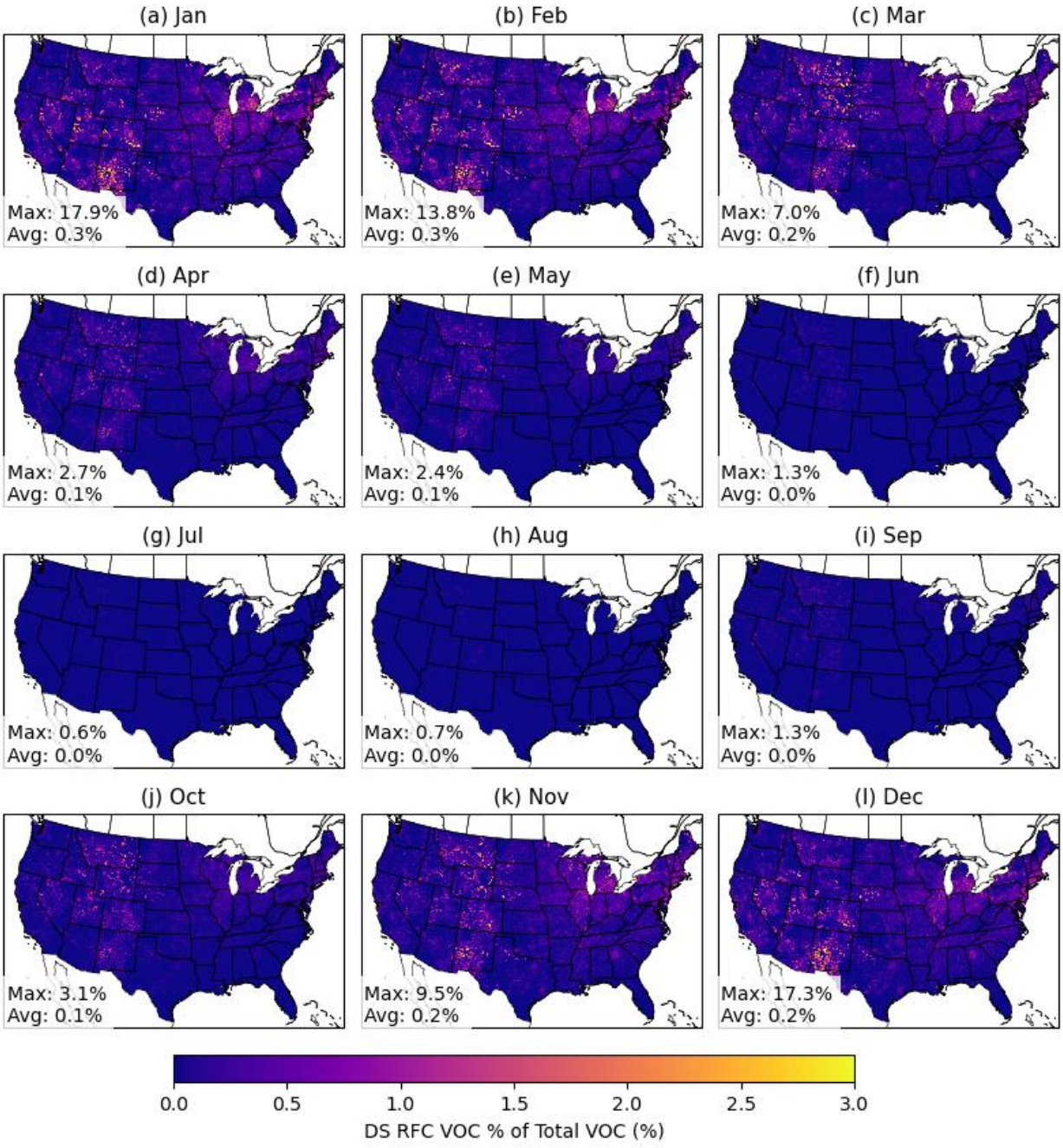

Figure 3.22. Monthly percent contribution of DS RFC VOC emissions to total anthropogenic VOC emissions.

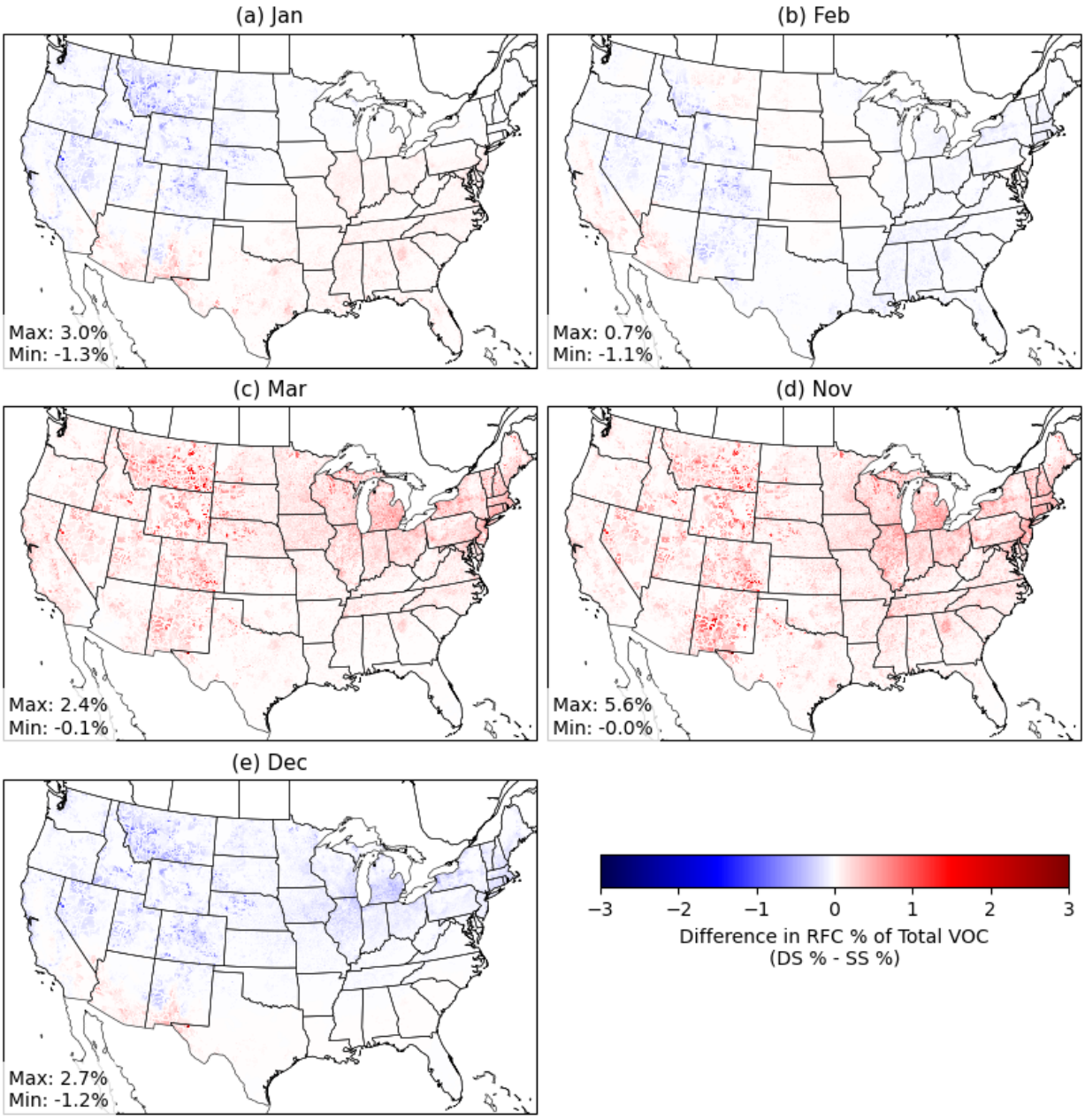

Figure 3.23. The difference between the percent contribution of RFC VOC emissions to total anthropogenic VOC emissions for DS and for SS in (a) January, (b) February, (c) March, (d) November, and (e) December.

3.3 Summary of Key Findings

In this chapter, we evaluated the impact of allocating RFC emissions using the DS approach based on daily heating demand, yielding five key results.

(1) DS increased the allocation of emissions to March and November relative to SS.

Across all climate regions, incorporating daily heating demand to allocate RFC emissions in the DS approach resulted in a redistribution of emissions toward March and November relative to the SS approach (Figure 3.1; Table 3.1). Median percent increases in emissions ranged from 33.3% to 103% in March, and 42.4% to 183.7% in November (Table 3.1). The increases in emissions in March and November were accompanied by decreases in emissions at other times during the year, particularly in May through September (Figure 3.2, Figure 3.3). The near universal increases during March and November when using the DS approach suggest that the SS approach may underestimate RFC emissions in the beginning and end of the winter heating season (Gesangyangji et al., 2024).

(2) DS had a greater range in hourly emission rates relative to SS, with higher median peak emission rates across all climate regions.

Incorporating heating demand in the DS approach introduced daily variability in RFC heating emissions. As the daily variability in DS emissions is derived from temperature variability, daily NO_X emission rates were directly correlated with outdoor air temperatures (Figure 3.6c-d). Median percent change in maximum daily value ranged from 7.1% percent in the cool-marine climate (zone 5C) to 223.0% in the hot-humid climate (zone 2A) (Figure 3.7).

(3) Incorporating a diurnal profile designed to represent heating behavior increased the allocation of emissions to night hours compared to the U.S. EPA diurnal profile for RFC.

Applying the diurnal profile developed to represent outdoor hydronic heaters (U.S. EPA, 2025) allocated 18% to 28% more emissions to nighttime hours than the U.S. EPA default profile, which could be impactful for simulations of NO_X, ozone, and PM chemistry (Figure 3.8).

(4) RFC NO_X emissions contributed the most to total gridded anthropogenic NO_X emissions in rural areas with few NO_X sources, and urban areas with high RFC emissions, and that contribution was highest in January.

On average, RFC NO_X emissions contributed 4.7% to total annual anthropogenic NO_X emissions, with a maximum contribution of 68.7% (Figure 3.9). On a monthly basis, RFC emissions allocated using the DS approach contributed to a greater fraction of total anthropogenic NO_X during the heating season months (November through March)—between 7.7% and 9.7% on average (Figure 3.10).

(5) On annual and monthly timescales, the contribution of RFC to total anthropogenic emissions for chemical species other than NO_X was highest for SO_2, followed by primary $PM_{2.5}$ and CO, while contributions to VOCs were minimal.

On a monthly basis, RFC SO_2 emissions allocated using the DS approach contributed to an average of between 20.6% and 23.6% of total anthropogenic SO_2 in the heating season months (November through March). The highest RFC SO_2 concentrations occurred in New England due to the highest reliance on residential fuel oil for space heating. During the heating season months, RFC using DS contributed to an average of between 1.6% and 2.1% to total anthropogenic $PM_{2.5}$, between 1.3% and 1.6% to total anthropogenic CO, and between 0.2% and 0.3% to total anthropogenic VOCs.

Chapter 4 Discussion and Conclusions

We developed a method for temporally allocating annual emissions from non-wood residential fuel combustion (RFC) to each day based on a temperature-dependent proxy for heating demand, heating degree days (HDD). This method was applied to estimate RFC emissions across the contiguous United States (CONUS) to prepare an emissions inventory for use with the Community Multiscale Air Quality model (CMAQ). This chapter discusses the implications of the key findings and conclusions in the context of previous studies, and poses future research directions.

4.1 Distribution of Emissions Across the Heating Season

The temperature-based daily scaling (DS) approach changed the monthly emissions for all climate regions compared to the seasonal-scaling (SS) approach, primarily as an increase in emissions allocated to March and November. The increases in emissions in March and November were accompanied by decreases in emissions during other parts of the year, particularly May through September. The reallocation of emissions caused a decrease in emissions in core winter months (December through February) in some regions—particularly in colder climates—as the SS approach overallocated emissions to winter months compared to March and November, which often had comparable heating demand. For the U.S., Gesangyangji et al. (2024) identified March and November as part of the heating season—months when heating demand exceeded cooling demand—for all states except for Florida based on historical data from 1986-2010. Studies in other countries with temperate climates also consider March and November to be part of the heating season (Belova et al., 2018; Hartley & Robinson, 2000; Shen & Liu, 2016). By including heating demand-based temporal scaling that relied on local daily ambient air temperatures, the DS approach adapts the timing of RFC emissions to be responsive to the variability of heating and

cooling seasons experienced across U.S. states (Gesangyangji et al., 2024). The reallocation of emissions to adapt to local heating and cooling seasons is likely more representative of when RFC emissions occur than the fixed SS approach.

4.2 Daily Emissions Variability and Maximum Emission Rates

Allocating emissions based on local heating demand in the DS approach increased the range of hourly and daily emission rates compared to the SS approach, resulting in a median increase in the maximum emission rates across all climate regions. For warmer climates with sporadic heating demand, DS concentrated RFC emissions to fewer days, resulting in the greatest increases to maximum emission rates.

Because of the co-variability of emissions with atmospheric dynamics, meteorology, and chemistry, the timing and magnitude of daily emissions may have substantial impacts to atmospheric concentrations. Colder ambient temperatures in winter increase the atmospheric lifetime of NO_X by slowing chemical loss pathways (Jaeglé et al., 2018; Kenagy et al., 2018). Atmospheric dynamics play a role in the physical loss pathways of NO_X. For example, a shallow boundary layer and stable atmospheric conditions, often caused in winter by temperature inversions, can lead to a rapid increase in pollution (Sun et al., 2021; Ying, 2011). One of the National Ambient Air Quality Standard (NAAQS) for NO_X is a 1-hour standard, and capturing peak emission rates from RFC may be important for simulating maximum concentrations in atmospheric modeling that may exceed the NAAQS. The variability in the daily allocation of RFC emissions with the DS approach may be better able to capture the timing of peak NO_X emissions, and likely ambient NO_X concentrations, compared to the fixed SS approach.

4.3 Diurnal Allocation

To further improve the representation of RFC in emissions inventories, we compared the impact on RFC emissions of using a diurnal allocation profile that was developed to represent wood-burning outdoor hydronic heaters (OHH) in the DS approach, to the default profile used in current EPA methods for RFC emissions processing (U.S. EPA, 2025) with the SS approach. By their definitions, the OHH profile allocates more emissions to evening and morning hours local time, whereas the default profile allocates most emissions to midday hours local time (Figure 2.3). Applying the OHH profile allocated 18% to 28% more emissions to nighttime hours than the default profile across CONUS (Figure 3.8). Spatial differences in the percent of emissions allocated to nighttime were impacted both by the change in diurnal profile, and the daily allocation of emissions; the DS approach allocates more emissions to the heating season months, which also have longer nights in the midlatitudes.

A higher allocation of emissions to nighttime may increase the importance of nocturnal chemical processes to determining the fate of NO_X in the atmosphere. Analysis of the WINTER aircraft campaign showed that the nocturnal NO_X lifetime is shorter than the daytime NO_X lifetime (Kenagy et al., 2018). Furthermore, chemical loss of NO_X via N_2O_5 and HNO_3 chemistry becomes more important at night compared to the day, when photochemical reactivity dominates chemical processes (Jaeglé et al., 2018; Kenagy et al., 2018).

RFC emissions encompass fuel combustion from a range of space heating appliances that use various fuel sources (e.g., natural gas, fuel oil, etc.). Ideally, each appliance would be represented with diurnal allocation profiles specific to the daily usage activity for each appliance type. Though the OHH profile was developed to represent wood-burning heating appliances, a study by Gouveia et al. (2017) suggested that space heating from electricity follows a similar

diurnal allocation. Using observations of hourly consumption of electricity to track usage for space heating, Gouveia et al. (2017) found that the typical use profile for space heating was highest in the evening hours. However, unlike the OHH profile which also allocates emissions to early morning hours, the electricity usage for space heating was lowest in the early morning hours. While the assumption to use the OHH profile is likely an improvement in the representation of heating activity over the default profile, appliance- or fuel-specific diurnal allocations could be a future improvement for hourly RFC emissions estimations.

4.4 Contribution of RFC to Total Anthropogenic Emissions

Isolating gridded, temporally-allocated RFC emissions from other nonpoint sources for this research allowed us to quantify the contribution of RFC emissions to total anthropogenic emissions on an annual and monthly basis. Previously, available data only allowed for estimating the contribution of RFC to annual, county-level emissions. On an annual basis, RFC contributed to an average of 4.7% of total anthropogenic NO_X by grid cell, and up to 68.7%. The contribution of RFC to total NO_X emissions increased during the heating season, with average contributions between 7.7% and 9.7%. RFC NO_X emissions had the highest contribution to total gridded anthropogenic NO_X emissions in rural areas with limited NO_X sources and urban areas with relatively high RFC emissions. Quantifying the impact to gridded emissions shows that previous estimates using county-level totals underestimate the relative importance of RFC to total anthropogenic NO_X in some grid cells, especially in the winter.

On annual and monthly timescales, the contribution of RFC to total anthropogenic emissions for other chemical species was highest for SO_2. RFC SO_2 emissions contributed a substantial portion of gridded total anthropogenic SO_2 emissions, particularly in New England, with average contributions between 20.6% and 23.6% during the heating season. The largest SO_2

emissions sources are coal-fired power plants, industrial fuel combustion, and other industrial processes such as chemical manufacturing (U.S. EPA, 2023a). Though these large stationary sources have SO_2 emissions that are three orders of magnitude higher than RFC SO_2 emissions, RFC is one of the only sources of SO_2 emissions in areas without large sources. High RFC SO_2 emissions in the U.S. are primarily from the sulfur content in fuel oil, which is predominantly used in New England states (Kroetz & Friedland, 2008; Northeast States for Coordinated Air Use Management (NESCAUM), 2005). Outside of the U.S., residential heating is a substantial source of SO_2 due to reliance on coal for central heating systems (Mutlu & Bayraktar, 2021; Su et al., 2011). Since 2011, the NEI has not reported any RFC from coal combustion as coal is no longer a primary fuel source used in residential heating (U.S. EPA, 2021c). Chemical transport model evaluations of RFC emissions could be done to understand the impact of RFC emissions on ambient SO_2 concentrations to identify potential NAAQS exceedances in areas without regulatory surface-level monitors.

4.5 Potential Implications for CMAQ Biases

Model performance of CMAQ in simulating atmospheric composition is limited by the accuracy of emissions inventory inputs, as well as chemical mechanisms and meteorological inputs (Appel et al., 2021b). CMAQ simulations have regional and seasonal biases in the estimation of ambient NO_X, ozone, $PM_{2.5}$, and other chemical species. While the DS approach reflects an improvement in the representation of the temperature-dependence of RFC emissions compared to the SS approach, the implications for potentially improving CMAQ performance are unclear.

CMAQ tends to underestimate NO_X concentrations throughout the year, but especially in the winter months (Appel et al., 2021a; Harkey et al., 2015; Kaynak et al., 2013; Pan et al., 2014) In an evaluation of CMAQ version 5.3.1, winter NO_X concentrations were biased low compared

to surface monitor observations for all regions across CONUS (Appel et al., 2021a). The reallocation of RFC NO_X emissions in time using the DS approach could potentially improve the CMAQ low bias by allocating more emissions to cold days when longer NO_X lifetimes and atmospheric stagnation may result in rapid increases to concentrations. Alternatively, the distribution of RFC emissions to an extended heating season, increasing emissions in March and November but decreasing emissions in the winter months, may decrease NO_X concentrations and contribute to the low CMAQ bias.

While CMAQ performs well in simulating summer ozone concentrations, winter ozone concentrations are underestimated compared to observations (Appel et al., 2021b; Matichuk et al., 2017). Winter season ozone in CMAQ version 5.3.1 was biased low in all regions across CONUS compared to surface monitor observations (Appel et al., 2021b). CMAQ ozone estimations are especially low in the mountain west and northeastern states, where RFC emissions are highest (Appel et al., 2021a). A study using CMAQ to investigate a high winter ozone episode which coincided with a temperature inversion during the 2013 Uinta Basin Winter Ozone Study (UBWOS) similarly showed that CMAQ predictions of ozone were biased low compared to surface and aircraft observations (Matichuk et al., 2017). Depending on local ozone formation chemistry, increases to RFC NO_X emissions during cold weather events due to the DS temporal allocation could improve performance of CMAQ ozone simulations during the winter.

Studies have shown that chemical transport models have worse performance in simulating chemical processes impacting nocturnal chemistry compared to daytime processes (Chang et al., 2011; Hoffman et al., 2024). Though the poor performance is primarily tied to simplifications in the chemical mechanisms impacting nocturnal chemistry, including a more accurate allocation of RFC emissions to nighttime may improve the characterization of wintertime atmospheric

composition. For example, Hoffman et al. (2024) identified low biases in estimations of winter concentrations of dinitrogen pentoxide (N_2O_5) and nitryl chloride ($ClNO_2$) using various chemical mechanisms in CMAQ compared to observations. As N_2O_5 and $ClNO_2$ are produced by the oxidation of NO_X at night (e.g., Jaeglé et al., 2018), higher NO_X emissions allocated to nighttime hours may improve the CMAQ low bias for these species.

4.6 Assumptions and Limitations

Estimating hourly, gridded emissions from annual county-level emissions totals is inherently based on assumptions and simplifications. Using HDDs as the temperature-based proxy for heating demand in the DS approach assumes that all RFC emissions are directly correlated with ambient air temperatures. HDDs are a widely used proxy for heating demand and energy use for residential space heating, which are based solely on outdoor ambient temperature (e.g., Gesangyangji et al., 2024; Kennard et al., 2022; Quayle & Diaz, 1980; Thom, 1954). Other meteorological variables can also have an impact on residential heating demand, such as humidity (Kheiri et al., 2023), which is not incorporated directly in this method. In the evaluation of emissions impacts to different IECC climate regions, we observed systematic differences in the impact of DS on humid compared to dry climates (Figure 3.8), indicating that our scaling approach may indirectly represent the influence of humidity on building heating.

The assumption that all RFC emissions are proportional to HDDs in the DS approach is a simplification when considering RFC emissions from other end uses for fuel besides space heating. Though space heating is the largest end use of residential fuels in the U.S., it is not the only end use. Based on the 2020 Residential Energy Consumption Survey from the U.S. Energy Information Administration (U.S. EIA), 46% to 78% of residential natural gas use across census regions is for space heating, with between 17% and 43% of usage toward water heating. An evaluation of

outdoor temperature on the efficiency of water heaters found that lower temperatures increase the energy demand for water heating (Hart & De Dear, 2004). While there is an inverse relationship between temperature and water heater energy demand, water heaters are still used on days when there is no space heating demand. The DS simplification to only allocate RFC emissions based on space heating demand is comparable to the assumptions made by the U.S. EPA for residential wood combustion, where it is assumed that no emissions are present on days above a reference outdoor temperature threshold (U.S. EPA, 2023b).

When this research was initiated, EQUATES 2019 was the most recent platform available from the U.S. EPA, which has been used in peer-reviewed publications (e.g., Harkey & Holloway, 2024; Hoffman et al., 2024). The EQUATES 2019 platform uses the SS approach to allocate RFC emissions, which was used for comparison to DS in this study. After this research was initiated, the U.S. EPA released model-ready emissions inventories for model years 2020 through 2023 with a monthly scaling approach for residential natural gas emissions (U.S. EPA, 2025). The monthly allocation method is based on monthly natural gas purchases by state reported by the U.S. EIA. All other RFC fuel types use the SS approach, and emissions for all fuel types are flatly allocated for each day of the month. The monthly allocations are constant for each state, which does not account for intrastate heterogeneity in heating demand. Based on the IECC climate zones, most states have more than one climate zone, with some larger states having as many as six or seven climate zones (Figure 2.4). While the monthly allocation approach is an improvement in precision compared to the SS approach, the temperature-based DS approach offers further improvements to the representation of heating demand on daily RFC emissions.

4.7 Future Research Directions

Developing this temperature-dependent emissions inventory (EI) of RFC will allow us to investigate the co-variability between emissions, meteorology, and chemistry impacting wintertime air quality. As I continue in my graduate research, I plan to implement the new RFC EI into the EQUATES 2019 modeling platform to simulate wintertime air pollution using the CMAQ, focusing on NO_X and secondary particulate nitrate concentrations. I will evaluate the model results by comparing output to surface and satellite observations where available. Because more recent emissions estimates are now available, I plan to apply the DS allocation approach to the 2020 NEI for the 2024 model year, using 2024 meteorology. The 2024 model year coincides with observations from the Tropospheric Emissions: Monitoring of Pollution (TEMPO) satellite mission. For the 2024 model year, I plan to use CMAQ to isolate the effects of RFC emissions from other meteorologically-dependent chemical processes on wintertime atmospheric composition.

References

(1) Adelman, Z. (2016). *2014 Emissions Modeling Platform Spatial Surrogate Document*. UNC Institute for the Environment, Chapel Hill, NC. https://gaftp.epa.gov/Air/emismod/2014/v1/spatial_surrogates/US_SpatialSurrogate_Documentation_10012016.pdf

(2) Adelman, Z., Arora, G., Xiu, A., Baek, B., Houyoux, M., Eyth, A., & Strum, M. (2010). *Development and preliminary results for a model of temporal variability in residential wood combustion emissions*.

(3) Allen, D., Pickering, K. E., Bucsela, E., Van Geffen, J., Lapierre, J., Koshak, W., & Eskes, H. (2021). Observations of Lightning NO_x Production From Tropospheric Monitoring Instrument Case Studies Over the United States. *Journal of Geophysical Research: Atmospheres*, *126*(10), e2020JD034174. https://doi.org/10.1029/2020JD034174

(4) Almaraz, M., Bai, E., Wang, C., Trousdell, J., Conley, S., Faloona, I., & Houlton, B. Z. (2018). Agriculture is a major source of NO_x pollution in California. *Science Advances*, *4*(1), eaao3477. https://doi.org/10.1126/sciadv.aao3477

(5) Antonopoulos, C., Gilbride, T., Margiotta, E., & Kaltreider, C. (2022). *Guide to Determining Climate Zone by County: Building America and IECC 2021 Updates*. Pacific Northwest National Laboratory (PNNL). https://doi.org/10.2172/1893981

(6) Appel, K. W., Bash, J. O., Fahey, K. M., Foley, K. M., Gilliam, R. C., Hogrefe, C., Hutzell, W. T., Kang, D., Mathur, R., Murphy, B. N., Napelenok, S. L., Nolte, C. G., Pleim, J. E., Pouliot, G. A., Pye, H. O. T., Ran, L., Roselle, S. J., Sarwar, G., Schwede, D. B., … Wong, D. C. (2021a). Supplement of The Community Multiscale Air Quality (CMAQ) model versions 5.3 and 5.3.1: System updates and evaluation. *Geoscientific Model Development*, *14*(5), 2867–2897. https://doi.org/10.5194/gmd-14-2867-2021-supplement

(7) Appel, K. W., Bash, J. O., Fahey, K. M., Foley, K. M., Gilliam, R. C., Hogrefe, C., Hutzell, W. T., Kang, D., Mathur, R., Murphy, B. N., Napelenok, S. L., Nolte, C. G., Pleim, J. E., Pouliot, G. A., Pye, H. O. T., Ran, L., Roselle, S. J., Sarwar, G., Schwede, D. B., … Wong, D. C. (2021b). The Community Multiscale Air Quality (CMAQ) model versions 5.3 and 5.3.1: System updates and evaluation. *Geoscientific Model Development*, *14*(5), 2867–2897. https://doi.org/10.5194/gmd-14-2867-2021

(8) Arunachalam, S., Woody, M., Omary, M., Penn, S., Chung, S., Woo, M., Tambouret, Y., & Levy, J. (2016). Modeling the Air Quality and Public Health Benefits of Increased Residential Insulation in the United States. In *Springer Proceedings in Complexity* (pp. 135–140). Springer International Publishing. https://doi.org/10.1007/978-3-319-24478-5_22

(9) Aste, N., Adhikari, R. S., Compostella, J., & Pero, C. D. (2013). Energy and environmental impact of domestic heating in Italy: Evaluation of national NOx emissions. *Energy Policy*, *53*, 353–360. https://doi.org/10.1016/j.enpol.2012.10.064

(10) Aste, N., Adhikari, R. S., & Del Pero, C. (2009). Estimation of NO<inf>x</inf> emissions associated with the natural gas consumption for residential heating in Italy. *2009 International Conference on Clean Electrical Power*, 202–206. https://doi.org/10.1109/iccep.2009.5212057

(11) Baek, B. H., & Seppanen, C. (2021). *CEMPD/SMOKE: SMOKE v4.8.1 Public Release (June 2023)* (Version SMOKEv481_Jan2021) [Computer software]. Zenodo. https://doi.org/10.5281/ZENODO.1421402

(12) Beelen, R., Raaschou-Nielsen, O., Stafoggia, M., Andersen, Z. J., Weinmayr, G., Hoffmann, B., Wolf, K., Samoli, E., Fischer, P., Nieuwenhuijsen, M., Vineis, P., Xun, W. W., Katsouyanni, K., Dimakopoulou, K., Oudin, A., Forsberg, B., Modig, L., Havulinna, A. S., Lanki, T., … Hoek, G. (2014). Effects of long-term exposure to air pollution on natural-cause mortality: An analysis of 22 European cohorts within the multicentre ESCAPE project. *The Lancet*, *383*(9919), 785–795. https://doi.org/10.1016/S0140-6736(13)62158-3

(13) Beidler, J. (2025, March 14). *Temporal Allocation of Residential Fuel Combustion for 2019? Comment: "Profile 26 is often used for source categories where source-specific diurnal activity data is either not available or has not been assessed."* [Online post]. CMAS Forum. https://forum.cmascenter.org/t/temporal-allocation-of-residential-fuel-combustion-for-2019/5034/5?u=crscalpone

(14) Belova, I. N., Ginzburg, A. S., & Krivenok, L. A. (2018). Heating seasons length and degree days trends in Russian cities during last half century. *Energy Procedia*, *149*, 373–379. https://doi.org/10.1016/j.egypro.2018.08.201

(15) Cai, Y., Zhang, B., Ke, W., Feng, B., Lin, H., Xiao, J., Zeng, W., Li, X., Tao, J., Yang, Z., Ma, W., & Liu, T. (2016). Associations of Short-Term and Long-Term Exposure to Ambient Air Pollutants With Hypertension: A Systematic Review and Meta-Analysis. *Hypertension*, *68*(1), 62–70. https://doi.org/10.1161/HYPERTENSIONAHA.116.07218

(16) Chang, W. L., Bhave, P. V., Brown, S. S., Riemer, N., Stutz, J., & Dabdub, D. (2011). Heterogeneous Atmospheric Chemistry, Ambient Measurements, and Model Calculations of N_2O_5: A Review. *Aerosol Science and Technology*, *45*(6), 665–695. https://doi.org/10.1080/02786826.2010.551672

(17) Chatoutsidou, S. E., & Lazaridis, M. (2024). Investigating the role of photochemistry and impact of regional and local contributions on gaseous pollutant concentrations (NO, NO2, O3, CO, and SO2) at urban and suburban sites. *Atmospheric Pollution Research*, *15*(12), 102322. https://doi.org/10.1016/j.apr.2024.102322

(18) Chen, T.-M., Kuschner, W. G., Gokhale, J., & Shofer, S. (2007). Outdoor Air Pollution: Nitrogen Dioxide, Sulfur Dioxide, and Carbon Monoxide Health Effects. *The American Journal of the Medical Sciences*, *333*(4), 249–256. https://doi.org/10.1097/MAJ.0b013e31803b900f
(19) Cheng, B., Alapaty, K., & Arunachalam, S. (2024). Spatiotemporal trends in PM2.5 chemical composition in the conterminous U.S. during 2006–2020. *Atmospheric Environment*, *316*, 120188. https://doi.org/10.1016/j.atmosenv.2023.120188
(20) Clean Air Act, 42 U.S.C. (1970).
(21) Cornette, J. F. P., & Blondeau, J. (2024). Emissions and levelized cost of urban residential building heating: The Brussels perspective. *Energy Strategy Reviews*, *54*, 101443. https://doi.org/10.1016/j.esr.2024.101443
(22) Dedoussi, I. C., Eastham, S. D., Monier, E., & Barrett, S. R. H. (2020). Premature mortality related to United States cross-state air pollution. *Nature*, *578*(7794), 261–265. https://doi.org/10.1038/s41586-020-1983-8
(23) Environment and Climate Change Canada. (2025). *Canada's Air Pollutant Emissions Inventory Report 1990-2023*. https://publications.gc.ca/collections/collection_2025/eccc/En81-30-2023-eng.pdf
(24) Foley, K. M., Pouliot, G. A., Eyth, A., Aldridge, M. F., Allen, C., Appel, K. W., Bash, J. O., Beardsley, M., Beidler, J., Choi, D., Farkas, C., Gilliam, R. C., Godfrey, J., Henderson, B. H., Hogrefe, C., Koplitz, S. N., Mason, R., Mathur, R., Misenis, C., … Adams, E. (2023). 2002–2017 anthropogenic emissions data for air quality modeling over the United States. *Data in Brief*, *47*, 109022. https://doi.org/10.1016/j.dib.2023.109022
(25) Gesangyangji, G., Holloway, T., Vimont, D. J., & Acker, S. J. (2024). Future changes in state-level population-weighted degree days in the U.S. *Environmental Research Letters*, *19*(3), 034029. https://doi.org/10.1088/1748-9326/ad28dd
(26) Gouveia, J. P., Seixas, J., & Mestre, A. (2017). Daily electricity consumption profiles from smart meters—Proxies of behavior for space heating and cooling. *Energy*, *141*, 108–122. https://doi.org/10.1016/j.energy.2017.09.049
(27) Hall, S. J., Matson, P. A., & Roth, P. M. (1996). NO_x EMISSIONS FROM SOIL: Implications for Air Quality Modeling in Agricultural Regions. *Annual Review of Energy and the Environment*, *21*(1), 311–346. https://doi.org/10.1146/annurev.energy.21.1.311
(28) Hand, J. L., Schichtel, B. A., Pitchford, M., Malm, W. C., & Frank, N. H. (2012). Seasonal composition of remote and urban fine particulate matter in the United States. *Journal of Geophysical Research: Atmospheres*, *117*(D5). https://doi.org/10.1029/2011jd017122
(29) Harkey, M., & Holloway, T. (2024). Simulated Surface-Column NO_2 Connections for Satellite Applications. *Journal of Geophysical Research: Atmospheres*, *129*(21). https://doi.org/10.1029/2024jd041912

(30) Harkey, M., Holloway, T., Oberman, J., & Scotty, E. (2015). An evaluation of CMAQ NO_2 using observed chemistry-meteorology correlations. *Journal of Geophysical Research: Atmospheres*, *120*(22). https://doi.org/10.1002/2015JD023316
(31) Hart, M., & De Dear, R. (2004). Weather sensitivity in household appliance energy end-use. *Energy and Buildings*, *36*(2), 161–174. https://doi.org/10.1016/j.enbuild.2003.10.009
(32) Hartley, S., & Robinson, D. A. (2000). A shift in winter season timing in the Northern Plains of the USA as indicated by temporal analysis of heating degree days. *International Journal of Climatology*, *20*(4), 365–379. https://doi.org/10.1002/(sici)1097-0088(20000330)20:4<365::aid-joc478>3.0.co;2-7
(33) Hoek, G., Krishnan, R. M., Beelen, R., Peters, A., Ostro, B., Brunekreef, B., & Kaufman, J. D. (2013). Long-term air pollution exposure and cardio- respiratory mortality: A review. *Environmental Health*, *12*(1), 43. https://doi.org/10.1186/1476-069X-12-43
(34) Hoffman, A., Bertram, T. H., Holloway, T., & Harkey, M. (2024). Assessment of Nocturnal NO_x Heterogeneous Reaction Mechanisms in the Community Multiscale Air Quality (CMAQ) Model. *Journal of Geophysical Research: Atmospheres*, *129*(10). https://doi.org/10.1029/2023jd040290
(35) International Code Council. (2025, February). *2021 International Energy Conservation Codes (IECC); Section C301 Climate Zones*. https://codes.iccsafe.org/content/IECC2021V1.0/chapter-3-ce-general-requirements#IECC2021V1.0_CE_Ch03_SecC301
(36) Jacob, D. J. (1999). *Introduction to Atmospheric Chemistry*. Princeton university press.
(37) Jaeglé, L., Shah, V., Thornton, J. A., Lopez-Hilfiker, F. D., Lee, B. H., McDuffie, E. E., Fibiger, D., Brown, S. S., Veres, P., Sparks, T. L., Ebben, C. J., Wooldridge, P. J., Kenagy, H. S., Cohen, R. C., Weinheimer, A. J., Campos, T. L., Montzka, D. D., Digangi, J. P., Wolfe, G. M., … Weber, R. J. (2018). Nitrogen Oxides Emissions, Chemistry, Deposition, and Export Over the Northeast United States During the WINTER Aircraft Campaign. *Journal of Geophysical Research: Atmospheres*, *123*(21). https://doi.org/10.1029/2018jd029133
(38) Jeong, C.-H., Evans, G. J., Dann, T., Graham, M., Herod, D., Dabek-Zlotorzynska, E., Mathieu, D., Ding, L., & Wang, D. (2008). Influence of biomass burning on wintertime fine particulate matter: Source contribution at a valley site in rural British Columbia. *Atmospheric Environment*, *42*(16), 3684–3699. https://doi.org/10.1016/j.atmosenv.2008.01.006
(39) Kaynak, B., Hu, Y., & Russell, A. G. (2013). Analysis of NO, NO2, and O3 Between Model Simulations and Ground-Based, Aircraft, and Satellite

Observations. *Water, Air, & Soil Pollution*, *224*(9). https://doi.org/10.1007/s11270-013-1674-2

(40) Kenagy, H. S., Sparks, T. L., Ebben, C. J., Wooldrige, P. J., Lopez-Hilfiker, F. D., Lee, B. H., Thornton, J. A., McDuffie, E. E., Fibiger, D. L., Brown, S. S., Montzka, D. D., Weinheimer, A. J., Schroder, J. C., Campuzano-Jost, P., Day, D. A., Jimenez, J. L., Dibb, J. E., Campos, T., Shah, V., … Cohen, R. C. (2018). NO_x Lifetime and NO_y Partitioning During WINTER. *Journal of Geophysical Research: Atmospheres*, *123*(17), 9813–9827. https://doi.org/10.1029/2018JD028736

(41) Kennard, H., Oreszczyn, T., Mistry, M., & Hamilton, I. (2022). Population-weighted degree-days: The global shift between heating and cooling. *Energy and Buildings*, *271*, 112315. https://doi.org/10.1016/j.enbuild.2022.112315

(42) Kheiri, F., Haberl, J. S., & Baltazar, J.-C. (2023). Impact of outdoor humidity conditions on building energy performance and environmental footprint in the degree days-based climate classification. *Energy*, *283*, 128447. https://doi.org/10.1016/j.energy.2023.128447

(43) Kroetz, K. M., & Friedland, A. J. (2008). Comparing costs and emissions of northern New England space heating fuel options. *Biomass and Bioenergy*, *32*(12), 1359–1366. https://doi.org/10.1016/j.biombioe.2008.04.003

(44) Krug, E. C., & Frink, C. R. (1983). Acid Rain on Acid Soil: A New Perspective. *Science*, *221*(4610), 520–525. https://doi.org/10.1126/science.221.4610.520

(45) Lange, K., Richter, A., & Burrows, J. P. (2022). Variability of nitrogen oxide emission fluxes and lifetimes estimated from Sentinel-5P TROPOMI observations. *Atmospheric Chemistry and Physics*, *22*(4), 2745–2767. https://doi.org/10.5194/acp-22-2745-2022

(46) Laughner, J. L., & Cohen, R. C. (2019). Direct observation of changing NO_x lifetime in North American cities. *Science*, *366*(6466), 723–727. https://doi.org/10.1126/science.aax6832

(47) Lee, D. S., Köhler, I., Grobler, E., Rohrer, F., Sausen, R., Gallardo-Klenner, L., Olivier, J. G. J., Dentener, F. J., & Bouwman, A. F. (1997). Estimations of global no, emissions and their uncertainties. *Atmospheric Environment*, *31*(12), 1735–1749. https://doi.org/10.1016/S1352-2310(96)00327-5

(48) Likens, G. E., Bormann, F. H., & Johnson, N. M. (1972). Acid Rain. *Environment: Science and Policy for Sustainable Development*, *14*(2), 33–40. https://doi.org/10.1080/00139157.1972.9933001

(49) Mansfield, M. L., & Hall, C. F. (2013). Statistical analysis of winter ozone events. *Air Quality, Atmosphere & Health*, *6*(4), 687–699. https://doi.org/10.1007/s11869-013-0204-0

(50) Matichuk, R., Tonnesen, G., Luecken, D., Gilliam, R., Napelenok, S. L., Baker, K. R., Schwede, D., Murphy, B., Helmig, D., Lyman, S. N., & Roselle, S. (2017). Evaluation of the Community Multiscale Air Quality Model for Simulating Winter

Ozone Formation in the Uinta Basin. *Journal of Geophysical Research: Atmospheres*, *122*(24). https://doi.org/10.1002/2017jd027057

(51) Mezuman, K., Bauer, S. E., & Tsigaridis, K. (2016). Evaluating secondary inorganic aerosols in three dimensions. *Atmospheric Chemistry and Physics*, *16*(16), 10651–10669. https://doi.org/10.5194/acp-16-10651-2016

(52) Mutlu, A., & Bayraktar, O. M. (2021). Urban scale air quality analysis due to coal-based residential heating. *Air Quality, Atmosphere & Health*, *14*(9), 1487–1503. https://doi.org/10.1007/s11869-021-01063-1

(53) Northeast States for Coordinated Air Use Management (NESCAUM). (2005, December). *Low Sulfur Heating Oil in the Northeast States: An Overview of Benefits, Costs and Implementation Issues*. https://www.nescaum.org/documents/report060101heatingoil.pdf

(54) Pan, L., Tong, D., Lee, P., Kim, H.-C., & Chai, T. (2014). Assessment of NOx and O3 forecasting performances in the U.S. National Air Quality Forecasting Capability before and after the 2012 major emissions updates. *Atmospheric Environment*, *95*, 610–619. https://doi.org/10.1016/j.atmosenv.2014.06.020

(55) Petri, Y., & Caldeira, K. (2015). Impacts of global warming on residential heating and cooling degree-days in the United States. *Scientific Reports*, *5*(1). https://doi.org/10.1038/srep12427

(56) Quayle, R. G., & Diaz, H. F. (1980). Heating degree day data applied to residential heating energy consumption. *Journal of Applied Meteorology and Climatology*, *19*(3), 241–246.

(57) Ranson, M., Morris, L., & Kats-Rubin, A. (2014). *Climate Change and Space Heating Energy Demand: A Review of the Literature*. https://doi.org/10.22004/AG.ECON.280923

(58) Schroder, J. C., Campuzano-Jost, P., Day, D. A., Shah, V., Larson, K., Sommers, J. M., Sullivan, A. P., Campos, T., Reeves, J. M., Hills, A., Hornbrook, R. S., Blake, N. J., Scheuer, E., Guo, H., Fibiger, D. L., McDuffie, E. E., Hayes, P. L., Weber, R. J., Dibb, J. E., … Jimenez, J. L. (2018). Sources and Secondary Production of Organic Aerosols in the Northeastern United States during WINTER. *Journal of Geophysical Research: Atmospheres*, *123*(14), 7771–7796. https://doi.org/10.1029/2018jd028475

(59) Schumann, U., & Huntrieser, H. (2007). The global lightning-induced nitrogen oxides source. *Atmospheric Chemistry and Physics*, *7*(14), 3823–3907. https://doi.org/10.5194/acp-7-3823-2007

(60) Shen, X., & Liu, B. (2016). Changes in the timing, length and heating degree days of the heating season in central heating zone of China. *Scientific Reports*, *6*(1). https://doi.org/10.1038/srep33384

(61) Simon, H. (2015). *CMAQv5.0 PMother speciation* [CMASWIKI]. U.S. EPA. https://cmascenter.org/cmaq/wiki/airqualitymodeling.org/index.php/CMAQv5.0_PMother_speciation
(62) Su, S., Li, B., Cui, S., & Tao, S. (2011). Sulfur Dioxide Emissions from Combustion in China: From 1990 to 2007. *Environmental Science & Technology*, *45*(19), 8403–8410. https://doi.org/10.1021/es201656f
(63) Sun, X., Ivey, C. E., Baker, K. R., Nenes, A., Lareau, N. P., & Holmes, H. A. (2021). Confronting Uncertainties of Simulated Air Pollution Concentrations during Persistent Cold Air Pool Events in the Salt Lake Valley, Utah. *Environmental Science & Technology*, *55*(22), 15072–15081. https://doi.org/10.1021/acs.est.1c05467
(64) Thom, H. C. S. (1954). The rational relationship between heating degree days and temperature. *Monthly Weather Review*, *82*(1), 1–6.
(65) Turkiewicz, K., Magliano, K., & Najita, T. (2006). Comparison of Two Winter Air Quality Episodes during the California Regional Particulate Air Quality Study. *Journal of the Air & Waste Management Association*, *56*(4), 467–473. https://doi.org/10.1080/10473289.2006.10464525
(66) Turner, M. C., Krewski, D., Diver, W. R., Pope, C. A., Burnett, R. T., Jerrett, M., Marshall, J. D., & Gapstur, S. M. (2017). Ambient Air Pollution and Cancer Mortality in the Cancer Prevention Study II. *Environmental Health Perspectives*, *125*(8), Article 8. https://doi.org/10.1289/EHP1249
(67) U.S. Census Bureau. (2020). *CO-EST2019-alldata: Annual Resident Population Estimates, Estimated Components of Resident Population Change, and Rates of the Components of Resident Population Change for States and Counties* [Dataset]. https://www.census.gov/data/tables/time-series/demo/popest/2010s-counties-total.html
(68) U.S. EIA. (2023). *Residential Energy Consumption Survey (RECS) 2020: Table CE4.1 Annual household site end-use consumption by fuel in the United States—Totals, 2020* [Dataset]. https://www.eia.gov/consumption/residential/data/2020/c&e/pdf/ce4.1.pdf
(69) U.S. EIA. (2024, October 19). Units and calculators explained: Degree days. *US EIA Energy Explained*. https://www.eia.gov/energyexplained/units-and-calculators/degree-days.php
(70) U.S. EPA. (1996). *Compilation of Air Pollutant Emission Factors, 5th Edition, AP-42, Volume I: Stationary Point and Area Sources.* https://www.epa.gov/air-emissions-factors-and-quantification/ap-42-compilation-air-emission-factors#5thed
(71) U.S. EPA. (2012, December). *Technical Support Document (TSD) Preparation of Emissions Inventories for the Version 5.0, 2007 Emissions Modeling Platform*. https://www.epa.gov/sites/default/files/2015-10/documents/2007v5_2020base_emismod_tsd_13dec2012.pdf

(72) U.S. EPA. (2021a). *2017 National Emissions Inventory: January 2021 Updated Release, Technical Support Document*. https://www.epa.gov/sites/default/files/2021-02/documents/nei2017_tsd_full_jan2021.pdf
(73) U.S. EPA. (2021b). *EQUATESv1.0: Emissions, WRF/MCIP, CMAQv5.3.2 Data -- 2002-2019 US_12km and NHEMI_108km* [Dataset]. UNC Dataverse. https://doi.org/10.15139/S3/F2KJSK
(74) U.S. EPA. (2021c). *NEI 2017 Supporting Data, Residential Heating—Coal, Distillate Oil, Kerosene, Natural Gas, and LPG*. https://gaftp.epa.gov/Air/nei/2017/doc/supporting_data/nonpoint/
(75) U.S. EPA. (2022, February). *Technical Support Document (TSD) Preparation of Emissions Inventories for the 2017 North American Emissions Modeling Platform*. https://www.epa.gov/system/files/documents/2022-03/2017_emismod_tsd_february2022_0.pdf
(76) U.S. EPA. (2023a, March). *2020 National Emissions Inventory Technical Support Document: Fuel Combustion – Residential Heating -Natural Gas, Oil, and Other*. https://www.epa.gov/system/files/documents/2023-03/NEI2020_TSD_Section26_FuelComb_Res_NonWood.pdf
(77) U.S. EPA. (2023b, March). *2020 National Emissions Inventory Technical Support Document: Fuel Combustion – Residential Heating -Wood*. https://www.epa.gov/system/files/documents/2023-03/NEI2020_TSD_Section27_RWC.pdf
(78) U.S. EPA. (2025, March). *Technical Support Document (TSD): Preparation of Emissions Inventories for the 2022v1 North American Emissions Modeling Platform*. https://www.epa.gov/system/files/documents/2025-06/2022v1_emismod_tsd_base_and_2026_may2025_508_6.pdf
(79) U.S. EPA Office of Research and Development. (2024). *CMAQ* (Version 5.5) [Computer software]. Zenodo. https://doi.org/10.5281/ZENODO.13883210
(80) Valin, L. C., Russell, A. R., & Cohen, R. C. (2013). Variations of OH radical in an urban plume inferred from NO_2 column measurements. *Geophysical Research Letters*, *40*(9), 1856–1860. https://doi.org/10.1002/grl.50267
(81) Van Der A, R. J., Eskes, H. J., Boersma, K. F., Van Noije, T. P. C., Van Roozendael, M., De Smedt, I., Peters, D. H. M. U., & Meijer, E. W. (2008). Trends, seasonal variability and dominant NO_x source derived from a ten year record of NO_2 measured from space. *Journal of Geophysical Research: Atmospheres*, *113*(D4). https://doi.org/10.1029/2007jd009021
(82) Yang, B.-Y., Qian, Z., Howard, S. W., Vaughn, M. G., Fan, S.-J., Liu, K.-K., & Dong, G.-H. (2018). Global association between ambient air pollution and blood pressure: A systematic review and meta-analysis. *Environmental Pollution*, *235*, 576–588. https://doi.org/10.1016/j.envpol.2018.01.001

(83) Ying, Q. (2011). Physical and chemical processes of wintertime secondary nitrate aerosol formation. *Frontiers of Environmental Science & Engineering in China*, *5*(3), 348–361. https://doi.org/10.1007/s11783-011-0343-1